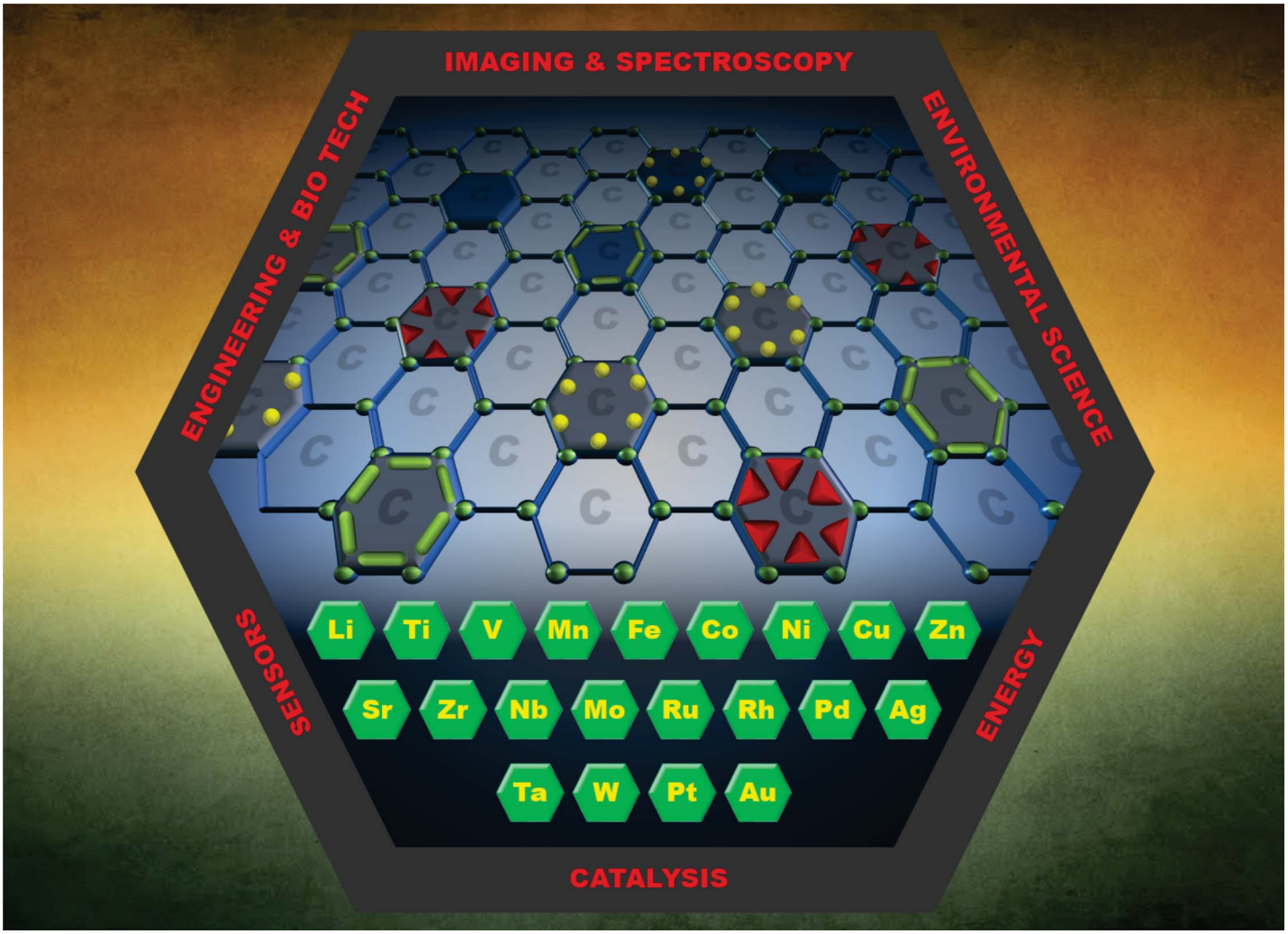

A detailed review by Prof. Wolfgang Tremel, Institute of Inorganic Chemistry, Johannes Gutenberg University of Mainz, Germany and Prof. Abdulrahman A. Al-warthan, Department of Chemistry, College of Science, King Saud University, Saudi Arabia.

Title: Graphene based metal and metal oxide nanocomposites: synthesis, properties and their applications

Graphene, an atomically thin two-dimensional carbonaceous material has attracted tremendous attention in the scientific community due to its unique properties. Especially, in combination with inorganic nanoparticles, it offers great opportunities in various fields of research including electronics, sensing, catalysis, energy storage and conversion. Therefore, we have reviewed in detail the current developments of graphene based metal and metal oxide nanocomposites, their synthesis and applications.

As featured in:

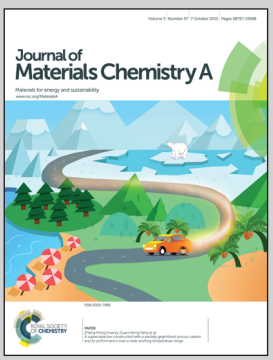

See Muhammad Nawaz Tahir, Abdulrahman A. Al-warthan, Wolfgang Tremel *et al.*, *J. Mater. Chem. A*, 2015, **3**, 18753.

ROYAL SOCIETY OF CHEMISTRY

www.rsc.org/MaterialsA

Registered charity number: 207890

Journal of Materials Chemistry A

REVIEW

Cite this: J. Mater. Chem. A, 2015, 3, 18753

Graphene based metal and metal oxide nanocomposites: synthesis, properties and their applications

Mujeeb Khan,[a] Muhammad Nawaz Tahir,*[b] Syed Farooq Adil,[a] Hadayat Ullah Khan,[cd] M. Rafiq H. Siddiqui,[a] Abdulrahman A. Al-warthan*[a] and Wolfgang Tremel*[b]

Received 27th March 2015
Accepted 10th June 2015

DOI: 10.1039/c5ta02240a

www.rsc.org/MaterialsA

Graphene, an atomically thin two-dimensional carbonaceous material, has attracted tremendous attention in the scientific community, due to its exceptional electronic, electrical, and mechanical properties. Indeed, with the recent explosion of methods for a large-scale synthesis of graphene, the number of publications related to graphene and other graphene based materials has increased exponentially. Particularly the development of easy preparation methods for graphene like materials, such as highly reduced graphene oxide (HRG) *via* reduction of graphite oxide (GO), offers a wide range of possibilities for the preparation of graphene based inorganic nanocomposites by the incorporation of various functional nanomaterials for a variety of applications. In this review, we discuss the current development of graphene based metal and metal oxide nanocomposites, with a detailed account of their synthesis and properties. Specifically, much attention has been given to their wide range of applications in various fields, including electronics, electrochemical and electrical fields. Overall, by the inclusion of various references, this review covers in detail the aspects of graphene-based inorganic nanocomposites.

[a]*Department of Chemistry, College of Science, King Saud University, P.O. Box 2455, Riyadh 11451, Saudi Arabia. E-mail: awarthan@ksu.edu.sa*

[b]*Institute of Inorganic Chemistry, University of Mainz, 55099 Mainz, Germany. E-mail: tremel@uni-mainz.de; tahir@uni-mainz.de*

[c]*Materials Science and Engineering Program, Division of Physical Science and Engineering, King Abdullah University of Science and Technology, Thuwal 23955-6900, Saudi Arabia*

[d]*Thin Film Electronics AB, Westmansgatan 27B, 58216 Linköping, Sweden*

Mujeeb Khan is an Assistant Professor in the Department of Chemistry at King Saud University, Riyadh, KSA. He received his MSc degree in materials chemistry and PhD (2008) from Johannes Gutenberg University of Mainz in Germany. Later he worked as a post-doctoral fellow at Max Planck Institute for Polymer Research Mainz, Germany. His research interests are in the areas of synthesis and in-depth structural, physical characterization as well as to explore potential applications of graphene/inorganic nanocomposites, especially in the field of catalysis. He is an editorial board member of the Arabian Journal of Chemistry.

Dr. Muhammad Nawaz Tahir received his M.Phil. degree from Quaid-i-Azam University Islamabad, Pakistan, in 2001 and then joined Prof. Wolfgang Tremel's group at the Johannes Gutenberg University of Mainz, Germany. He was awarded his PhD in 2006 from Johannes Gutenberg University of Mainz with distinction "Summa Cum Laude". Later he undertook many research projects funded by DFG, MWFZ and the Max Planck Society. Since 2010, he has been working as a senior scientist and group leader for nanomaterials synthesis at Johannes Gutenberg University of Mainz. His research interests involve the synthesis of innovative nanomaterials, characterization and surface functionalization, for biomedical and energy storage applications.

1 Introduction

Graphene is a carbon allotrope comprising a densely packed atomically thin layer of sp^2 *hybridized* carbon atoms in a honeycomb crystal lattice.[1–3] This precisely two-dimensional material exhibits unique high crystal and electronic quality[4,5] and has emerged as a promising new nanomaterial for a variety of exciting applications despite its short history.[6–8] For nearly three decades, carbonaceous materials such as fullerenes and carbon nanotubes (CNTs) have drawn considerable attention due to their exceptional electronic and mechanical properties.[9] Specifically, after the discoveries of zero-dimensional (0D) buckminsterfullerene[10] and shortly later one-dimensional 1D CNTs,[11] enthusiasm in the research of carbon based nanomaterials has increased further.[12] Both fullerenes and CNTs have been proposed to be derived from 2D graphene sheets that are viewed as key building blocks of all other graphitic carbon allotropes (*cf.* Fig. 1), such as "graphite" made up of graphene sheets stacked on top of each other (separated by an interlayer distance of 3.37 Å),[13] "fullerenes" and "CNTs" can be virtually made by wrapping and rolling a section of a graphene sheet.[14] In reality, however, they are not synthesized from graphene.

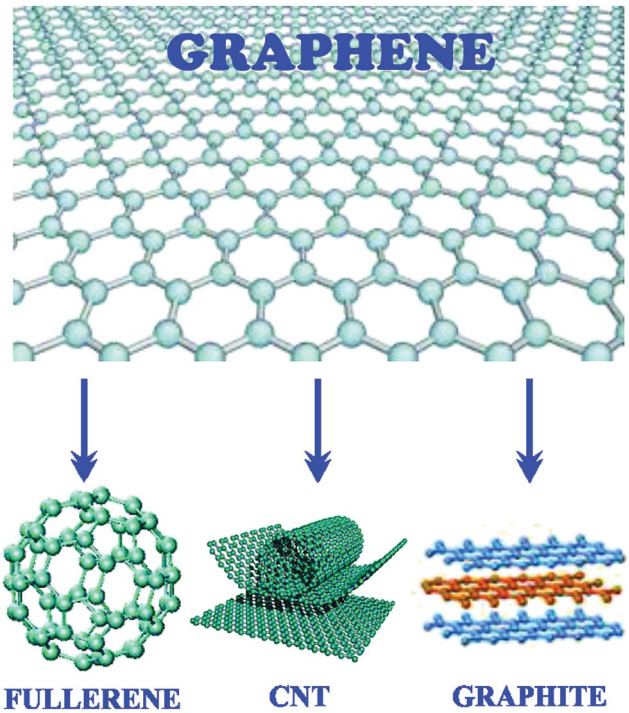

Fig. 1 Graphene is a two-dimensional building block for carbonaceous materials of all other dimensions. It can be wrapped up into 0-D buckyballs, rolled into 1-D nanotubes or stacked into 3-D graphite.[1]

Although graphite is a naturally occurring material and has been in use for centuries,[15] the first reported method for producing graphene can only be traced back to 1970 [16] and rather, the free standing single-layer of graphene was first obtained in 2004 by the isolation of graphene from graphite *via*

S. F. Adil was born in Hyderabad, Telangana, and obtained his Bachelor's and Master's degree from Osmania University. He carried out his doctoral research work at the Indian Institute of Chemical Technology, and his PhD degree was awarded by the Jawaharlal Nehru Technological University, Hyderabad. He later joined the chemistry department at the King Saud University, KSA as an assistant professor in the year 2008. His research is focused on Nanomaterials, Material Sciences and their applications. He worked as a visiting associate at CALTECH, Pasadena, CA. He is also an editorial assistant with the Journal of Saudi Chemical Society.

Prof. M. Rafiq H. Siddiqui was awarded his PhD in 1986 from Aligarh Muslim University. He worked for over four years as a scientist in a national laboratory in India. He then moved to the UK in 1992 where he worked for nearly fourteen years as a senior scientist in the Leverhulme Centre for Innovative Catalysis, Department of Chemistry, University of Liverpool. In 2004 he joined the Department of Chemistry, King Saud University in 2004, where he is a full professor. His main research interests are catalysis, nanotechnology and materials chemistry. He has over 100 publications and translated two books.

Wolfgang Tremel is an inorganic materials chemist. He earned a PhD in chemistry in 1984 from the University of Münster with B. Krebs. Subsequently he joined the group of R. Hoffman at Cornell University (1984-1986) and spent one summer at Ames Laboratory with H. F. Franzen after having returned to Münster in 1987. In 1991 he was appointed associate professor and, in 1996, full professor at the Johannes Gutenberg University in Mainz. His research focuses on the synthesis and structural and physical characterization as well as the design and potential applications of new materials, in particular the chemistry of organized matter.

micromechanical cleavage.[17] The delay in the discovery of free standing graphene sheets can be partially attributed to their single-atom-thick nature, which was initially believed to be thermodynamically unstable.[18] However, graphene is not only stable but also exhibits excellent electronic and mechanical properties such as a charge-carrier mobility of 250 000 $cm^2 V^{-1} s^{-1}$ at room temperature,[19] a thermal conductivity of 5000 W $m^{-1} K^{-1}$,[20] an electrical conductivity of up to 6000 S cm^{-1},[21] and a large theoretical specific surface area of 2630 $m^2 g^{-1}$.[22,23] In addition, graphene is highly transparent, with absorption of <2.3% towards visible light[24] and indeed, with a Young's modulus of 1 TPa and an ultimate strength of 130 GPa, single-layer graphene is the strongest material ever measured.[25]

Despite the fact that graphene has been used as a theoretical model to describe the electronic structure of graphitic species for over half a century,[26] researchers have had difficulty in obtaining experimentally relevant amounts of this material until very recent development of mechanical[17] and chemical methods for graphene production.[27,28] Therefore, due to the great interest generated by the unique structural characteristics and exceptional properties of graphene, and also with the advent of facile production methods,[29,30] graphene has attracted enormous research interest in both scientific and engineering communities all over the world.

The novel catalytic, magnetic and optoelectronic properties of graphene nanocomposites based on the hybridization with nanoparticles (NPs) have attracted significant attention.[31] Particularly, due to the unique sp^2 hybridization of carbon bonds present in graphene, which facilitates the delocalization of electrons, graphene possesses excellent electronic conduction.[17] This electronic conduction of graphene can be enhanced by incorporating various inorganic nanoparticles, including different metal and metal oxide NPs. Due to the enhanced electrical and electronic properties and the synergistic effect between graphene and inorganic nanoparticles, graphene/nanoparticle nanocomposites offer great potential for various applications including energy storage and energy conversion devices.[32] Therefore, the interest in graphene based materials has been ever-growing, due to their peculiarities in combining desirable properties of building blocks for a given application. To date, great efforts have been made to uniformly combine different varieties of nanomaterials with graphene and explore their application in fields like electronics, chemical and biological sensors, electrochemical, energy conversion and storage, solar energy harvesting, *etc.*[33–35] In order to further enhance the properties and to broaden the applications of graphene, various metal and metal oxide NPs have been decorated on graphene.[5] Apart from enhancing the properties of graphene, the NPs act as a stabilizer against the aggregation of individual graphene sheets, which is caused by strong van der Waals interactions between graphene layers. Therefore, more efforts and new strategies to synthesize graphene-based nanocomposites are indispensable.

In this review, we highlight the latest literature with a clear focus on graphene-based metal and metal oxide nanocomposites. In the beginning we review different methods for the synthesis of graphene or highly reduced graphene oxide sheets (HRG) with a particular emphasis on the latest scalable methods (*top-down approaches*) for the production of graphene using graphite oxide (GO) as a precursor, suitable for the preparation of graphene-based nanocomposites. Simultaneously, we discuss some of the *most recently* developed methods for the large-scale synthesis of graphene-based metal and metal oxide nanocomposites, with a particular focus on solution based *in situ* processes. This is followed by an extensive review of the literature about the properties and morphologies of a variety of HRG-metal and HRG–metal oxide nanocomposites and their applications in various fields, such as catalysis or energy storage. Finally, we conclude with challenges for the future growth of the class of nanocomposites. Readers interested in the electronic properties of pristine graphene, various methods for the preparation and characterization of graphene and graphene-based materials and the corresponding background can consult excellent reviews by Neto *et al.*, Zhang *et al.*, Geim *et al.*, Müllen *et al.*, and Singh *et al.*[36–39]

2 Synthesis of graphene and graphene based nanocomposites

The interactions in graphite between adjacent 2D layers of graphene by their overlapping p_z orbitals[40] inhibit the complete delamination of bulk graphite into individual graphene under typical mechanical actions. Although single sheets of graphene can be obtained from bulk graphite by mechanical exfoliation using Scotch tape,[17,41] attempts to mechanically exfoliate graphite result only in stacks of sheets, or a few isolated sheets in low yield.[7] Chemical exfoliation strategies such as sequential oxidation–reduction of graphite often result in a class of graphene-like materials best described as highly reduced graphene oxide (HRG), with graphene domains, defects and residual oxygen containing groups on the surface of the sheets.[27,42,43] Indeed, none of the currently available methods for graphene production yields *bulk* quantities of *defect free* sheets.[7] Apart from the difficulty of producing bulk quantities of *defect free* graphene, most of the currently available synthetic methods also suffer from limited control over size, shape, edge and layers of graphene due to random exfoliation, growth or assembly processes.[44]

Nevertheless, some important advances have already been made and efforts are ongoing to obtain *bulk* quantities of controlled and *defect free* graphene. Several methods have been reported for the synthesis of graphene that can be mainly classified into two different approaches (*cf.* Fig. 2): the *bottom-up* and *top-down* approach.[29] The *bottom-up* growth of graphene sheets is an alternative to the mechanical exfoliation of bulk graphite. In *bottom-up* processes, graphene is synthesized by a variety of methods such as chemical vapor deposition (CVD),[45,46] arc discharge,[47] epitaxial growth on SiC,[48] chemical conversion,[49] reduction of CO,[50] unzipping carbon nanotubes[51,52] and self-assembly of surfactants.[53] The CVD approach to produce graphene relies on dissolving carbon in metal surfaces, such as Ni and Cu that act as catalysts[54,55] and then forcing it to separate by cooling the metal. The thickness and crystalline ordering of

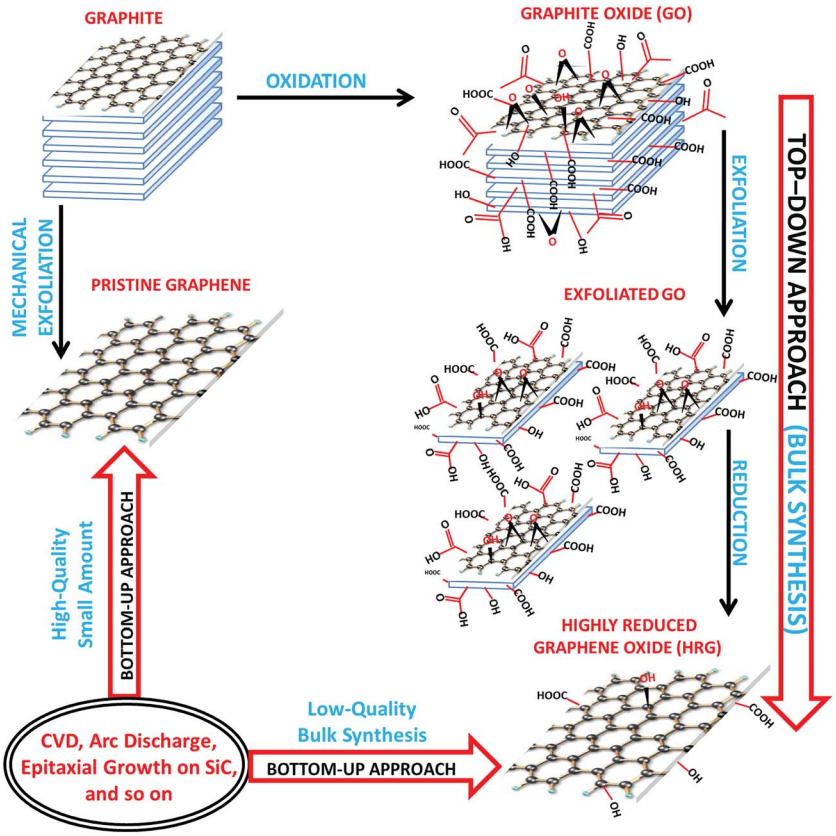

Fig. 2 Schematic representation of the methods used for the synthesis of graphene, which are classified into *top-down* and *bottom-up* approaches. The *top-down* approach is widely used for the *scalable* synthesis of graphene that produces a relatively *low quality* of a graphene-like material commonly known as Highly Reduced Graphene Oxide (HRG) or graphene in *large quantity* required for the preparation of graphene-based nanocomposites.

the precipitated carbon are controlled by the cooling rate and by the concentration of carbon dissolved in the metal.[56] This direct CVD synthesis provides high quality layers of graphene without intensive mechanical or chemical treatments. The epitaxial growth of graphene is achieved *via* high temperature thermal annealing of carbon containing substrates such as SiC.[57]

Notably, CVD and epitaxial growth usually produce large-sized, *defect free* graphene in small quantity suitable for fundamental studies and electronic applications and they are more attractive than the mechanical cleavage method. However, these and other methods mentioned before are not suitable for the synthesis of graphene needed for the preparation of graphene-based *nanocomposites* that usually require *large* amounts of graphene sheets preferably with a *modified* surface structure.[5,9,58,59] While mechanical exfoliation using *Scotch-tape* is a laborious procedure and rarely leads to good quality individual graphene sheets, epitaxial growth requires high-vacuum conditions and a specialized, expensive fabrication system to generate films on small areas. Still, the production of graphene monolayers with large surface areas has been attainable due to the more recent advances in CVD techniques, the uniform growth of single layers of graphene is still a challenge and indeed suitable methods have yet to be fully developed.[56] Similarly, *bulk* quantities of graphene nanoribbons can be potentially produced *via* longitudinal unzipping of CNTs, however, the width of the nanoribbons depends on the CNT diameter.

Therefore, for the manufacturing of graphene-based nanocomposites, which generally requires *bulk* quantities of homogeneously distributed graphene sheets, the *top-down* approach (*i.e.*) chemical and/or thermal reduction of graphite derivatives such as graphite oxide (GO)[60] and graphite fluoride[61] appears to be the most suitable and efficient strategy (*cf.* Fig. 2). These techniques yield low-cost *bulk* amounts of graphene-like sheets that albeit not *defect free*, and they are highly processable and can be fabricated into a variety of materials. Additionally, graphite is a commodity material and easily available with a current annual global production of over 1.1 million tons at $897 per ton in 2009.[62] Hence, the application of graphite or graphite derivatives for the synthesis of graphene offers considerable economic advantages over *bottom-up* methods.[29] Therefore, currently the primary interest in the synthesis of graphene based *nanocomposites* focuses on the oxidation and exfoliation of graphite oxide (GO), followed by chemical reduction[63] that produces graphene as highly reduced graphene oxide (HRG)[64,65] or chemically modified graphene (CMG).[66,67]

2.1 Graphene *via* direct exfoliation of graphite

The exfoliation of graphite into single layers of graphene sheets has attracted considerable attention because of the unusual

electronic properties of monolayers of the graphite lattice.[1,36,68] Among the many exfoliation techniques including micromechanical and liquid exfoliation methods, the micromechanical cleavage of graphite is the most reliable method that renders large-sized, high-quality graphene sheets but in very limited quantities, which makes it only suitable for fundamental studies or electronic applications.[17,69,70] However, recently graphite has also been directly exfoliated into single- and multi-layer graphene *via* sonication in the presence of polyvinylpyrrolidone[71] or diazaperopyrenium dications,[72] electrochemical functionalization of graphite assisted with ionic liquids,[73] and through dissolution in superacids[74] and solvents (liquid phase exfoliation).[75] For the dissolution of graphite certain solvents such as *N*-methyl pyrrolidone (NMP), dimethylformamide (DMF), and *o*-dichlorobenzene (ODCB)[76,77] are particularly interesting, as graphite could be directly exfoliated into monolayer sheets, while preserving its intrinsic electrical properties.[78] Alternatively, surfactant molecules, in aqueous solutions, have also been used to directly exfoliate graphite flakes with concentrations up to 1 mg mL^{-1}.[79] Recently, the direct exfoliation of graphite has been achieved by surface functionalization of graphene sheets with aromatic carboxylic acids in aqueous solutions.[80,81] The aqueous dispersions of graphene sheets in these cases originate from the non-covalent functionalization of graphene with hydrophilic carboxylic acids through aromatic interactions between graphene surfaces and fused aromatic units. The carboxylic acid groups positioned at the out of plane graphene surface stabilize aqueous dispersions of graphene flakes. Moreover, it has also been speculated that selective dispersions of the 2D graphene sheet, out of all graphite allotropes, in aqueous solutions can also be achieved by an elaborate molecular design of amphiphilic molecules.[82] Indeed, more recently an aromatic amphiphile consisting of a hydrophilic dendron and an aromatic segment with planar conformation has been reported which selectively exfoliates graphite powder into single and double layer graphene sheets in aqueous solutions through hydrophilic functionalization of graphene surfaces.[83]

In another example, graphite powder was exfoliated directly in an aqueous solution of pyrene derivatives, which acts as a dispersion agent, a healing agent and an electric glue during the thermal annealing process to produce high-quality single layer graphene sheets.[84] Furthermore, ionic liquids have also been used to exfoliate graphite in a recent example, where a solution-phase technique has been applied for the production of large-area, bilayer or trilayer graphene from graphite.[85] Interhalogen compounds like iodine chloride (ICl) or iodine bromide have been used, which intercalate the graphite starting material at every second or third layer creating second- or third stage controlled graphite intercalation compounds. More recently, the exfoliation of graphite has been carried out under ambient conditions by an electrochemical method (*cf.* Fig. 3) using an environmentally friendly glycine–bisulfate ionic complex.[86] The ionic complex plays a key role in the anodic graphite exfoliation *via* electrochemical-potential-induced intercalation, leading to an efficient expansion of graphite sheets *via* the insertion of oxygen functional groups. Similarly, in a more recent study, an

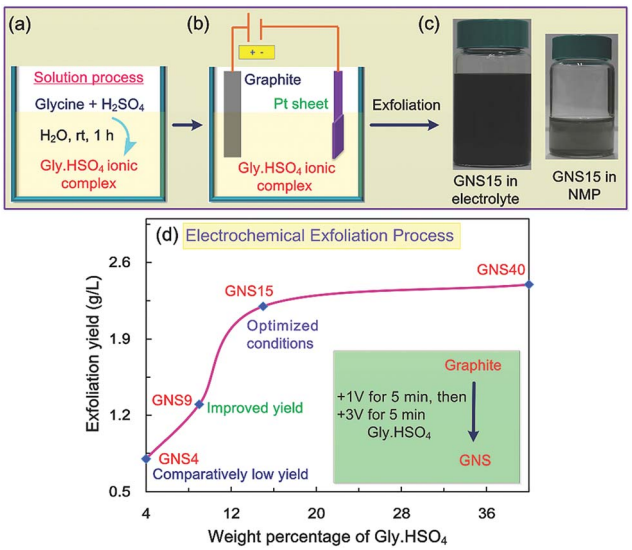

Fig. 3 Preparation process of graphene. (a) A simple solution-process approach for Gly·HSO_4 ionic complex preparation in aqueous solution. (b) Diagram of the electrochemical experimental setup. (c) Photographs of graphene directly in electrolyte (left) and re-dispersed in NMP after purification (right). (d) Exfoliation yields *versus* weight ratios of Gly·HSO_4 ionic complex to water used in exfoliation experiments. Copyrights reserved to the John Wiley and Sons.[86]

industrially scalable method has been developed for the commercial production of large quantities of defect free graphene.[87] During this study, large-scale exfoliation of graphite was carried out in stabilizing liquids, such as *N*-methyl-2-pyrrolidone and by a high-shear mixing method (*cf.* Fig. 4). In this way, the exfoliation of high quality graphene could be achieved in liquid volumes from hundreds of milliliters up to hundreds of liters and even beyond.

Therefore, direct sonication and dissolution methods (liquid phase exfoliation methods) have great potential to be scaled up to produce large quantities of single and multiple layer graphene or functionalized graphene that can be used for the fabrication of composites. Furthermore, gram-scale production of high quality graphene can be achieved using these methods by utilizing custom made molecules or polymers as stabilizing agents, which not only help in increasing the yield, but also inhibit the re-aggregation of graphene. The interaction of these functional molecules with graphene enhances the properties of the 2D material. However, the separation of exfoliated graphene sheets from bulk graphite could still be a challenge.[29] Therefore, further improvement in liquid phase exfoliation methods is required,[77] and more efforts are needed to design and synthesize new molecules with enhanced affinity to the basal plane, reducing the yield of by-products and enhancing the solubility of the produced graphene in other organic solvents, *etc.*

2.2 Graphite oxide (GO)

Although graphene has only emerged as a potential material very recently,[1] the history of GO extends over many decades, even back to the earliest studies involving the chemistry of

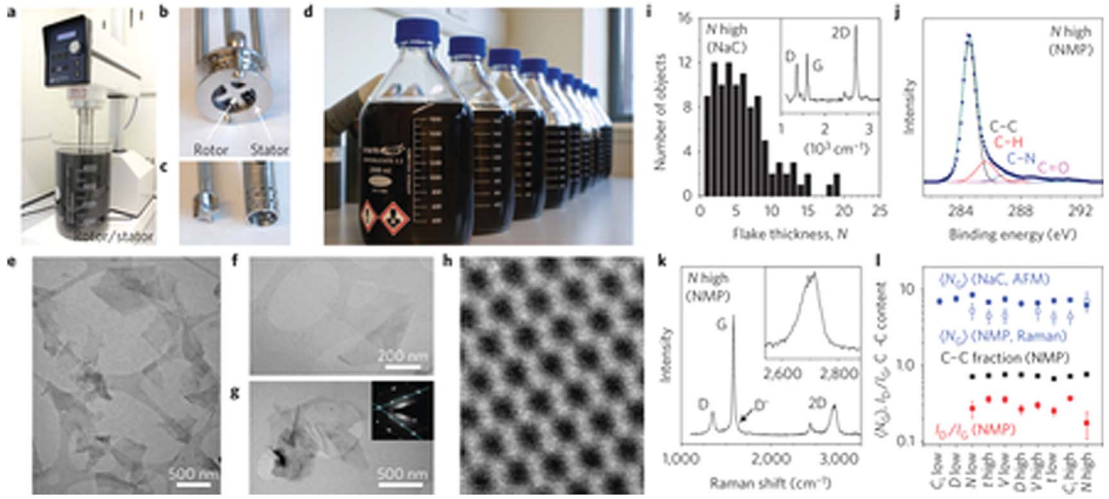

Fig. 4 Production of graphene by shear exfoliation. (a) Silverson model L5M high-shear mixer with a mixing head in a 5 L beaker of graphene dispersion. (b and c) Close-up view of the mixing heads. (d) Graphene dispersed in NMP. (e–h) TEM images of graphene nanosheets. (i) XPS and (j) Raman spectra of exfoliated graphene. (k and l) Rotor and stator for large-scale trials. (m) Shear exfoliation of graphite in 100 L water-surfactant solution. Copyright reserved to the Nature Publishing Group.[87]

graphite.[88,89] GO has been mainly produced by different variations of Brodie,[90,91] Staudenmaier,[92] and Hummers[93] methods that involve the oxidation of graphite in the presence of strong acids (nitric acid or its mixture with sulfuric acid) and oxidants ($KMnO_4$, $KClO_3$, $NaNO_3$). Since then many other slightly modified versions have also been developed. However, to date mainly these three methods comprise the primary routes for the synthesis of GO.[27,65] Notably, it has been demonstrated that the product obtained from these reactions shows strong variance in the level of oxidation depending on the type of oxidant, reaction conditions and the graphite precursor used.[27] Currently, the naturally occurring *flake graphite* is the most common source of graphite used for the preparation of GO that is purified to remove heteroatomic contaminants. Although the localized defects in the p-structure of the flake graphite may serve as seed points for the oxidation process, unfortunately they also *inhibit* the continuation of precise oxidation.[94]

The structure and properties of GO mainly depend on three parameters: the particular synthesis methods, the degree of oxidation and the source of graphite used.[95,96] Although over many decades the precise chemical structure of GO has been the subject of considerable debate, the detailed structure of GO and its oxidation mechanism are still not completely understood due to its complex structure (with strong disorder, irregular packing of the layers, nonstoichiometric atomic composition and lack of consistent and reproducible samples).[97–100] Significant efforts are still underway to understand the exact chemical structure of GO, despite the great success that has already been achieved over the years.[101–104]

Typically, the oxidation of graphite (producing GO) results in its functionalization by epoxy, hydroxyl and other functional groups. The oxidation methods, the variety of oxygen species, and the reaction conditions are well known.[27] However, little work has been done to understand the connection between the oxidation chemistry and morphology of GO sheets. In this context, during their work on the effect of oxidation on the morphology of GO, Li and co-workers have observed cracks in GO that were directly related to the oxidation process. The cracks occurred due to the strain from the cooperative alignment of epoxy groups.[105] Moreover, they also suggested that during the oxidation process graphene oxide sheets undergo an unzipping resulting in size reduction compared to the parent graphite flake size. Typically, slight variations in the degree of oxidation can cause substantial changes in the structure and properties of the materials. Furthermore it is difficult to achieve complete oxidation as well as reduction of GO (down to the level of pure graphene) because of the large number of defects present in its structure.[106] This has also been supported by density functional calculations of GO which predicted that partial oxidation is thermodynamically favored over complete oxidation.[107]

2.3 Modified graphite oxide (GO)

The oxygen functionalities in the basal plane of GO alter the van der Waals interactions between the layers and render them hydrophilic, thus greatly facilitating the hydration and exfoliation of GO in aqueous media.[108] Moreover, in a recent study of the surface charge (zeta potential) of the as-prepared GO sheets, it has been shown that GO sheets (or graphene oxide sheets) acquire negative charges when dispersed in water, apparently because of the dissociation of carboxylic acid and phenolic hydroxyl groups.[63,103] As a result, GO readily forms stable colloidal dispersions in water, which is attributed to both the electrostatic repulsion and hydrophilicity of GO sheets. Thus, complete exfoliation of GO can be achieved by sonication[108] and by stirring the water–GO mixture for a sufficient time, to produce aqueous suspensions of graphene oxide sheets (*cf.* Fig. 5).[42,109]

In particular, GO would serve as an excellent precursor for a variety of graphene-based composite materials if it could be

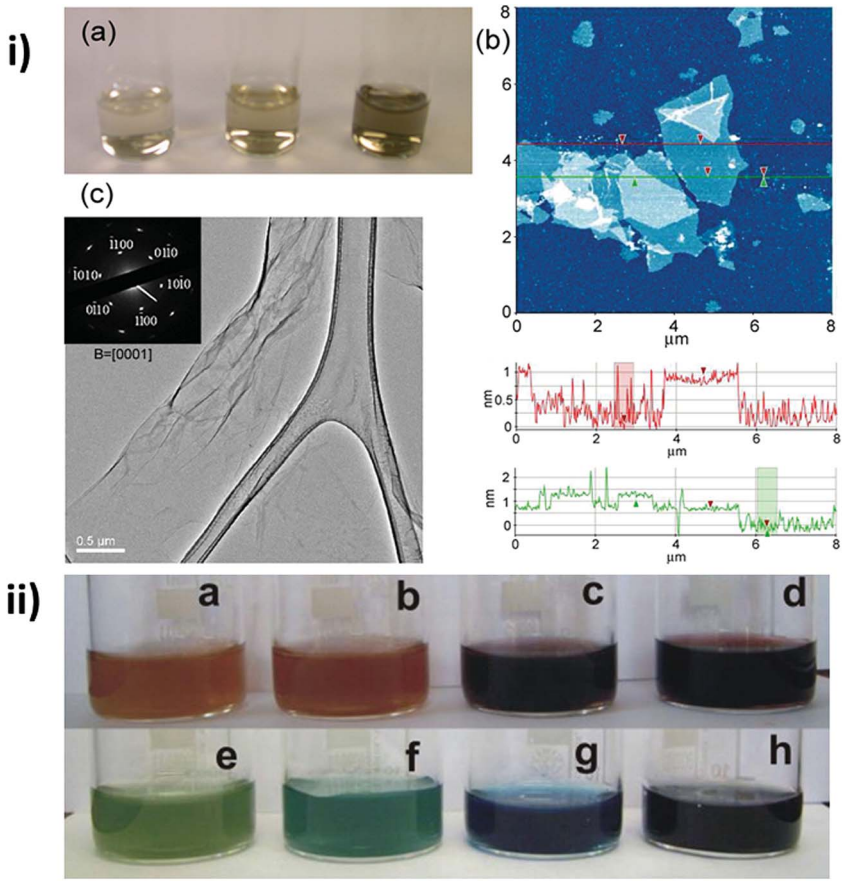

Fig. 5 Aqueous dispersion of GO (i-a) aqueous colloidal suspension from left: graphene oxide, KOH-modified graphene oxide (KMG), hydrazine-reduced KMG (hKMG), (i-b) AFM image of hKMG sheets on a mica substrate. (i-c) TEM image of hKMG sheets, inset, selected area diffraction pattern of what were found to be two overlapping hKMG sheets. Copyrights reserved to the American Chemical Society.[42] (ii) Aqueous suspension of GO in congo red solutions of various concentrations. (ii-a–d) samples without sonication. (ii-e–h) samples after 1 h sonication. Copyrights reserved to the Elsevier Ltd.[109]

completely exfoliated in a wide range of media including water and other organic solvents. However, the hydrophilic nature of GO precludes its direct exfoliation in non-aqueous solvents due to the strong interlayer hydrogen bonding interactions between the adjacent graphene oxide layers.[110] Nevertheless, significant efforts have been made to prepare homogeneous suspensions of GRO sheets in water as well as in various non-aqueous solvents by chemical functionalization of GO.[68,111–113] Usually, chemical functionalization would decrease the density of hydrogen bonding donor groups such as the hydroxyl groups in GO and thus undermine the strength of the hydrogen bonding, thereby rendering less hydrophilic GRO sheets.[110] The oxygen containing groups (such as carboxyl and hydroxyl groups) that exist in GO facilitate the functionalization by providing reactive sites for chemical modification.

Chemical functionalization also prevents the agglomeration of individually separated graphene oxide sheets in dispersion, which is the most important and challenging part in any synthetic route of graphene.[68,70] Thus bulk graphene or GRO sheets spontaneously agglomerate and even restack to form graphite or GO when left unprotected.[108] Several protocols have been reported regarding the homogeneous dispersion, chemical functionalization, and applications of modified graphite oxides (GO) or graphene oxides, such as synthesis of graphene oxide paper like materials[114] and thin films,[115] the ability of modified GO to recognize aromatic molecules[116] for controlling the aggregation state and orientation of organic dyes as well as their application as anode materials for lithium batteries.[117] Other than these, modified GO was also used for water purification in a recent example. For this purpose the hydrophilic character of GO is retained by covalently attaching thiol groups to GO.[118] This particular modification is achieved *via* carbon–carbon attachment of benzene–thiol groups to the sp^2 lattice within the nanosheets. In this regard, the preparation of several functionalized graphite oxides, by treatment of organic isocyanates, has been reported by Stankovich *et al.*[110] They dispersed isocyanate modified graphite oxides (GO) in polar aprotic solvents to form a stable dispersion. The synthesis of modified GO was facilitated by the functionalization of carboxyl and hydroxyl groups such as amides and carbamate esters. In another study, Paredes *et al.* reported the direct dispersion of GO in polar solvents like ethylene glycol, DMF, NMP and THF at about 0.5 mg mL^{-1}.[112]

2.4 Synthesis of highly reduced graphene oxide (HRG)

The reduction of GO or GRO can be performed by various methods including chemical,[119] thermal,[120] electrochemical[121] and photochemical methods[122,123] to obtain graphene-like materials which are generally referred to in the literature as highly reduced graphene oxide (HRG), reduced graphene oxide (rGO), chemically reduced graphene oxide (CReGO), chemically converted graphene (CCG), *etc.*[94] Throughout the article, we will use the term graphene or HRG to refer to the product obtained from the reduction of GO or GRO whereas a distinction will be made with pristine graphene (defect free graphene) when necessary. Despite the significant structural differences between pristine graphene and HRG, the striking similarities between them, particularly in terms of their electrical, thermal and mechanical properties render the reduction process as one of the most important reactions of GO or GRO. Indeed, for large scale applications such as for the preparation of graphene based composite materials, the reduction of GRO by chemical and thermal methods is the most benign and desirable route to obtain graphene or HRG. Therefore, we focus in this review mainly on chemical and thermal methods (*top-down* approaches), which are more suitable for the reduction of GRO and the *in situ* preparation of highly reduced graphene oxide (HRG) based nanocomposites. The properties of HRG obtained *via top-down* methods by the reduction of GO strongly depend on reduction processes. Therefore, in order to customize the properties of devices and enhance the performance of materials made up of HRG, more efforts needs to be directed towards the development of reduction processes.

2.4.1 Chemical methods. Graphene oxide (GRO or single layers of graphite oxide) can be reduced chemically to graphene or HRG by applying a variety of reducing agents such as hydrazine monohydrate,[124] sodium borohydride,[125] hydrogen spillover[126] and various other chemicals.[127] Among all reductants hydrazine monohydrate is the most important and certainly the most common and widely used reductant due to its strong reactivity and stability in aqueous media. The reduction of graphene oxide *via* hydrazine restores the π-electron conjugation within the aromatic system of graphite resulting in an enhancement of electrical conductivity. Hitherto the highest conductivity of 99.6 S cm^{-1} combined with a C/O ratio of around 12.5 has been reported for HRG films solely obtained from hydrazine reduction, and an electronic conductivity of up to 300 S cm^{-1} was observed after replacing hydrazine with less toxic hydroiodic acid and acetic acid.[128,129] Although hydrazine effectively removes oxide functional groups, it also introduces heteroatom impurities such as nitrogen that remains covalently bound to the surface of graphene sheets in the form of amines, hydrazones or other similar functional groups.[125] Although it has been reported that high quality graphene can be obtained by reducing GO with H_2, the requirement of high temperature and inert conditions limits its applications.[119,130] Similarly, the long reaction time (several hours or even a few days) required for the reduction of GRO using chemical reductants such as hydrazine poses a hindrance for the wide scale applications of such methods.

Hence, several other reducing agents have been explored in the literature that may allow the reduction at low temperature and in less time, are more environmentally friendly and also produce homogeneous suspensions of graphene unlike hydrazine and other chemical reductants. For this purpose, Feng *et al.* demonstrated a less toxic method for the mass production of high quality HRG with low oxygen content.[131] A sodium–ammonia solution was used as a reducing agent (*cf.* Fig. 6),

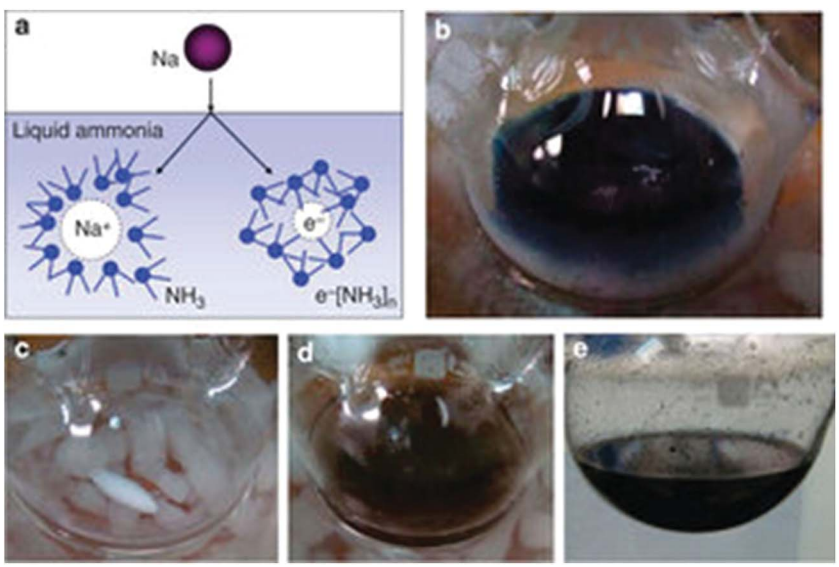

Fig. 6 Experimental procedures of the reduction of GO in the Na–NH_3 system. (a) The generation of solvated electrons by dissolution of sodium in liquid ammonia. (b) Several lumps of sodium metal were then dissolved in anhydrous liquid ammonia. The deep blue color is the color of the solvated electrons. (c) Liquid ammonia was kept in a dry ice-acetone bath. (d) GO powder was dispersed in liquid ammonia to show a brown color. (e) Black HRG solution was obtained after the reduction of GO with solvated electrons. Copyrights reserved to the Nature Publishing Group.[131]

where the solvated electrons facilitated the reduction of GRO and the restoration of the conjugated network of HRG with an oxygen content of 5.6 wt%. In the following paragraphs we only provide some of the most recent examples of such reductants, for more details about the structure, properties and reduction of GRO we refer the reader to recent reviews by Pei and Dreyer *et al.*[65,94,132,133]

Esfandiar *et al.* in their recent work have applied melatonin for the reduction of a GO suspension as a replacement for hydrazine. Melatonin is a biocompatible antioxidant that has led to results comparable with those for hydrazine under similar conditions. Furthermore, due to the π–π adsorption of MLT molecules on the reduced sheets, the MLT-reduced GRO suspension is more stable compared to a hydrazine-reduced suspension, where more aggregation is observed.[134] More recently, metal-mediated reduction of graphene oxide has been reported that is environmentally friendly and leads to faster reduction.[135] In a recent report Fan *et al.* described an efficient route for the synthesis of graphene *via* reduction of GRO with aluminum powder.[136] The reaction was carried out in acidic medium (HCl solution) and completed in a short time (~30 min). The resulting graphene sheets have a high bulk electrical conductivity of 2.1×10^3 S m^{-1} (*cf.* Fig. 7). Similarly, Mei and Ouyang replaced aluminum with Zn, to carry out reduction under mild acidic conditions under ultrasonication at room temperature.[137] The reaction is fast and completed within one minute, *i.e.* much less time than reported for the reduction of graphene oxide with iron[138] and aluminum powder.[136] The low reduction potential of Zn^{2+}/Zn and the ultrasonication facilitated fast and efficient reduction of GRO. In addition the HRG sheets obtained by this method show good electrical conductivity and thermal stability (*cf.* Fig. 7).

More recently, the trend of applying plant extracts as both reducing and stabilizing agents during the preparation of nanomaterials has attracted considerable attention in the scientific community.[139,140] The plant extracts (PE) are relatively easy to handle, readily available, low cost, and have been greatly exploited due to their biocompatibility in the field of nanotechnology. Although a number of different metallic nanoparticles have been synthesized successfully using plant extracts as bioreductants,[141,142] their reducing abilities have only recently been tested for the reduction of GO. Khan *et al.* demonstrated an efficient route for the synthesis of highly reduced graphene oxide *via* green reduction of GRO using *Pulicaria glutinosa* (*P. glutinosa*) plant extract (PE). The phytomolecules present in the *P. glutinosa* PE were not only responsible for the reduction of GRO but also functionalize the surface of HRG nanosheets to stabilize them in various solvents, thereby limiting the use of any other external and harmful chemical reductants and surfactants (*cf.* Fig. 8).[143] Similarly, Li *et al.* described a method that employs gallic acid, which acted both as a reductant and stabilizer for the reduction of GRO.[144]

Apart from this, a new trend of microbial reduction of GRO has been reported in several studies.[145,146] In one such example, Kuila *et al.* used carrot root as a biocatalyst and reducing agent. Here the endophytic microorganisms present in the carrot root reduce the exfoliated GO to HRG at room temperature.[147] In another example, Wang *et al.* demonstrated the reduction of graphene oxide mediated by microbial respiration of *Shewanella* cells in a normal aerobic setup under ambient conditions.[148]

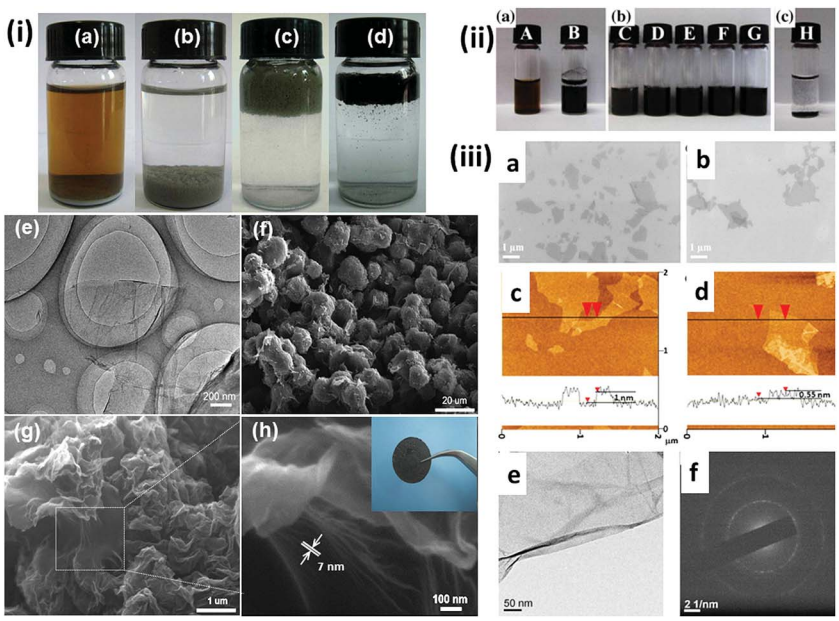

Fig. 7 Metal assisted reduction of GO. (i-a–d) Digital photographs of the reduction process. (i-e) TEM image of GO (i-f) SEM images of GO/aluminum particles (i-g and h) SEM images of HRG. Copyright reserved to the Elsevier Ltd.[136] (ii-a) Photographs of a GO solution (A) before and (B) after the reduction with Zn powder. (ii-b) Photographs of Zn/HRG dispersed in various solutions. (ii-c) Photographs of hydrazine reduced HRG dispersed in water. (iii-a) SEM image of GO. (iii-b) SEM images of Zn/HRG. (iii-c) AFM image of GO. (iii-d) AFM image of Zn/HRG. (iii-e) TEM image of a free standing Zn/HRG sheet suspended on a lacey carbon TEM grid. (iii-f) Selected area electron diffraction (SEAD) pattern of the Zn/HRG sheet in iii-e. Figures (ii) and (iii) Copyrights reserved to the Elsevier Ltd.[137]

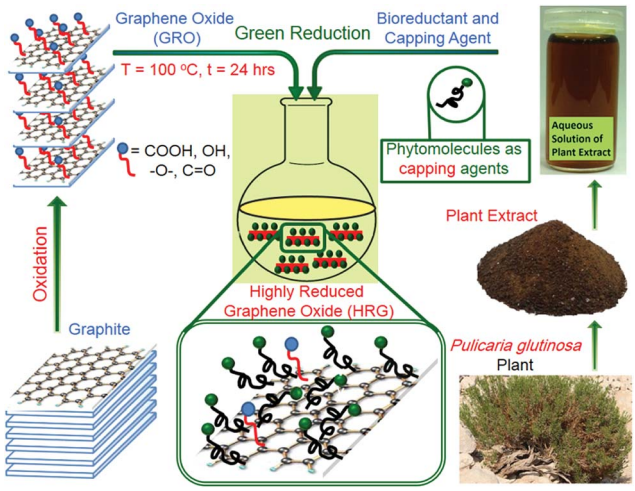

Fig. 8 Green reduction of graphene oxide (GRO) using an aqueous extract of the *Pulicaria glutinosa* plant. Copyrights reserved to the Royal Society of Chemistry.[143]

Shewanella, a *metal-reducing* bacterium, is known to transfer metabolically generated electrons from the interior part of the cell to external electron acceptors such as solid metal oxides. For the reduction of graphene oxide, extracellular electron transfer is mediated by both self-secreted electrons and outer membrane c-type cytochromes (Mtr/Ornc). It has also been reported that the microbially reduced HRG exhibits excellent electrochemical properties that are comparable to those prepared by chemical methods.

2.4.2 Thermal methods. HRG can be prepared by thermal exfoliation and reduction of GO by rapid heating (>200 °C min^{-1}) of dry GO under inert gas and high temperature (1050 °C).[149] The rapid heating led to the decomposition of oxygen containing functional groups attached on the carbon plane of GO, releasing gaseous CO and CO_2 gas. The released gas gradually evolves into the space between graphene oxide sheets and creates a local pressure between stacked layers, which ultimately leads to the exfoliation of GO. Such thermal treatment not only exfoliates but also reduces the GO to graphene simultaneously by eliminating oxygen containing functional groups also referred to as TRG (thermally reduced graphene), thus making it an attractive strategy to produce a bulk quantity of graphene.[150]

However, the release of gases (CO and CO_2) during the thermal exfoliation process causes significant structural damage to the platelets. The decomposition of oxygen containing groups also removes carbon atoms from the basal plane, thereby fragmenting the graphene sheets (TRG).[106] About ~30% of the mass of GO is lost during the exfoliation process due to the decomposition of oxygen containing groups and evaporation of water. Therefore, these methods only produce small sized and wrinkled graphene sheets with severe topological defects and etch holes throughout the plane of TRG sheets.[151] These defects significantly decrease the ballistic transport path length and also introduce several scattering sites in TRG sheets which have adverse effects on their electronic properties. Such high temperature processing is unlikely to be compatible with fabrication techniques used for most electronic applications but is useful for producing a bulk quantity of HRG sheets required for the synthesis of graphene based composites.[94,133]

Thermal treatment at such a high temperature with a fast heating rate involves huge energy consumption and difficulties in operation. Thus significant efforts have been invested to develop methods for thermal exfoliation of GO at reduced temperatures.[152] Recently, few-layered graphene sheets by thermally exfoliating GO under high vacuum at a significantly low temperature of 200 °C were prepared, which is far below the proposed critical exfoliation temperature of 550 °C.[149] However, the surface area of the TRG sheets produced by this method is much lower (368 m^2 g^{-1}) than that of conventional thermally exfoliated graphene (around 600–900 m^2 g^{-1}).[153] In a similar approach Zhang *et al.* prepared HRG sheets with an average thickness of 0.9 nm and a high specific surface area of 758 m^2 g^{-1} under vacuum at lower temperature (135 °C). The surface area obtained is comparable to that of conventional graphene (700 m^2 g^{-1}) generated at 1050 °C at atmospheric pressure. Here GO was thermally exfoliated and reduced *in situ* to few layered graphene sheets.[154] Furthermore, a high yield, hydrazine-free method has been reported that produces single-layer high quality HRG sheets at considerably *lower* temperature and at *atmospheric* pressure. The reduction of GO by this method was carried out in deionized water at pH ≈3 at 95 °C. It has been speculated that the oxygen reduction and simultaneous transformation of carbon sp^3 into sp^2 bonds by this method resulted from the *dehydration* of HRG in DI water.[155]

However, in certain cases the special atmosphere (*i.e.*, ultra-high vacuum and/or rapid heating) greatly hinders the preparation of graphene-based composite materials that necessarily require an oxidizing atmosphere; thus the need to thermally reduce GO under *mild* conditions is ever-increasing.[156] Recently, Wang *et al.* have demonstrated a facile and efficient method for the scalable synthesis of high quality TRG sheets by thermal reduction of GO in *air*. The reduction was carried out at 300 °C in 5 min. The low temperature facilitated the preparation of a vanadium pentoxide/graphene composite wherein the oxidizing atmosphere played a critical role.[157] Although thermal reduction methods are highly effective, more work needs to be done to further lower the annealing temperatures of GO, in order to achieve high quality large scale synthesis of HRG. In essence, high annealing temperatures not only require a higher energy consumption, but also need critical treatment conditions, which call for sophisticated and expensive instruments. Additionally, the preparation of HRG films on organic substrates which are required for certain electronic devices is also difficult using thermal reduction methods at high annealing temperatures.

2.4.3 Microwave assisted reduction methods. Although the reduction of GO by high temperature annealing is highly efficient and widely applied, it poses some obvious drawbacks.[133] Thermal annealing is usually carried out by thermal irradiation; however some unconventional heating resources have been examined for thermal reduction, such as microwave irradiation (MWI).[158,159] In this process, microwave energy is transformed into heat through a microwave absorbent. Other conventional heating methods lead to heating of the reaction mixture

uniformly and rapidly. In addition, due to the different dielectric constants of reactants and solvent, selective dielectric heating can also be carried out using MWI. Such a kind of heating provides a significant enhancement in the transfer of energy directly to the reactants, which causes an instantaneous increase of the internal temperature.

Recently, MWI has demonstrated excellent ability to produce graphene from GO. The interaction of microwaves with GO and graphene is not fully understood. Hu *et al.* reported that for carbon based materials the microwave absorption capacity is highly dependent on their chemical composition and structure.[160] During their study, by varying the oxygen content in GO and/or graphene based materials, the microwave absorption capacity of GO decreased remarkably with increase of oxygen content due to the decrease of sp^2 domains. Therefore, pristine graphene is an excellent microwave absorbent compared to GO, which has a relatively poor microwave absorption capacity. The non-oxidized graphitic regions act as "impurities" and absorbents to initiate microwave-induced reduction. Moreover, it has been speculated that the reduction process of GO can be greatly enhanced by addition of small amounts of pristine graphene. MWI has been used to prepare exfoliated graphite (EG) from a wide range of graphite intercalation compounds (GICs).[161] EG has also been prepared by MWI quickly (4 min); the mixture of natural graphite with nitric acid and potassium permanganate was directly heated in a microwave oven.[162] The preparation of reduced graphene oxide has also been reported by simultaneous exfoliation and reduction of GO under dry conditions (without using any chemicals or solvents) by rapid MWI in ~1 min.[163]

2.4.4 Hydrothermal and solvothermal methods. Hydrothermal processing is another powerful and emerging chemical reduction method for the *green* synthesis of graphene and its composites.[133] This single-pot process produces highly crystalline homogeneous nanostructures without the need for post-synthetic annealing or calcination.[164] Hydrothermal reduction of GO is carried out in a closed system in the presence of water or solvent (solvothermal processing) at a temperature close to or above its boiling point to generate high pressure.[165] Supercritical (SC) water can also act as a reducing agent, thereby providing an environmentally friendly alternative to hazardous chemical reductants. For instance, during the reduction of GO *via* a "water-only" route by hydrothermal treatment of a GO solution, the SC water not only partly removed the oxygen containing functional groups, but also restored the aromatic structure.[166] During this process, water acts as a source of H^+ ions for the protonation of hydroxyl groups. This leads to a dehydration of HRG, thereby facilitating the reduction process. Moreover, the true pH may be different in such reduction processes. The nominal pH of the solution plays a critical role, *i.e.*, a basic solution (pH = 11) yields a stable HRG solution while the HRG sheets aggregate in an acidic solution (pH = 3).

Deoxygenation of GO has been studied by solvothermal reduction.[167] In a procedure described by Wang *et al.* the reduction of GO was carried out in *N*,*N*-dimethylformamide (DMF) at 180 °C using hydrazine monohydrate as a reductant.[165] HRG sheets were dispersed in DMF, and the C/O ratio of the HRG sheets reached 14.3 (which is much higher than that obtained by hydrazine reduction at normal pressure). However, the resulting HRG sheets exhibited poor conductivity due to the nitrogen-doping caused by the hydrazine reductant. In another study, Dubin *et al.* considered the solvothermal reduction using *N*-methyl-2-pyrrolidinone (NMP) as a solvent.[168] Here the reduction was *not* performed in a sealed container, and the reaction temperature was below (200 °C) the boiling point of NMP (202 °C at 1 atm). It has been proposed that the oxygen-scavenging properties of NMP at elevated temperature and the moderate thermal annealing facilitated the reduction of GO. Although a homogeneous dispersion of HRG sheets could be obtained solvothermally in DMF, graphene sheets usually suffer from limited dispersibility and irreversible agglomeration due to increased hydrophobicity and π–π stacking during such a process. To avoid the aggregation of graphene sheets, covalent or non-covalent modifications of HRG sheets must be introduced. This introduces extra stabilizers into the reducing system that may hinder the necessary functionalization of HRG and its further applications. In this regard, Zhou *et al.* have demonstrated a simple surfactant-free approach to prepare a homogeneous dispersion of HRG sheets in DMF by solvothermal reduction of GO.[169] The high temperature and the autogenous high pressure promote the reduction of GO, wherein DMF acts as a weak reducing agent and stabilizer which keeps the dispersion homogeneous and stable. The resulting HRG sheets could be re-dispersed in solvents such as *N*-methylpyrrolidone, *N*,*N*-dimethylacetamide and acetonitrile.

2.5 Chemical and thermal reduction mechanisms

To make progress in optimization and design of reduction processes that meet the increasing demand for *tailored* graphene-based composite materials, GO needs to be well characterized and the mechanism of its thermal deoxygenation to be well understood.[170] Insight into how the oxygen containing functional groups of graphene oxide evolve during the thermal reduction is particularly important.[171] Several studies have been conducted to this end. For instance, an X-ray diffraction and a Fourier transform infrared spectroscopy (FTIR) study of the thermal stability of GO during heat treatment under an argon atmosphere could identify the removal of water, hydroxyl, epoxide and carboxyl groups.[172] It has also been suggested that the interlayer distance between the GO adjacent layers decreases gradually with annealing time. In a theoretical study Gao *et al.* have identified three possible mechanisms for the elimination of epoxide groups of GO with hydrazine.[173] This detailed theoretical study also provided an elucidation for reduction of GO, and also suggested details of the product structures and of the ways to optimize the reaction conditions.

Ganguly *et al.* proposed a mechanism for the thermal decomposition of GO using a combination of high-resolution temperature-dependent *in situ* spectroscopies (X-ray photoemission and X-ray absorption).[174] They suggested that the edge plane carboxyl groups are highly unstable, whereas carbonyl groups (C=O) are more difficult to remove. However, the formation of phenol groups was facilitated through the reaction of basal plane epoxide groups with adjacent hydroxyl groups at

moderate temperature (~400 °C). The phenol groups are predominant over carbonyl groups (C=O) and survive even at temperatures as high as 1000 °C (*cf.* Fig. 9). Moreover, they observed for the first time a drastic increase in the density of states (DOS) near the Fermi level at 600 °C suggesting a progressive restoration of the aromatic structure in TRG. In another report, Acik and co-workers described a systematic study of the chemical and thermal reduction mechanism and characterized the structural composition of GO.[175] They performed *in situ* transmission IR measurements of GO films upon thermal annealing at 60 to 850 °C *in vacuo* (10^{-3} to 10^{-4} Torr) to study the complex mechanism of oxygen removal in reduced GO. Apart from a detailed illustration of interactions between randomly arranged oxygen species, they have suggested that thermal annealing fosters the formation of free radicals containing oxygen in the presence of trapped water in GO, which further attach carboxyls, hydroxyls and carbonyls, preferentially at the edges rather than on basal plane defects.

Liao *et al.* demonstrated that the reduction and transformation of C–C bonds from sp^3 to sp^2 in GO are mainly facilitated by dehydration.[155] In an acidic environment the neighboring hydroxyl groups and hydrogen atoms attached to carbon atoms are eliminated as water. This results in the formation of HRG sheets with sp^2 bonded carbon atoms. The reduction of epoxy groups is a two-step process: in the first step, the transformation of two neighboring epoxy (–O–) to hydroxyl groups occurs *via* hydration in an acidic environment followed by a dehydration step, where water and HRG sheets are formed. They further explained that for the reduction of GO in water a low pH environment and moderately high temperatures are needed. The reduction is initiated by protonation while the reaction kinetics is governed by temperature. Notably, OH^- anions can act as a catalyst when reduction is carried out in a basic environment.[176] In both cases, the extent of oxygen reduction is dependent on the number of hydrogen atoms bonded to carbon atoms carrying hydroxyl groups.

2.6 Synthesis of HRG/nanoparticle nanocomposites

The binding or loading of metal and metal oxide NPs on graphene for the preparation of graphene-based *nanocomposites* is generally realized in two different ways (*cf.* Fig. 10): *post immobilization* (*ex situ* hybridization) or *in situ* binding (*in situ* crystallization). *Post immobilization* involves mixing of separate solutions of graphene nanosheets and pre-synthesized NPs. Before mixing, the NPs *and/or* graphene sheets are surface functionalized to enhance the processability of the resulting products. The conjugated graphene sheets can readily be functionalized by non-covalent π–π stacking or *covalent* C–C coupling reactions. The functionalization of graphene *and/or* NPs significantly enhances their solubility and hence broadens the opportunities for the preparation of graphene-based composites. However, *post immobilization* may suffer from low density and non-uniform coverage of nanostructures by graphene sheets. In this review the *in situ* methods for the preparation of metal and metal oxide decorated graphene-based *nanocomposites* will be discussed in some detail. In the following paragraphs we describe the most recent methods for the synthesis of graphene-based metal and metal oxide nanocomposites by *in situ* methods, *i.e.* by the simultaneous reduction of graphite oxide (GO) or graphene oxide (GRO) and the respective metal salts. Readers interested in details of the *post immobilization* methods (*e.g.* materials used for the functionalization and the preparation of functionalized graphene based metal nanocomposites) can consult excellent reviews by Yang or Shi and co-workers.[177–181]

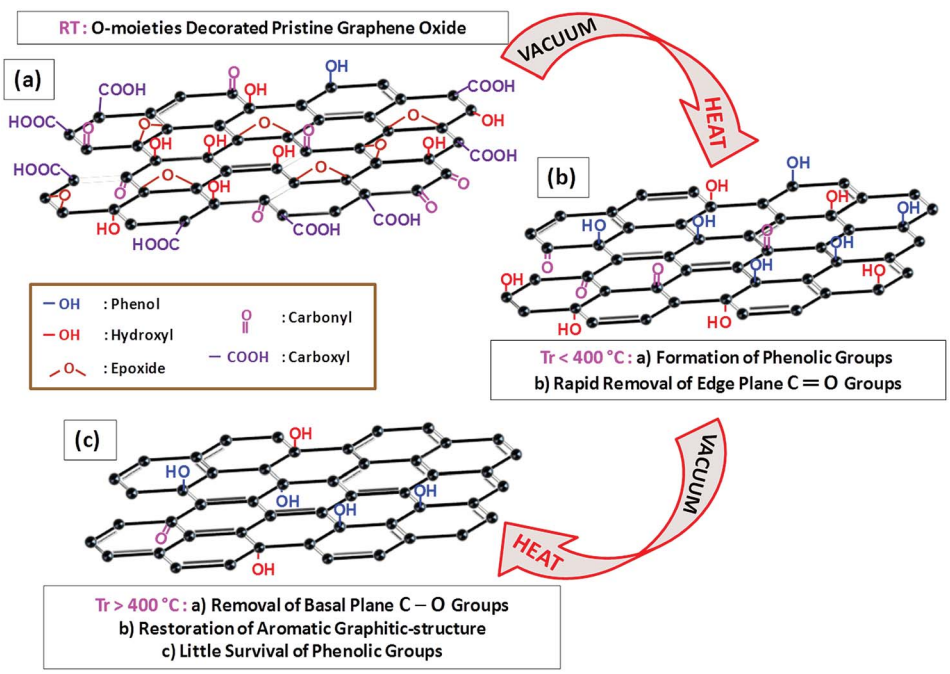

Fig. 9 Schematic representation of GO reduction mechanisms. Copyright reserved to the American Chemical Society.[174]

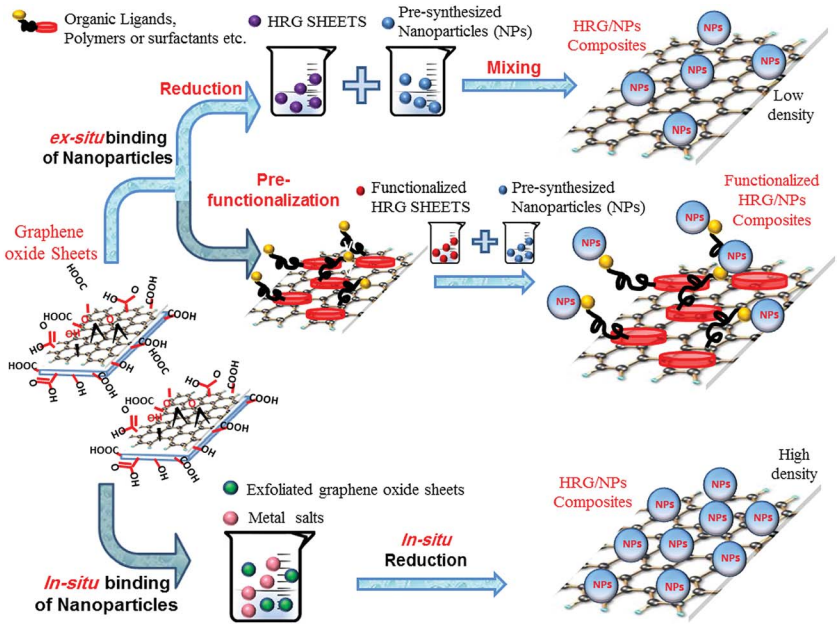

Fig. 10 Schematic illustration of the binding mechanisms of nanoparticles (NPs) onto HRG sheets. The NPs can be loaded onto HRG sheets in two different ways by *in situ* or *ex situ* binding. A high density of NPs can be achieved *via in situ* binding. Both HRG sheets and NPs can be functionalized either *via* non-covalent π–π stacking or *covalent* C–C coupling reactions.

Methods for the preparation of graphene based metal and metal oxide nanocomposites by *in situ* chemical reduction of metal precursors such as $HAuCl_4$, $AgNO_3$, K_2PtCl_4, and H_2PdCl_6 with reductants like hydrazine hydrate, amines, and $NaBH_4$ are more common and widely applied.[182] For instance, HRG/Au nanocomposites were prepared by reduction of $HAuCl_4$ with $NaBH_4$ [183] and graphene-based bimetallic HRG/Pt/Pd nanocomposites were synthesized by *in situ* reduction of H_2PdCl_4 and K_2PtCl_4 with HCOOH and ascorbic acid.[184] In another example, Ji *et al.*, in their recent work, have described a facile method for the preparation of HRG/Co nanocomposites and also demonstrated their magnetic properties.[185] Cobalt (Co) NPs with a size of *ca.* 3 nm were densely and homogeneously deposited onto graphene sheets by *in situ* hydrazine hydrate reduction in ethylene glycol. Nanocomposites of HRG/Ag were synthesized by a green, cost-effective single-pot method, where the *in situ* reduction of $AgNO_3$ and GO was carried out in aqueous solution using tannic acid (water-soluble polyphenol) as a reducing agent.[186] The resulting material exhibited excellent SERS (Surface Enhance Raman Scattering) activity as a SERS substrate, and notable catalytic performance for the reduction of H_2O_2.

Apart from metallic and bimetallic NPs, the composites of metal oxides with graphene have been synthesized by *in situ* chemical reduction.[187,188] Kim *et al.* prepared HRG/Co_3O_4 nanocomposites as anode materials, by the reduction of GO and cobalt acetate ($(C_2H_3O_2)_2Co\cdot 4H_2O$) in deionized water (DI) with NH_4OH and hydrazine as reductants.[189] The homogeneous HRG dispersion provides nucleation sites for Co_3O_4 NPs, resulting in a uniform growth of small (~5 nm) Co_3O_4 NPs on the conductive surface of HRG sheets. In addition, the HRG layers act as a mechanical buffer that accommodates a large volume change of Co_3O_4 NPs and inhibits their isolation. Similarly, HRG/SnO_2 and ternary HRG/SnO_2–Au nanocomposites were prepared by *in situ* chemical reduction, and they could find applications as anode materials in lithium-ion batteries as well.[190] HRG/SnO_2/Au hybrid materials were prepared from an aqueous dispersion of GO and $SnCl_2$. The key step of the synthesis is that $SnCl_2$ acts as a source of tin and as a reducing agent for both GO and $HAuCl_4$ in a sonication-assisted process, which also has the potential for preparing other multicomponent nanocomposites starting from different metal salts.

Apart from this, MWI is also widely applied for the synthesis of graphene-based nanocomposites.[191,192] Particularly, the preparation of HRG/metal nanoparticle (NP) composites by simultaneous (*in situ*) reduction of various metal salts and GO is highly effective. Hassan *et al.* demonstrated that HRG/NP composites can be obtained by a scalable microwave-assisted chemical reduction.[193] This method allows a rapid chemical reduction of GO with a variety of reducing agents in aqueous and organic media; the simultaneous reduction of GO and metal salts leads to the formation of metallic and bimetallic NPs supported on graphene sheets. HRG/NP composites of Cu, Pd, Au, and Ag have been prepared by *in situ* reduction of GO and appropriate metal salts ($HAuCl_4$, Pd nitrate) with reducing agents like hydrazine hydrate, ammonium hydroxide, or ethylenediamine by MWI. Such *in situ* reductions have produced homogeneous dispersions of NPs on HRG sheets due to the specific interaction between the NPs and graphene sheets, different from the aggregates of the NPs with poor dispersion on HRG sheets obtained by physical mixing.

Additionally, *in situ* MWI has been used to prepare HRG/metal oxide and metal sulfide nanocomposites such as HRG/MnO_2, HRG/ZnO and HRG/ZnS.[194] In the latter case, the reaction was carried out in aqueous medium assisted by MWI. The HRG sheets act not only as a precursor of graphene but also as a

template for the growth of ZnS nanospheres.[160] Recently, MWI combined with an ionic liquid (IL) assisted dispersion of NPs on HRG sheets, *e.g.* in the synthesis of HRG/PdPt NPs composites, has been reported.[195] MWI has attracted attention due to its ease of processing and scalable production. Moreover, due to the rapid and uniform heating, MWI prevents the aggregation of graphene layers. A major drawback is the difficulty in controlling the size, uniformity and surface distribution of NPs on HRG surfaces.

Hydrothermal and solvothermal reduction processes have been applied for the synthesis of graphene-based metal and metal oxide nanocomposites.[196–198] Previously, HRG/TiO_2 nanocomposites were prepared in an ethanol–water mixture under hydrothermal conditions. In a recent report Shen *et al.* used glucose as an eco-friendly reductant.[199] It has been speculated that under hydrothermal conditions the reducing ability of glucose may be enhanced as it was found to yield highly reduced suspensions of graphene (HRG) in a way comparable to those obtained with hydrazine. The reduction process was accompanied by the formation of HRG/TiO_2 nanocomposites, where the photocatalytic ability of TiO_2 was enhanced by the interaction between HRG and TiO_2. The preparation of magnetic HRG/Fe_3O_4 nanocomposites by an *in situ* hydrothermal reduction was reported.[209] Li *et al.* prepared nanocomposites by simultaneous formation of Fe_3O_4 NPs and reduction of GO in ethylene glycol.[200] Ferric acetylacetonate ($Fe(acac)_3$) was used as a precursor for the preparation of Fe_3O_4 nanoparticles, which were uniformly assembled in a 3D pattern on HRG sheets while their loading could be controlled by altering the Fe^{3+} starting concentration. In order to have better control over the morphology of NPs on the surface of HRG sheets during the reduction process, ionic liquids (ILs) were applied that are commonly used as solvents, reactants, and templates for the synthesis of inorganic nanomaterials with novel morphologies and improved properties.[201] In their recent work Shen *et al.* described a one-pot hydrothermal method to prepare HRG/TiO_2 nanocomposites using GO, tetrabutyl titanate and [BMIM][PF_6] ionic liquid as starting materials.[201] Here, GO was reduced *in situ* with ascorbic acid in the presence of 1-butyl-3-methylimidazolium hexafluorophosphate ([BMIM][PF_6]) under pressure. The hydrothermal conditions not only favored the reduction of GO but also facilitated the generation of TiO_2 NPs in the presence of ILs.

From the results discussed above, it becomes clear that graphene and graphene-based materials can be prepared on a large scale with very satisfactory structure and properties by top-down methods. There are several advantages of these methods. Inexpensive graphite is used as a raw material for the production of graphene like materials (HRG) in high yield, which makes them very cost effective. Graphene or HRG obtained from these methods is highly processable, and can be used for the production of macroscopic structures and devices on a large scale by simple and cheap solution processes. Therefore, these approaches have gained significant attention in the scientific community, and extensive research is still going on in this field. Still, several challenges and questions remain to be answered. It is a challenge to completely remove the functional groups from the surface of HRG, and the restoration of the defects formed during the oxidation process is very difficult. Apart from this, it is difficult to keep the long-range conjugated structure of HRG intact, which is needed to enhance the electrical conductivity. Although the functional groups are relatively easy to remove by reduction, it is a challenge to restore the defects.

Extensive research is required to prepare HRG on an industrial scale, which is similar or close to the structure of single layer graphene obtained by the Scotch tape method. A two-step strategy for the reduction of GO proved to be efficient compared to single-step processes. A combination of chemical reactions and thermal annealing was used here for the effective deoxygenation of GO: the chemical reactions maintained the structure of the carbon plane, while thermal annealing facilitated the desorption of functional groups.[202] In order to fully exploit these methods for the large scale synthesis of HRG, a mechanistic understanding of the reduction is needed. So far, much research has been performed using computer simulations at the molecular level. Experimental research is required to fully understand the mechanism of GO reduction. Additionally, most of the defects in HRG are formed during the oxidation process; therefore, controlling the oxidation of graphite is also a key step in obtaining non-defective HRG.

3 Properties and applications

In the last few decades, huge efforts have been made to synthesize composites of graphene with *inorganic* NPs, mostly based on transition metal and metal oxide NPs.[31,32] A lack of knowledge in graphene chemistry prevented a significant advancement of this field for a long time. However, the advent of methods for the preparation of stable and homogeneous dispersions of graphene on a large scale has changed the scenario. In particular, tremendous interest has been generated in making graphene-based nanocomposites and exploring them for different applications.[203] The majority of graphene-based nanocomposites are comprised of only two components, but multicomponent composites have been prepared for special applications as well.[32] Although a variety of second components have been involved, the architectures of graphene based composites can be classified into three types:[31] (i) composites, graphene sheets form a continuous phase and act as a substrate for supporting a second component, which adheres to graphene sheets. (ii) These second components are typically an inorganic nanoparticle (*e.g.* metals, metal oxide, or and CNTs); occasionally polymeric nanostructures have been applied.[29,204] (iii) Graphene sheets act as nano-fillers, incorporated into the continuous matrix of the second component.[205] In type II composites, both HRG sheets and the second component act as continuous phases. An example could be graphene-based composite films fabricated *via* layer-by-layer self-assembly of individual components.[206,207]

The following sections are organized in such a way that the most common applications of graphene/metallic NP based nanocomposites, such as energy storage, sensing, catalysis, are discussed. For each individual application the discussion, which is focused mostly on type I composites, follows the sequence from group 4 to group 12 of the periodic table (*cf.* Table 1).

Table 1 Typical synthetic method and the type of precursor used for the preparation of graphene supported nanocomposites based on metal and metal oxide NPs belonging to group 4 to 12 of the periodic table, and their related applications

Materials	Synthetic routes	Precursors	Applications	References
TiO_2/HRG	*In situ preparation*: hydrothermal synthesis	GO–NH_4TiF_6	Photocatalytic activity	437
	Ex situ preparation: hydrothermal synthesis	GO–$TiCl_4$	Photocatalytic activity	599
	In situ preparation: thermal hydrolysis	GO–titania peroxo complex (ethyl glycol)	Photocatalytic activity	600
	In situ preparation: sol–gel method	GO–tetra butyl titanate (sodium borohydrate)	Photocatalytic activity	601
	In situ preparation: sonochemical synthesis	GO–$TiCl_4$	Photocatalytic activity	602
	In situ preparation: solvothermal synthesis		Photocatalytic activity	603
	In situ preparation: microwave-assisted synthesis	GO–tetra butyl titanate	Photocatalytic activity	604
	In situ preparation: hydrothermal synthesis	GO–titanium isopropoxide (hydrazine hydrate)	Electrochemical sensor and biosensor	379
	Self-assembly method (template free)	GO–$TiSO_4$	Lithium ion batteries and photocatalytic activity	220
	In- situ preparation: hydrothermal synthesis		Lithium ion batteries and photocatalytic activity	605
	In situ preparation: hydrothermal synthesis (ionic liquid-assisted)	GO–tetrabutyl titanate [BMIM] [PF_6] (ascorbic acid)		606
ZrO_2/HRG	*Ex situ*: electrochemical deposition	GO–$ZrOCl_2$ (sodium borohydrate)	Electrochemical sensing	477
	In situ preparation: hydrothermal synthesis	GO–$ZrO(NO_3)_2 \cdot 3H_2O$	Supercapacitors	315
V_2O_5/HRG	*In situ preparation*: hydrothermal synthesis	GO–V_2O_5	Cathode material in LIBs	225
	Ex situ mixing: electrochemical synthesis	GO–$V_2O_5 \cdot nH_2O$ (H_2O_2)	Cathode material in LIBs	227
	In situ preparation: thermal synthesis	GO–$(NH_4)_2V_6O_{16}$	Cathode material in LIBs	157
	In situ preparation: solvothermal synthesis	GO–vanadium oxy triisopropoxide	Supercapacitors	316
Nb_2O_5/HRG			Photocatalytic activity	444
$InNbO_4$/HRG	*Ex situ mixing*: hydrothermal synthesis	GO–$In(NO)_3 \cdot 5H_2O$–$NbCl_5$	Photocatalytic activity	446
$Sr_2Ta_2O_{7-x}N_x$/HRG	*Ex situ mixing*: photo-induced synthesis	GO–$Sr_2Ta_2O_7$ (sodium borohydride)	Photocatalytic hydrogen production	447
Ta/HRG/MgO	*Ex situ deposition:* electrochemical deposition		Biosensor	607
MoO_3/HRG	*In situ preparation*: hydrothermal synthesis	GO–$Na_2MoO_4 \cdot 2H_2O$		228
WO_3/HRG	*In situ preparation*: photo-irradiation (UV-assisted)	GO–$SrWO_4$	Gas sensing	483
	In situ preparation: hydrothermal synthesis		Photochemical conversion	608
MnO_2/HRG	*In situ preparation*: microwave irradiation	GO–KmNO4	Supercapacitors	321
	In situ deposition: electrodeposition	GO–$Mn(CH_3COO)_2$	Supercapacitors	322
	Ex situ mixing: thermal synthesis	GO–K_xMnO_2	Supercapacitors	609
	Ex situ deposition: electrostatic co-precipitation method	GO–$Mn(NO_3)_2$ (hydrazine hydrate)	Supercapacitors	610
MnO_2/HRG/CNT	*Ex situ deposition*: electrodeposition	GO–$Mn(NO_3)_2$–SWCNT	Supercapacitors	611
MnO_2/HRG	*Ex situ deposition*: ultrafiltration method	GO–$KMNO_4$	Anode material in LIBs	238
	In situ preparation: redox-like method	GO–$KMNO_4$	Water purification	543
Mn_3O_4/HRG	*Ex situ mixing*: thermal synthesis	GO–MnO_2 organosol	Supercapacitors	242
	In situ preparation: hydrothermal synthesis	GO–$MnAc_2 \cdot 4H_2O$	Supercapacitors	327
	In situ preparation: solvothermal synthesis	GO–$MnAc_2 \cdot 4H_2O$	Supercapacitors	612
	In situ preparation: hydrothermal synthesis	GO–$Mn(CH_3COO)_2$	Anode material in LIBs	613
	In situ preparation: solvothermal synthesis	$Mn(COOH)_2 \cdot 4H_2O$	Catalyst	544
Fe/HRG	*In situ preparation*: thermal synthesis	GO–$FeCl_3 \cdot 6H_2O$	Anode material in LIBs	246
Fe_3O_4/HRG	*In situ preparation*: hydrothermal synthesis	GO–$FeCl_3 \cdot 6H_2O$ (hydrazine hydrate)	Anode material in LIBs	252
	In situ preparation: hydrothermal synthesis	GO–Fe powder	Anode material in LIBs	614
	In situ preparation: sol–gel synthesis (microwave-assisted)	GO–$Fe(acac)_3$(benzyl alcohol)	Anode material in LIBs	615
	In situ preparation: chemical synthesis	GO–ferric citrate	Anode material in LIBs	616
	In situ preparation: hydrothermal synthesis	GO–$FeCl_3 \cdot 6H_2O$, $FeCl_2 \cdot 4H_2O$	Supercapacitors	329
	In situ preparation: chemical synthesis	GO–Cu catalyzed	Adsorber material	546
	In situ preparation: chemical synthesis	GO–$FeCl_3$, $FeCl_2$	Adsorber material	548
	In situ preparation: hydrothermal synthesis	GO–$FeCl_3$	Cellular magnetic resonance imaging	585
	In situ preparation: chemical precipitation	GO–$FeCl_3 \cdot 6H_2O$, $FeCl_2 \cdot 4H_2O$	Targeted drug delivery	617
	In situ preparation: chemical precipitation	GO–$FeCl_3 \cdot 6H_2O$, $FeCl_2 \cdot 4H_2O$	Sensors	590
Fe_3O_4/HRG/CNT	*In situ preparation*		Targeted drug delivery	618

Table 1 (*Contd.*)

Materials	Synthetic routes	Precursors	Applications	References
Fe_2O_3/HRG	*In situ preparation*: hydrothermal synthesis	GO–$FeCl_3 \cdot 6H_2O$	Anode material in LIBs	619
	In situ preparation: hydrothermal synthesis (microwave-assisted)	GO–$FeCl_3$ and $NH_4H_2PO_4$	Anode material in LIBs	259
	In situ preparation: microwave-assisted synthesis	GO–$FeCl_3$ (hydrazine hydrate)	Anode material in LIBs	260
	In situ preparation: hydrothermal synthesis	GO–$Fe(NO_3)_3$	Supercapacitors	620
	In situ preparation: thermal synthesis	GO–$Fe(CO)_5$	Adsorber material	550
	In situ preparation: chemical hydrolysis	GO–$FeCl_3 \cdot 6H_2O$	Tribological activities	591
$LiFePO_4$/HRG	*Ex situ mixing*: thermal synthesis (spray-drying and annealing)	GO–H_3PO_4 and LiOH (H_2O_2)	Cathode material in LIBs	263
RuO_2/HRG	*In situ preparation*: sol–gel method (annealing assisted)	GO–$RuCl_3$	Supercapacitors	337
	In situ preparation: hydrothermal synthesis	GO–$RuCl_3$	Supercapacitors	338
Co_3O_4/HRG	*In situ preparation*: chemical synthesis		ORR Catalysts in lithium–air batteries	267
	In situ preparation: thermal synthesis	GO–$CoCl_2 \cdot 6H_2O$ ($NaBH_4$)	Anode material in LIBs	266
	In situ preparation: solvothermal synthesis	GO–$CoSO_4 \cdot 7H_2O$	Anode material in LIBs	270
	In situ preparation: chemical synthesis	GO–$(C_2H_3O_2)_2Co \cdot 4H_2O$ (NH_2NH_2)	Anode material in LIBs	189
	In situ preparation: thermal synthesis	GO–CoC_2O_4	Supercapacitors	341
	In situ preparation: microwave-assisted synthesis	GO–$Co(NO_3)_2 \cdot 6H_2O$	Supercapacitors	340
	In situ preparation: hydrothermal synthesis	GO–$Co(C_2H_3O_2)_2$	Catalyst (ORR & OER)	393
CoO/HRG	*In situ preparation*: ultrasonic synthesis	GO–$Co_4(CO)_{12}$	Anode material in LIBs	276
	In situ preparation: thermal synthesis	GO–$Co(acac)_3$	Anode material in LIBs	275
Co@graphite/HRG	*In situ preparation*: chemical Vapor deposition	GO–$Co(NO_3)_2 \cdot 6H_2O$		621
Co/HRG	*In situ preparation*: thermal synthesis (pyrolysis)	GO–cobalt phthalocyanine (NH_2NH_2)	Anode material in LIBs	268
	In situ preparation: mechanical ball milling	GO-	Hydrogen storage	281
Co–Al LDH/HRG	*Ex situ mixing*: self-assembly	GO–$CoCl_2 \cdot 6H_2O$, $AlCl_3 \cdot 6H_2O$	Supercapacitor	344
	Ex situ mixing: layer-by-layer assembly	GO–$CoCl_2 \cdot 6H_2O$, $AlCl_3 \cdot 6H_2O$	Supercapacitor	345
$CoFe_2O_4$/HRG	*In situ preparation*: hydrothermal synthesis	GO–$Co(CH_3COO)_2 \cdot 4H_2O$, $FeCl_3 \cdot 6H_2O$	Adsorbent material	622
Rh/HRG	*In situ preparation*: sonochemical synthesis	GO–$RhCl_3 \cdot xH_2O$ ($NaBH_4$)	Catalytic activity	461
NiO/HRG	*In situ preparation*: thermal synthesis (multi-step process)	GO–$Ni(NO_3)_2$	Supercapacitor	352
	Ex situ deposition: electrochemical deposition	HRG–$Ni(OH)_2$	Supercapacitor	353
	In situ preparation: thermal synthesis (self-assembly)	GO–$Ni(NO_3)_2 \cdot 6H_2O$	Supercapacitor	354
	In situ preparation: thermal synthesis (liquid-phase deposition)	GO–$Ni(NO_3)_2 \cdot 6H_2O$	Anode material in LIBs	289
	In situ preparation: hydrothermal synthesis	GO–$Ni(NO_3)_2 \cdot 6H_2O$	Anode material in LIBs	287
	Ex situ mixing: thermal synthesis (Doctor blade method)	GO–$NiCl_2$	Solar cells	382
$Ni(OH)_2$/HRG	*In situ preparation*: solid-state synthesis (mechanically assisted)	GO–$Ni(C_2O_4) \cdot H_2O$	Supercapacitor	360
	In situ preparation: hydrothermal synthesis	GO–$Ni(NO_3)_2 \cdot 6H_2O$	Pseudocapacitor	356
	In situ preparation: hydrothermal synthesis	GO–Ni foam	Supercapacitor	623
	In situ preparation: chemical synthesis (deposition)	GO–$Ni(NO_3)_2$ ($NaBH_4$)	Anode material in LIBs	290
$Ni(OH)_2$/HRG	*Ex situ deposition: electrochemical deposition*	HRG–Ni_2SO_4	Sensors	624
Ni-AL LDH/HRG	*In situ preparation*: hydrothermal synthesis	GO–$Ni(NO_3)_2 \cdot 6H_2O$, $Al(NO_3)_2 \cdot 9H_2O$ (glucose)	Supercapacitor	363
$NiCo_2O_4$/HRG	*In situ preparation*: hydrothermal synthesis (microwave-assisted)	GO-	Sensing application	625
Pd/HRG	*In situ preparation: chemical synthesis*	GO–H_2PdCl_4	Electrocatalyst in DMFCs	397
	In situ preparation: chemical synthesis	GO–H_2PdCl_4	Electrocatalyst in DFAFCs	398
	In situ preparation: electrochemical synthesis	GO	Electrocatalyst in DEFCs	401
	In situ preparation: hydrothermal synthesis (microwave-assisted)	GO–$PdNO_3$ (hydrazine)	Catalytic activity for C–C coupling	468
	In situ preparation: electrochemical synthesis	GO–$Pd(CH_3COO)_2$ (hydrazine)	Biosensor	506
PdPt/HRG	*In situ preparation: chemical synthesis*	GO–Na_2PtCl_6 and Na_2PdCl_4 (ethylene glycol)	Electrocatalyst for ORR	626

Table 1 (*Contd.*)

Materials	Synthetic routes	Precursors	Applications	References
Pt/HRG	*In situ preparation*: electrochemical deposition	GO–H_2PtCl_6 + 10 mM KH_2PO_4	Electrocatalyst in DMFCs	411
	In situ preparation: chemical synthesis	GO–H_2PtCl_6 ($NaBH_4$)	Electrocatalyst in DMFCs	412
	In situ preparation: chemical synthesis	GO–$H_2PtCl_6 \cdot H_2O$ (hydrazine hydrate)	Electrocatalyst for ORR	425
	In situ preparation: layer-by-layer self-assembly	GO–H_2PtCl_6	Counter electrode in solar cells	384
	In situ preparation: microwave-assisted synthesis	GO–H_2PtCl_6 (ethylene glycol)	Biosensor for H_2O_2	508
	In situ preparation: chemical synthesis	GO–$H_2PtCl_6 \cdot 6H_2O$ ($NaBH_4$)	Biosensor for cholesterol	511
Pt–Ru/HRG	*In situ preparation*: hydrothermal synthesis	GO–$H_2PtCl_6 \cdot H_2O$ + $RuCl_3$	Electrocatalyst in DMFCs	415
Pt–Ru/HRG	*In situ preparation*: hydrothermal synthesis	GO–H_2PtCl_6 + $RuCl_3$	Electrocatalyst in DMFCs and DEFCs	416
	In situ preparation: chemical synthesis	GO–H_2PtCl_6 + $RuCl_3$	Electrocatalyst in DMFCs	414
Pt–Au/HRG	*Ex situ preparation*: electrodeposition	GO–$H_2PtCl_6 \cdot 6H_2O$ (hydrazine hydrate)	Electrocatalyst in DMFCs and ORR	418
	In situ preparation: chemical synthesis	GO–H_2PtCl_6 + $HAuCl_4$ ($NaBH_4$)	Electrocatalyst in DFAFCs	421
	In situ preparation: chemical synthesis	GO–H_2PtCl_6 + $HAuCl_4$ (ethylene glycol)	Electrocatalyst in DFAFCs	422
Pt–Pd/HRG	*In situ preparation*: electrochemical deposition	GO–$PdCl_2$ + H_2PtCl_6 (hydrazine hydrate)	Electrocatalyst in DEFCs	417
Pt–Ni/HRG	*In situ preparation*: electrochemical deposition	GO–$NiSO_4 \cdot 6H_2O$ + $H_2PtCl_6 \cdot 6H_2O$ (hydrazine hydrate)	Biosensor for glucose	512
Pt_3Co/HRG	*In situ preparation*: chemical synthesis	GO–H_2PtCl_6 + $CoCl_2$ (ethylene glycol)	Electrocatalyst for ORR	627
Pt/TiO_2/HRG	*In situ preparation*: hydrothermal synthesis	GO–$TiCl_3$ + $H_2PtCl_6 \cdot 6H_2O$ ($NaBH_4$)	Catalyst for NB hydrogenation	471
Cu/HRG	*In situ preparation*: chemical synthesis	GO–$CuSO_4 \cdot 5H_2O$ (KBH_4)	Biosensor for carbohydrates	515
	Ex situ preparation: potentiostatic deposition	GO–$CuSO_4$ (hydrazine monohydrate)	Biosensor for glucose	516
Cu_2O/HRG	*Ex situ preparation*: physical adsorption	HRG–Cu_2O NPs	Biosensor for H_2O_2	517
	In situ preparation: ultrasound-assisted synthesis	GO–$Cu(CH_3COO)_2$ (glucose)	Anode material in LIBs	299
	In situ preparation: electrochemical deposition	GO–$CuSO_4$	Solar cells	386
	In situ preparation: chemical synthesis	GO–$CuSO_4$ (ascorbic acid)	Photocatalytic activity	628
	In situ preparation: chemical synthesis	GO–$Cu(OH)_2$ (glucose)	Adsorbent material	629
CuO/HRG	*In situ preparation*: chemical synthesis	GO–$Cu(NO_3)_2 \cdot H_2O$ (ethylene glycol)	Biosensor for glucose	518
	In situ preparation: microwave assisted synthesis	GO–($Cu(CH_3COO)_2 \cdot H_2O$)	Anode material in LIBs	630
	In situ preparation: hydrothermal synthesis	GO–$Cu(CH_3COO)_2$ (hydrazine hydrate)	Anode material in LIBs	293
	In situ preparation: chemical synthesis	GO–$Cu(OAc)_2 \cdot H_2O$	Catalyst for NH_4ClO_4 decomposition	631
Ag/HRG	*In situ preparation*: chemical synthesis	GO–$AgNO_3$ (GO functional groups)	SERS substrate	186
	In situ preparation: microwave-assisted synthesis	GO–$AgNO_3$	Anti-bacterial activity	632
	In situ preparation: chemical synthesis	GO–$AgNO_3$ (tannic acid)	Biosensor for glucose and H_2O_2	520
	In situ preparation: chemical synthesis	GO–CH_3COOAg ($NaBH_4$)	Electrocatalyst in DMFCs	633
	In situ preparation: chemical synthesis	GO–$AgNO_3$ (hydrazine hydrate)	Supercapacitor	634
	In situ preparation: photochemical synthesis	GO–$AgNO_3$	Catalyst for 2-nitroaniline preparation	451
Ag/graphene oxide	*Ex situ preparation*: self assembly	GO–$AgNO_3$	Anti-bacterial activity	597
Ag/AgX/ graphene oxide	*In situ preparation*: chemical synthesis (surfactant-assisted assembly)	GO–$AgNO_3$	Photocatalyst for pollutant degradation	450
Ag/TiO_2/SiO_2/ HRG	*In situ preparation*: biomimetic synthesis	GO (lysozome)	Photocatalyst	635

Table 1 (*Contd.*)

Materials	Synthetic routes	Precursors	Applications	References
Au/HRG	*In situ preparation: electrochemical synthesis*	GO–$AuCl_4$	Biosensor	529
	Ex situ preparation: layer-by-layer self-assembly	HRG–$HAuCl_4$ (hydrazine)	Electrochemical sensor for dopamine	533
Au/HRG	*In situ preparation: chemical synthesis*	GO–$HAuCl_4$ (sodium citrate)	Electrochemical sensor for epinephrine	538
	In situ preparation: chemical synthesis	GO–$HAuCl_4$ (sodium citrate)	Electrochemical sensor for levofloxacin	491
	In situ preparation: chemical synthesis	GO–$HAuCl_4 \cdot 3H_2O$ (hexamethylenetetramine)	Electrocatalytic application	493
ZnO/HRG	*In situ preparation: hydrothermal synthesis*	GO	Photocatalytic activity	636
	In situ preparation: atomic layer deposition	GO	Anode material in LIBs	637
	In situ preparation: chemical synthesis	GO–$ZnCl_2$ (NaOH)	Photocatalytic activity	458
	In situ preparation: ultrasonication-assisted synthesis	GO–Zn	Photocurrent generation	496
	In situ preparation: chemical synthesis	HRG–zinc benzoate dihydrazinate complex	Antibacterial activity	540
	In situ preparation: microwave assisted synthesis	GO–$ZnSO_4 \cdot 7H_2O$ (NaOH)	Supercapacitor	368
$ZnFe_2O_4$/HRG	*In situ preparation: hydrothermal synthesis*	GO	Photocatalytic activity	559
CdS/HRG	*Ex situ preparation: layer-by-layer self-assembly*	HRG–CdS quantum dots	Photocatalytic activity	638
	In situ preparation: chemical synthesis	GO	Photochemical sensor	639

3.1 Energy storage and conversion

The development of alternative strategies for the production of clean energy is one of the biggest challenges for the scientific community. Due to the increasing global warming, air pollution and growing environmental concerns, the efforts directed towards the development of energy storage and energy conversion devices with high energy densities and power densities have increased tremendously.[208] Graphene-based metallic nanocomposites have gained immense popularity in the field of electrochemical energy storage.[209] Because of their physicochemical properties such as high thermal and chemical stability, large surface area, excellent electrical conductivity and superior thermal and mechanical properties, graphene-based materials have been exploited as electrode materials in electrical energy storage devices.[210] Additionally, their broad potential range and rich surface chemistry have allowed customizing the properties of storage devices.[211] Therefore, graphene-based metallic, bimetallic and metal oxide nanocomposites have found wide applications in energy storage and energy conversion devices, such as lithium ion batteries (LIBs), supercapacitors, fuel and solar cells.[212]

3.1.1 Lithium ion batteries (LIBs). The performance of LIBs is largely dependent on the physical and chemical properties of cathode and anode materials.[213] Due to its large theoretical lithium storage capacity of 372 mA h g^{-1}, graphite is commercially used as an anode material. However, such storage capacity is not sufficient for the requirement of high energy capacity, which sparked the search for other alternative anode materials. Although the theoretical lithium storage capacity (744 mA h g^{-1}) of a single graphene layer is much higher than that of graphite its practical applications in LIBs face severe limitations due its natural tendency for stacking. The incorporation of metal and metal oxide NPs with high specific capacity into graphene not only inhibits the aggregation of graphene layers but also enhances its lithium storage capacity.[214]

TiO_2 has long been targeted in high-performance lithium ion batteries (LIBs). In particular, mesoporous anatase NPs and carbon-coated TiO_2 nanoparticles facilitate rapid ion diffusion and increase the conductivity of bulk materials.[215–217] Several HRG/TiO_2 nanocomposites with enhanced lithium storage capabilities compared to pure TiO_2 have been reported.[218,219] Recently, Li *et al.* described a simple one-pot, template-free self-assembly route to prepare well-dispersed mesoporous anatase TiO_2 nanospheres on graphene sheets.[220] The uniform TiO_2 nanospheres with a size of *ca.* 100 nm act as pillars and effectively separate graphene sheets from each other. Unlike the conventional mesoporous anatase particles which are polycrystalline, these mesoporous anatase nanospheres on graphene sheets are single crystalline, with each nanosphere containing wormhole-like pores with a relatively uniform size of *ca.* 4 nm. Compared to reference TiO_2, the composite shows a substantial improvement of the lithium specific capacity of 97 mA h g^{-1} at a rate of 50 C, which is 6 times higher than that of TiO_2. Apart from TiO_2, the other group 4 elements (Zr, Hf) did not show applications in LIBs.

Moving further in the periodic table, vanadium pentoxide (V_2O_5) has found prominent applications as a cathode material in rechargeable lithium-ion batteries (LIBs) due to its layered structure, wide occurrence in nature and its high energy densities.[221] However, the diffusion coefficient of lithium ions and moderate electrical conductivity of V_2O_5 hampered its intercalation capacity and rate capacity in practical applications. The diffusion capabilities can be enhanced by the nanoscaled formulation of V_2O_5 (nanobelts, nanowires, nanoscrolls

and nanorods), whereas improving the electrical conductivity of V_2O_5 requires the support of conductive carbon materials such as CNTs and graphene.[222] To this end, a number of graphene-supported V_2O_5 nanocomposites have been reported.[223–225] A HRG/V_2O_5 nanocomposite prepared under hydrothermal conditions by Liu *et al.* exhibited excellent electrochemical properties.[226] The simultaneous assembly of ultralong 1D V_2O_5 nanowires on the surface of 2D HRG sheets during the *in situ* reaction inhibited the restacking of HRG sheets. The as-prepared HRG/V_2O_5 nanocomposites have shown a high performance for lithium ion storage, providing a high discharge capacity and improved rate capability, when applied as a cathode material. The nanocomposite exhibited an initial specific discharge capacity of 412 mA h g^{-1} at a lower current density of 50 mA g^{-1}. When the current density was increased to 1600 mA g^{-1}, the composite still delivered a capacity of 316 mA h g^{-1}. This excellent performance of the HRG/V_2O_5 nanocomposite is attributed to the unique morphology of V_2O_5 nanowires with a short diffusion pathway for lithium ions and a higher electrical conductivity of HRG sheets.

Apart from 1D nanowires thin 2D graphene-like nanoribbons of V_2O_5 have been incorporated into graphene sheets, as the layer-structured vanadium pentoxide is an excellent host for lithium ion intercalation.[227] Among the V_2O_5 phases the amorphous hydrated form of V_2O_5 ($V_2O_5 \cdot nH_2O$) has a higher intercalation capacity than the crystalline one. The nanocomposites of HRG/$V_2O_5 \cdot nH_2O$ with different ratios of 2D $V_2O_5 \cdot nH_2O$ xerogel ribbons and graphene sheets were prepared by stacking two components. The amount of graphene in the composites played an important role in their structure and morphology and the resulting electrochemical properties. Increasing the graphene content in the composites resulted in better cycling stability when the composites were tested as cathodes in different voltage ranges for LIBs. Furthermore, the phase transformation of HRG/$V_2O_5 \cdot nH_2O$ nanocomposites moved towards higher temperature compared to pristine $V_2O_5 \cdot nH_2O$, as the thermal stability of the sample is enhanced by the presence of graphene.

For group 6 metals, molybdenum trioxide (MoO_3) is one of the most important layered materials and n-type metal oxide semiconductor that has attracted attention for photochromic and eletrochromic devices and energy storage.[228] Very recently, it has been found that HRG/MoO_3 nanocomposites synthesized by self-assembly (graphene encapsulated α-MoO_3 nanoribbons) exhibit an excellent high specific capacitance and enhanced discharge capacity.[229] Yang *et al.* have reported the hydrothermal synthesis of high-quality HRG/MoO_3 nanocomposites using inexpensive inorganic salts (NaCl) as capping agents.[228] The composite exhibits a combination of stacked HRG sheets and uniform MoO_3 nanobelts. MoO_3 belts with a diameter of 200–300 nm were obtained by the controlled use of NaCl as a capping agent. In addition, nanocomposites of HRG with other Mo derivatives such as MoS_2 (molybdenum sulfide), MoN (molybdenum nitride) and GO-based MoO_2 nanocomposites find application in LIBs or for hydrogen evolution.[230–236]

Moreover, due to the high theoretical capacity (1232 mA h g^{-1}) of MnO_2 (based on heterogeneous Li_2O and Mn metal conversion reactions) HRG/MnO_2 nanocomposites have attracted attention for application in LIBs as anode materials.[203,237] Yu *et al.* have prepared free-standing layer-by-layer assembled hybrid HRG/MnO_2 films by ultra-filtration and studied their use as anodes for LIBs.[238] The hybrid material was comprised of ~1 μm long single crystalline MnO_2 nanotubes grown on HRG sheets with an average thickness of 1–2 nm. The adequate contact of graphene sheets with MnO_2 nanotubes provides a fast electron pathway with 2-D electron conducting behavior between MnO_2 nanotubes. In addition, the nanostructured thin film (~10 μm) shortens the diffusion path length for fast lithium ion transport into the electrode to enhance directly the power rating of the external circuit. HRG/MnO_2 composite films as an anode material exhibited excellent cycle and rate capabilities with a reversible specific capacity based on an electrode composite mass of 495 mA h g^{-1} at 100 mA g^{-1} after 40 cycles with current rates from 100 to 1600 mA g^{-1}.

Among the manganese oxides Mn_3O_4 has been studied as an anode material for LIBs aimed at achieving higher specific capacities than graphite.[239] The capacity of Mn_3O_4 has been significantly enhanced by the support of conducting substrates such as CNTs and graphene.[240,241] In their effort to enhance the capacity of Mn_3O_4 Wang *et al.* have prepared HRG/Mn_3O_4 hybrid materials in a two-step solution phase process.[242] The HRG/Mn_3O_4 nanocomposite is comprised of ~10–20 nm large and well-crystallized Mn_3O_4 NPs uniformly distributed on HRG sheets. The hybrid material showed an unprecedented high capacity of ~900 mA h g^{-1} based on the mass (~810 mA h g^{-1} based on the total mass of the hybrid) with good rate capability and cycling stability, which is attributed to the intimate interaction between graphene substrates and Mn_3O_4 NPs. In addition, mixed metal oxides of manganese have been tested as anode materials in LIBs. For instance, in the HRG/$Mn_2Mo_3O_8$ nanocomposite reported by Sun *et al.* the nanohybrids are composed of HRG-wrapped secondary microspheres of ~3–5 μm in diameter that are built from many $Mn_2Mo_3O_8$ nanosheets with a thickness of 10–15 nm and width of 80–120 nm.[243]

In group 8 ferromagnetic Fe and magnetic iron oxide NPs have potential applications in energy storage devices including LIBs.[244] The most important studies have been conducted on graphene-based nanocomposites of iron oxides (*e.g.* Fe_2O_3 and Fe_3O_4). However, studies on HRG/Fe composites are rare.[245] In a recent study, graphene-encapsulated iron microspheres (GEIMs) have been synthesized by heating graphene oxide nanosheets and $FeCl_3$.[246] They contain 68.32% of carbon and 28.32% of Fe with no traces of oxygen, confirming the unoxidized state of the Fe core due to graphene coating.

In addition to Fe, magnetic iron oxide NPs like Fe_2O_3 and Fe_3O_4 have been exploited as anode materials for LIBs due to their high theoretical capacities (~1005 mA h g^{-1} and 926 mA h g^{-1}, respectively).[247,248] However, the ability of Fe_3O_4 NPs as electrode materials has been affected greatly due to the large volume change and severe particle aggregation during the electrochemical cycling process, which ultimately leads to a high irreversible capacity loss and poor cycling stability.[249] Nevertheless, the electrochemical properties of Fe_3O_4 NPs have been improved considerably over the last couple of years by

using the support of graphene.[250,251] For instance, the HRG/Fe_3O_4 nanocomposites recently developed by Su *et al.* exhibit high reversible capacity, improved cyclic performance and excellent rate capability compared to pristine Fe_3O_4 NPs.[252] The as-prepared HRG/Fe_3O_4 electrode maintains a reversible capacity of 1102 mA h g^{-1} after 10 cycles at a current density of 100 mA g^{-1}, whereas that of the Fe_3O_4 electrode rapidly drops from 1011 to 193 mA h g^{-1}. Furthermore, the reversible capacity of the hybrid electrode is still as high as 474 mA h g^{-1}, even at a higher current density of 1600 mA g^{-1}, which is in sharp contrast to that of an electrode from pure Fe_3O_4 NPs that decays to nearly zero under similar conditions. In other studies, specific capacities of more than 1200 mA h g^{-1} have been achieved for HRG/Fe_3O_4 nanocomposites prepared *via* different methods, including the hydrothermal method. HRG/Fe_3O_4 nanocomposites prepared by ultrasonically assisted co-precipitation have a specific capacity of 1280 mA h g^{-1} at 0.1 C cycling and 860 mA h g^{-1} at a 4 C rate, compared to a specific capacity of 1257 mA h g^{-1} of hybrids synthesized under hydrothermal conditions.[253,254]

Although some achievements have been made for HRG/Fe_3O_4 nanocomposites, the aggregation of Fe_3O_4 NPs and graphene sheets during the synthesis process remains a challenge for the development of high capacity electrodes based on HRG/Fe_3O_4 nanocomposites.[249,254] The electrochemical properties of HRG/Fe_3O_4 electrodes are affected by the inaccessibility of the active material to the surface of HRG because of their zero-dimensional (0D) nature. Recently, three-dimensional (3D) hierarchical nanocomposites have been synthesized, where flowerlike Fe_3O_4 NPs are homogeneously encapsulated in graphene sheets.[255] Such a dimensional confinement of Fe_3O_4 nanoflowers by the surrounding graphene nanosheets limits the effect of volume expansion upon lithium insertion. In addition, the 3D nature of Fe_3O_4 NPs allows better contact with graphene sheets in the HRG/Fe_3O_4 nanocomposite, which serve as a diluting agent to prevent the aggregation of Fe_3O_4 NPs. Graphene nanosheets also provide a highly conductive network for electron transfer from the anchored nanoflowers within the whole electrode. This enhances the electrical conductivity of the HRG/Fe_3O_4 electrodes. The hybrid material (60 wt% of Fe_3O_4 in the composites) exhibits a stable capacity of ~605 mA h g^{-1} with a stability of up to 50 cycles in the voltage range of 0.001–3.0 V. In another approach to solve the problem of volume change in HRG/Fe_3O_4 nanocomposites, Chen *et al.* prepared graphene-encapsulated ordered aggregates of Fe_3O_4 NPs with a spherical geometry and hollow interior by self-assembly.[249] The composite exhibited an excellent and stable specific capacity of 900 mA h g^{-1} for up to 50 cycles. Even after 90 cycles of charge and discharge at different current densities, a specific capacity of 832 mA h g^{-1} at 100 mA g^{-1} was achieved, indicating a recoverability of about 92% of the initial capacity.

The electrochemical properties of Fe_2O_3 have been affected by similar problems, which were improved by the incorporation of graphene.[256,257] In addition, Fe_2O_3 electrodes are inclined to lose electrical contact and structural integrity during repetitive cycling at high charge and discharge rates. In an effort to enhance the electrical contact and to maintain the structural integrity of Fe_2O_3 electrodes Zhou *et al.* prepared HRG/Fe_2O_3 core–shell nanocomposites by complete coating of Fe_2O_3 NPs with a graphene shell.[258] The graphene-wrapped rose-like porous Fe_2O_3 NPs showed a high reversible capacity, enhanced rate capability and improved cycling stability with respect to pristine α-Fe_2O_3 when tested as an anode material in LIBs. The specific capacity of the HRG/Fe_2O_3 core–shell nanocomposite at a rate of 5 C and 10 C was 269 mA h g^{-1} and 143 mA h g^{-1}, respectively, which is 34 times higher than that of bare α-Fe_2O_3 NPs (8 mA h g^{-1} at a rate of 5 C. Pristine α-Fe_2O_3 cannot store charges at a rate of 10 C).

Zou *et al.* prepared HRG/Fe_2O_3 nanocomposites that also showed suitability as an anode material in LIBs.[259] The nanocomposite is comprised of uniformly distributed 150–200 nm long Fe_2O_3 rice-like NPs, which were obtained with phosphate anions as an additive. The tailored nanocomposite exhibited a high reversible capacity of 1184 mA h g^{-1} upon cycling and excellent rate capabilities at large currents: at a large current of 1000 mA g^{-1} it showed an initial reversible capacity of 825 mA h g^{-1}. A high capacity of 582 mA h g^{-1} could be retained even after 100 cycles. The synergetic effect due to better contact between the two components of HRG/Fe_2O_3 rice-on-sheet nanocomposites led to an improvement of their electrochemical properties. In another study HRG/Fe_2O_3 nanocomposites exhibited first discharge and charge capacities of 1693 and 1227 mA h g^{-1}, respectively, at a current density of 100 mA g^{-1} and also showed a good capacity retention with 1027 mA h g^{-1} after the 50th discharge.[260]

In addition to graphene-based nanocomposites of Fe_3O_4 and Fe_2O_3 NPs hybrids of graphene and other iron-based materials such as $LiFePO_4$ have been applied in LIBs.[261,262] Zhou *et al.* applied HRG/$LiFePO_4$ nanocomposites as a cathode material in LIBs, which showed excellent high rate capability and cycling stability, delivering a capacity of 70 mA h g^{-1} at 60 C discharge rate and showed a capacity decay rate of <15% when cycled under 10 C charging and 20 C discharging 1000 times.[263] The composite was prepared with $LiFePO_4$ NPs and graphene nanosheets by spray-drying and annealing; the NPs were embedded in micro-sized spherical secondary particles and wrapped homogeneously and loosely with a graphene 3D network.

Among the group 9 elements only graphene-based nanocomposites of cobalt oxides have been reported. They are applied as electrode materials in energy storage systems including LIBs and supercapacitors due to their excellent electrochemical properties such as high specific capacity (890 mA h g^{-1}), good cycling and high rate performance.[264,265] However, the large volume change (expansion/contraction) during the cycling process due to the pulverization and aggregation of cobalt oxide NPs leads to a deterioration of the electric contact between the particles. The support of highly conductive graphene reduces the aggregation of cobalt oxide NPs, whereas the highly active surface area of graphene significantly enhances the lithium storage capacity and cycling performance of the hybrid graphene-/cobalt oxide materials.

HRG/cobalt oxide nanocomposites can utilize the combinative merits of nanosized cobalt oxide and graphene to produce

LIBs with superior performance.[266,267] Yang *et al.* prepared HRG/Co_3O_4 hybrids *via* co-assembly between negatively charged GRO and positively charged cobalt oxide NPs in a process driven by the mutual electrostatic interactions of the two species.[268] The as-prepared nanocomposites were comprised of electrochemically active Co_3O_4 NPs encapsulated with highly conductive graphene sheets. They exhibited a reversible capacity of 1100 mA h g^{-1} during the first 10 cycles and over 1000 mA h g^{-1} after 130 cycles with excellent cycle performance. Similarly, Co_3O_4 NPs ($\xi \approx$ 10–30 nm) were anchored homogeneously on graphene sheets.[269] These composites effectively utilized the properties of both the components including conductivity, high surface area, mechanical flexibility as well as large electrode/electrolyte contact area and short path length for Li^+ transport to deliver an electrochemical performance with a reversible capacity of 935 mA h g^{-1} after 30 cycles, cyclic performance, high columbic efficiency (above 98%) and good rate capability. In another instance, extremely small Co_3O_4 (~5 nm) NPs were uniformly grown on highly conductive graphene nanosheets in an *in situ* reduction process.[189] In this case, the electrochemical performance delivered by the as-prepared nanocomposites is attributed to their unique nanostructure with a reversible capacity of 778 mA h g^{-1} with a Coulumbic efficiency of 97% after 42 cycles, where graphene sheets act as a buffer to mitigate the large volume change of Co_3O_4 NPs in the charge–discharge process.

Although HRG/Co_3O_4 nanocomposites exhibit good electrochemical performance compared to their pristine components, it is more likely that Co_3O_4 NPs tend to aggregate more easily into larger particles during the charge–discharge process, which will limit the ion/electron transportation and further affect the reversible lithium storage capacity. The multi-dimensional nature of the NPs enhances the gap between graphene layers more due to their larger aspect ratio, compared to simply spherical NPs. To this end, the synthesis of HRG/Co_3O_4 nanocomposites containing Co_3O_4 nano/microrods is intriguing because the unique structure of Co_3O_4 NPs prevents particle aggregation and therefore leads to an excellent electrochemical performance of the nanocomposites.[270] The as-prepared nanocomposite exhibits improved cycling stability, remarkably high reversible lithium storage capacity and superior rate capability compared to the previously reported HRG/Co_3O_4 nanocomposites (~1310 mA h g^{-1} and 1090 mA h g^{-1} of capacity are retained even after 40 cycles at a current density of 100 mA g^{-1} and 1000 mA g^{-1} respectively). Similarly, a HRG/Co_3O_4 nanocomposite, containing Co_3O_4 nanorods (around 20–40 nm in diameter), showed a reversible capacity of 975 mA h g^{-1} with an irreversible capacity loss of <3% after 100 cycles.[271]

Apart from Co_3O_4 NPs and nanorods, 2D Co_3O_4 nanosheets, which may show better compatibility and good coverage with 2D graphene nanosheets, have been utilized in the preparation of HRG/Co_3O_4 nanocomposites. For instance, a microwave-assisted synthesis of sheet-on-sheet HRG/Co_3O_4 nanocomposites has been reported by Chen *et al.* where graphene nanosheets were tightly stacked with 2D porous Co_3O_4 NPs.[272] Each graphene nanosheet in the composite was separated by a few Co_3O_4 nanosheets with porous Co_3O_4 nanosheets having a micrometer size and ~100 nm thickness. Notably, the 2D and porous structure of Co_3O_4 sheets promoted the fast diffusion of ions, electrons, and electrolytes in the composite that exhibits a very large capacity of 1235 mA h g^{-1} and superior rate capabilities. Moreover, in order to achieve enhanced electrochemical performances in HRG/Co_3O_4 nanocomposites, the grain size porosity and morphology of Co_3O_4 nanostructures were optimized.

Zhu *et al.* tailored the porosity of HRG/Co_3O_4 nanocomposites and the grain size of Co_3O_4 nanosheets by varying the annealing temperature and gas environment, which directly affected their performance in Li-ion battery electrodes.[273] HRG/Co_3O_4 nanocomposites consisting of ultrathin Co_3O_4 nanowall arrays on graphene sheets were synthesized *via* pyrolysis of as-prepared α-$Co(OH)_2$/HRG composites. The pores were generated in Co_3O_4 nanowalls by annealing, where pores with larger diameters were obtained at higher temperatures. Furthermore, under optimized conditions HRG/Co_3O_4 nanocomposites obtained at 350 °C showed better Li storage performance than hybrids obtained at other temperatures. Among several HRG/Co_3O_4 electrodes, the one prepared at 350 °C (HRG/Co_3O_4-350) showed excellent charge–discharge capacities and cycling stabilities with a discharge capacity of 884 mA h g^{-1} during the second cycle, and a high specific capacity of 673 mA h g^{-1} after 100 cycles at a discharge current density of 180 mA g^{-1}.

Cobalt monoxide (CoO) with higher theoretical Li-ion storage capacities (716 mA h g^{-1}) due to its completely reversible electrochemical reaction has attracted special attention for use in lithium ion batteries (LIBs).[274,275] Zhu *et al.* synthesized HRG/CoO nanocomposites under identical conditions except replacing air with argon.[273] The as-prepared HRG/CoO-350 electrode comprised ultrathin CoO nanowalls synthesized under controlled conditions and exhibited an optimum electrochemical performance with a capacity of 732 mA h g^{-1} after 100 cycles at a discharge current density of 150 mA g^{-1}. Some other examples in this regard with excellent electrochemical performance of CoO hybrids with graphene include the synthesis of HRG/CoO nanocomposites by facile ultrasonic action.[276] In these hybrids CoO particles are dispersed uniformly as quantum dots (QDs) with an average diameter of ~5 nm, where the strong interaction between graphene nanosheets and QDs inhibits aggregation and volume change of CoO during the cycling process. This leads to a short pathway for Li diffusion. Furthermore, the small size of CoO QDs and their high mass loading (60%), which afforded abundant active sites, greatly enhanced the lithium storage capacity. The as-prepared HRG/CoO nanocomposites showed extraordinary performance as an anode material for LIBs, including a high reversible lithium storage capacity of 1592 mA h g^{-1} after 50 cycles, high coulombic efficiency (>95%), excellent cycling stability, and a high rate capability of 1008 mA h g^{-1} with a total retention of 77.6% after 50 cycles at a current density of 1000 mA g^{-1}.

In addition to cobalt oxides, layered cobalt hydroxides such as $Co(OH)_2$ are also attractive in the field of LIBs because of their large interlayer spacings and their well-defined electrochemical redox activity.[277] However, due to an anxiety about "hydrogen" of the hydroxides, $Co(OH)_2$ has attracted limited

attention in energy storage systems compared to other cobalt oxides. So far, only a few reports are available on graphene-based $Co(OH)_2$ nanocomposites including a synthesis *via* chimie douce using Na_2S in a water–isopropanol system.[278,279] The as-prepared material delivered remarkable electrochemical performance and improved specific capacitance compared to the individual counterparts.[277] Apart from cobalt-based materials, some studies were carried out on the incorporation of pristine cobalt NPs into graphene sheets in order to improve the performance of LIBs and other applications.[280–282] The high reactivity and strong sensitivity of Co NPs to oxygen greatly inhibit their wider applications.[283]

In addition to cobalt oxide and cobalt hydroxides, cobalt sulfide is also an excellent electrode material for LIBs. The performance of this material can be further enhanced by incorporating graphene, which not only provides improved conductivity, but also facilitates the mobility of electrons and ions. For this purpose various attempts have been undertaken to synthesize HRG/cobalt sulfide nanocomposites. In a recent study, Co_3S_4 nanotubes have been successfully grown on the surface of graphene by a facile hydrothermal process.[284] Due the enhanced conductivity of the composite by the incorporation of graphene, it has demonstrated an excellent electrochemical performance compared to pristine Co_3S_4 nanotubes. The nanocomposite showed good cycling stability and a high discharge capacity of 720 mA h g^{-1} up to 100 cycles with 99.9% coulombic efficiency (*cf.* Fig. 11).

For *group 10 metals*, nickel oxides including NiO and $Ni(OH)_2$ have been applied as anode materials in LIBs because of their outstanding theoretical capacity.[285,286] However, they usually suffer from various problems such as poor cyclic stability, energy density loss, and large voltage hysteresis (when the discharge potential is lower than the charge potential), which have been effectively addressed by the support of graphene in the form of nanocomposites, (HRG/$Ni(OH)_2$ and HRG/NiO).[287,288] For instance, Mai *et al.* demonstrated an improved cycling stability and rate capability of a HRG/NiO hybrid applied as an anode material in LIBs.[289] It delivered a capacity of 646.1 mA h g^{-1} after 35 cycles at a current density of 100 mA g^{-1}, corresponding to an 86.3% capacity retention. In addition, the incorporation of graphene sheets partly reduces the voltage hysteresis due to their lithium storage mechanism, where Li^+ ions are intercalated into graphene sheets which are different from bare NiO, where lithium is stored by Li insertion. Graphene incorporation into $Ni(OH)_2$ was reported where the HRG/$Ni(OH)_2$ electrode delivered a high performance with a specific discharge capacity of 507 mA h g^{-1} after 30 cycles in LIBs.[290] This hybrid with a sandwich-like structure facilitated the diffusion, oxidation/reduction and also effectively prevented the aggregation of NPs, which is essential for good cyclic performance.

In group 11, copper oxides such as CuO and Cu_2O are often used due to their high theoretical capacity and are promising candidates for anode materials in LIBs.[291,292] However, they suffer from a large volume variation during the Li^+ insertion/extraction process, which causes severe mechanical strain and rapid capacity decay. Through the support of graphene the breakdown of copper-based anode materials can be prevented, and the stability and capacity of the material can be enhanced.[293–295] In one such example, graphene-based copper oxide nanocomposites (HRG/CuO, applied as an anode material for high performance LIBs) exhibit improved cycling and rate performance compared to pure CuO.[296] The hybrid electrode delivered a stable reversible capacity of 600 mA h g^{-1} at a current density of 65 mA g^{-1} for 100 cycles. In addition, the HRG/CuO composite electrode still exhibited a charge capacity as high as 150 mA h g^{-1} at a high current density of 6400 mA g^{-1}, where the specific charge capacity of pure CuO is nearly zero. The enhanced performance of the composite is attributed to its special design, where CuO particles are enwrapped by a thin layer of graphene elastic buffer.

P-type cuprous oxide (Cu_2O) (due to the presence of copper vacancies) with a band gap of 2.17 eV is also considered a promising material with potential applications in LIBs.[297,298] In order to circumvent the typical shortcomings, such as poor cycling and rate performance of Cu_2O, HRG/Cu_2O composite

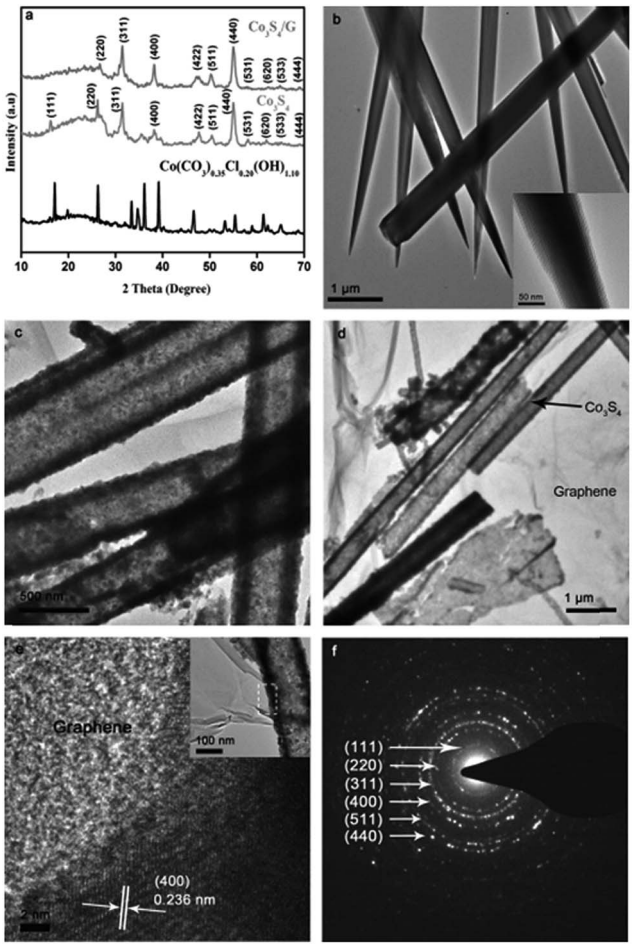

Fig. 11 (a) PXRD patterns of $Co(CO)_{0.35}Cl_{0.20}(OH)_{1.10}$, Co_3S_4, and Co_3S_4/HRG composites. TEM images of (b) $Co(CO)_{0.35}Cl_{0.20}(OH)_{1.10}$ wires (the inset is a high-resolution TEM image of $Co(CO)_{0.35}Cl_{0.20}(OH)_{1.10}$), (c) Co_3S_4, and (d) Co_3S_4/HRG composites. (e) HRTEM image (the area enclosed by the dashed lines in the inset shows the location of the HRTEM image) and (f) SAED pattern of Co_3S_4/HRG composites. Copyrights reserved to the John Wiley and Sons.[284]

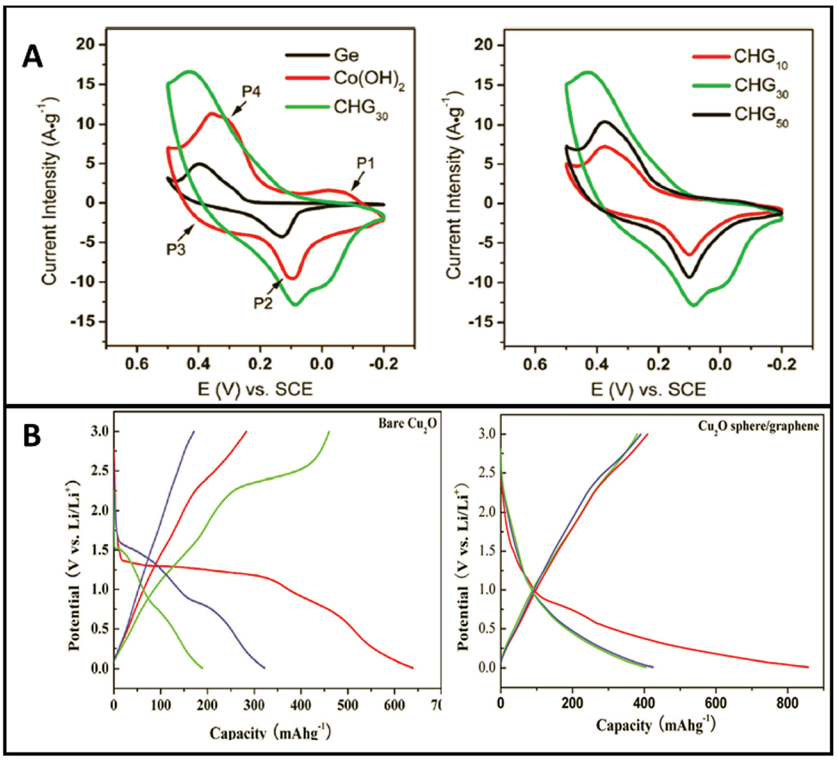

Fig. 12 (A) CV response of a graphene/$Co(OH)_2$ nanocomposite depicting great influence of graphene on the electrochemical properties of the composites. Copyrights reserved to the American Chemical Society.[278] (B) Comparisons were made between bare Cu_2O and Cu_2O NPs–GNS samples displaying superior cycling performance and highlighting the crucial role of graphene in alleviating the capacity degradation. Copyrights reserved to RSC Publishing.[299]

electrodes with graphite support have shown good cycling and excellent rate performance with a specific capacity of over 400 mA h g^{-1} at a rate of 100 mA g^{-1} after 20 cycles, whereas pure Cu_2O exhibited 100 mA h g^{-1} at the same current density (*cf.* Fig. 12).[299] During the preparation of HRG/Cu_2O nanocomposites, monodisperse Cu_2O spheres with diameters of 150–200 nm were loaded on the surface of graphene by sonication.

In addition to transition metals (group 4 to 12), graphene-based composites of other metals have been applied. The large theoretical specific capacity ~782 mA h g^{-1} of SnO_2, which is twice that of graphite, has attracted much attention.[300] The lithium storage properties of SnO_2 NPs have been enhanced by using the graphene support. Several studies describe the preparation of HRG/SnO_2 nanocomposites by hydrothermal or solvothermal methods, and demonstrate the enhanced electrochemical properties of the composites (improved lithium storage with high reversible capacity and great cycling stability).[301–303] HRG/SnO_2 hybrids, where rod-like SnO_2 nanocrystals were homogeneously distributed on the surface of graphene sheets, delivered a reversible capacity of 838 mA h g^{-1}.[304] In another study, a reversible capacity of 1304 mA h g^{-1} at a current density of 100 mA g^{-1} was achieved with a HRG/SnO_2 hybrid electrode.[305]

Despite the fact that graphene improves the electrochemical performance of the NPs, there are some limitations of the LIB performance of graphene-based hybrid anodes, because no proper contact between graphene and the NPs could be achieved, or the aggregation of the NPs increased the electronic path length in the electrodes, which in turn leads to an increase of the conductivity. These issues have been addressed through N-doping of graphene, which improved the electrochemical performance. The electrochemical performance of SnO_2 NPs by using the support of N-doped graphene was reported by Wang *et al.*[300] In addition to HRG/SnO_2, HRG/SnS_2 nanocomposites have found applications as anode materials in LIBs. Although these nanocomposites have demonstrated excellent electrochemical performances the stability of the nanocomposites and the capacity fading in the initial cycles are still challenges for their wide spread applications in LIBs. To find a solution to these problems, Hou *et al.* have demonstrated the preparation of HRG/SnS_2 nanocomposites in a single step solvothermal process by using ethylene glycol both as a solvent and capping agent.[306] In this composite, graphene not only enhanced the electrical conductivity but also provided stability to the anode material during the charge–discharge process (*cf.* Fig. 13).

Apart from graphene inorganic nanocomposites, graphene doped with boron, nitrogen, sulfur and phosphorus also exhibits excellent electrochemical performance in energy storage devices including LIBs. Hou *et al.* demonstrated a facile and scalable method for the preparation of phosphorus doped graphene (PHRG) by thermal annealing using triphenylphosphine and GO as phosphorus and carbon sources respectively.[307] The as-prepared PHRG was applied for the first time as

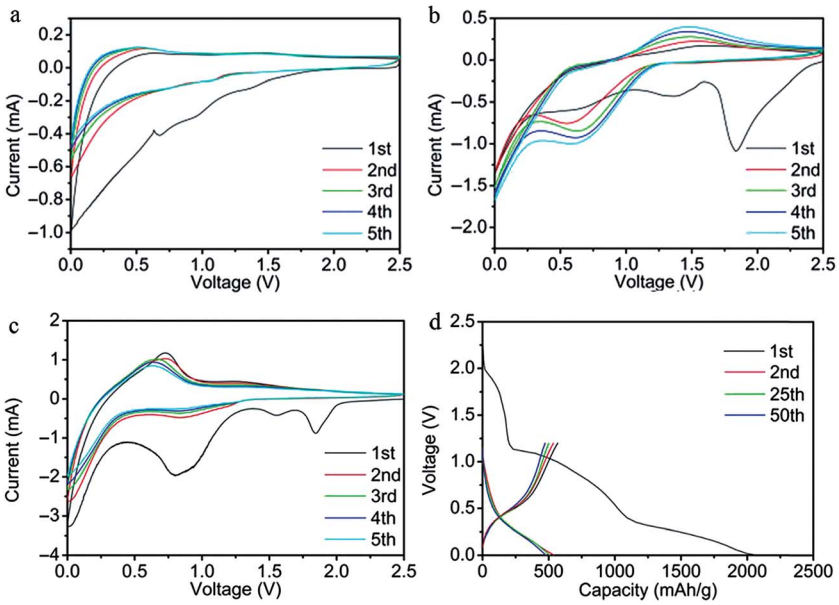

Fig. 13 Cyclic voltammograms of (a) HRG, (b) SnS_2 nanocrystals and (c) HRG/SnS_2 composites prepared at 200 °C for 12 h. (d) Charge–discharge voltage profiles of HRG/SnS_2 composites for the 1st, 2nd, 25th, and 50th cycles at a current of 500 mA g^{-1}. Copyright reserved to the American Scientific Publishers.[306]

an electrode material in LIBs and exhibited excellent current rate and enhanced reversible capacity compared to the undoped graphene (*cf.* Fig. 14). Furthermore, the combination of doped graphene and metal sulfides has attracted attention for energy storage applications.[308] The combination of the properties of both the components in these composites, such as high theoretical capacities and low cost of metal sulfides, combined with the excellent conductivities and rate capabilities of doped graphene, may be exploited in LIBs. In this regard, Hou *et al.* reported a hydrothermal synthesis of nickel sulfides, Ni_3S_4 and $NiS_{1.03}$, grown on nitrogen-doped graphene (NHRG) sheets.[309] The as-obtained nanocomposites demonstrated excellent

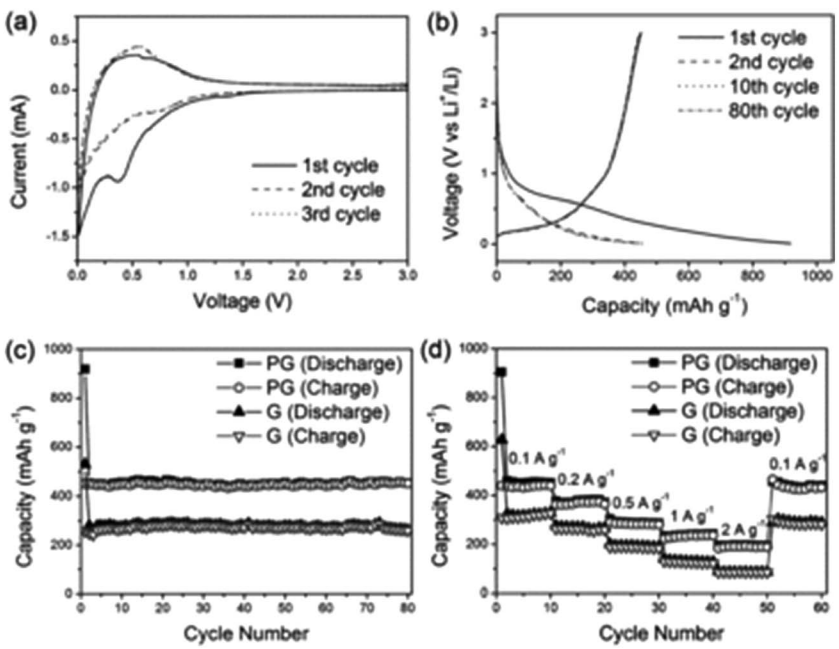

Fig. 14 (a) CV curves of PHRG at a scanning rate of 0.2 mV s^{-1} in the voltage range of 3–0.01 V *vs.* Li^+/Li. (b) Galvanostatic charge–discharge profile of PHRG at a current rate of 0.1 A g^{-1} in the voltage range of 3–0.01 V *vs.* Li^+/Li. (c) Cycle performance of PHRG and undoped graphene at a current rate of 0.1 A g^{-1} in the voltage range of 3–0.01 V *vs.* Li^+/Li. (d) Rate performance of PHRG and undoped graphene in the voltage range of 3–0.01 V *vs.* Li^+/Li. Copyrights reserved to the John Wiley and Sons.[307]

performance and remarkable capacity retention rate. The composite of Ni_3S_4/NHRG annealed at 250 °C showed ultrahigh performance with a discharge capacity of 558.2 mA h g^{-1} and a capacity retention of 95.19% after 100 cycles at 4 C. A NHRG/Co_3Sn_2@Co nanocomposite, which was prepared hydrothermally, exhibited good electrochemical performance in LIBs.[310] The deliberate design of a core@shell architecture of Co_3Sn_2@Co on the surface of doped graphene facilitated a reversible capacity of 1615 mA h g^{-1} at 250 mA g^{-1} after 100 cycles with a capacity retention of 102%. The hybrid also bears superior rate capability with a reversible capacity of 793.9 mA h g^{-1} at 2500 mA g^{-1} and coulombic efficiency close to 100%.

The combination of graphene with various metal oxide NPs not only maximizes the practical applications of LIBs, but the synergetic effects between both the active materials helped to increase the energy storage capacity and to enhance the electrochemical performance of LIBs.[208,213] In these composite materials, graphene provides a 2D support for the uniform dispersion of metal oxides, acts as a conductive template for building a 3D network to improve the electrical conductivity and to suppress the volume change and particle agglomeration during the charge–discharge process. The metal oxide NPs inhibit the agglomeration of graphene layers and thereby help to enhance the surface of graphene; ultimately leading to a high electrochemical activity of the resultant LIBs (*cf.* Table 2). The resulting composite is more than a mere combination of the individual components, but indeed, it is a new material with improved functionalities and properties. Despite several advantages, there remain challenges ahead for improvement of these composites in commercial applications of LIBs. So far, there has been a little control over the interface and interaction between graphene and metal oxide NPs, which is important in order to control the charge transfer processes. Therefore, there is a strong urge to develop strategies for the preparation of graphene/inorganic nanocomposites with well-defined uniform structure on graphene, which provide maximum control over surface interactions. Furthermore, controlling the phase and morphology of the NPs on the surface of graphene is necessary for enhancing the performance of LIBs.

3.1.2 Supercapacitors. Supercapacitors or electrochemical capacitors are an important class of energy storage devices that exhibit high power density, long cycle life and excellent charge–discharge rates compared to common batteries.[311] The energy storage mechanisms of supercapacitors mainly include a carbon-based electric double layer (EDL) and metal oxide- or polymer-based pseudo-capacitive charge storage. Electric double layer capacitors (EDLCs) store the charge electrostatically (physical process) using reversible adsorption of ions of the electrolyte onto active materials. In EDLCs the charge storage is mainly dependent on the properties of the electrode material, as the energy is stored by the adsorption of ionic charges on the surface of the electrode.[312] In order to increase the specific capacitance and the power density of EDLCs much attention has to be paid to the enhancement of electrode material properties. Recently, graphene has attracted attention as an electrode material in supercapacitors because of its high

Table 2 Electrochemical performance of graphene/inorganic NP nanocomposites as electrode materials in lithium-ion batteries

	Materials	Applications	Initial discharge capacity [mA h g^{-1}]	Potential window (V)	References
Anode	TiO_2/HRG	Lithium ion batteries and photocatalytic activity	97	1–3	220
	MnO_2/HRG	LIBs	208	0–3	238
	Fe/HRG	LIBs	440	0–3	246
	Co/HRG	LIBs	500	0–3	268
	$Ni(OH)_2$/HRG	LIBs	507	0–3	290
	NiO/HRG	LIBs	646.1	—	289
	Cu_2O/HRG	LIBs	857	0–3	299
	Mn_3O_4/HRG	LIBs	900	0–3	613
	Co_3O_4/HRG	LIBs	941	0–3	266
	Fe_3O_4/HRG	LIBs	988.5	0–3	614
		LIBs	1011	0–3	252
	CuO/HRG	LIBs	1043.3	0–3	630
	Fe_2O_3/HRG	LIBs	1561	0–3	619
	CoO/HRG	LIBs	1719	0–3	276
	TiO_2/HRG	Lithium ion batteries and photocatalytic activity	5000	3–0.05	605
	Materials	Applications	Current density	Potential range (V)	References
Cathode	V_2O_5/HRG	LIBs	600	2.0–4.0	225
		LIBs	299	1.5–4.0	227
		LIBs	383	2–4	157
	$LiFePO_4$/HRG	LIBs	70	2.0–4.2	263

surface area, chemical inertness, excellent flexibility, and superb electrical conductivity.[313] Single layer graphene exhibits an intrinsic capacitance of ~21 mF cm^{-2}, and a theoretical (if all the surface area of graphene can be used) electric double layer capacitance of ~550 F g^{-1} could be achieved.[314] However, the practical use of the whole surface area of graphene is difficult; therefore, graphene has been extensively used in combination with other electrochemically active metal oxides and hydroxides as electrode materials in supercapacitors.

Only a few reports on graphene-based composites of ZrO_2 and V_2O_5 in supercapacitors have appeared so far.[315,316] For metals of group VIIb reports have been found on supercapacitor applications of graphene/MnO_2 and Mn_3O_4 nanocomposites.[317] MnO_2 by virtue of its low cost, high specific capacitance, good cycle stability and environmental compatibility has attracted much attention.[318] However, its poor electrical conductivity (10^{-5} to 10^{-6} S cm^{-1}) and its densely packed structure limit its application for the development of high-performance supercapacitors. Therefore the combination of graphene and layered MnO_2 exhibited improved electrochemical performance. The distinct two-dimensional (2D) structure of graphene not only provides a highly reversible pseudocapacitance, but also the electrochemical double-layer capacitance.[319,320]

The synthesis of HRG/MnO_2 nanocomposites by microwave reaction and their use as electrode materials were reported by Yan *et al.*[321] Here, HRG sheets serve mainly as a highly conductive support, and they provide a large surface for the deposition of MnO_2 NPs (ξ 5–10 nm). The electrical conductivity of the electrode could be enhanced by the interfacial contact between MnO_2 and graphene. In addition, the easy surface accessibility of the nanocomposite by the electrolyte, and the improved electrochemical utilization of MnO_2 (resulted from the small particle size and high surface area of graphene and manganese oxides) provided both the high reversible pseudocapacity and excellent capacitive retention ratio at a high charge–discharge rate. The nanocomposite exhibits an overall specific capacitance of 310 F g^{-1} at 2 mV s^{-1} and even 228 F g^{-1} at 500 mV s^{-1} in an aqueous electrolyte, and a capacitance retention ratio at high charge–discharge rates of about 88% at 100 mV s^{-1} and 74% at 500 mV s^{-1}. In another study, the specific capacitance of 328 F g^{-1} at a charging current of 1 mA has been obtained after an electro-activation process in the nanocomposites of graphene sheets decorated with flower-like MnO_2 NPs.[322] The MnO_2 nanoflowers, containing rods with a thickness of less than 10 nm, were electrodeposited onto graphene sheets.

However, high energy storage and large capacitance usually obtained by a high mass loading of active MnO_2 materials often lead to an increased electrode resistance and decreased specific capacitance. The mass loading leads to densely packed MnO_2 NPs on the surface of graphene sheets with limited electrochemically active surface area, and only a thin top layer of the oxide participates in the charge storage process. To resolve these critical problems, Yu *et al.* developed a "three-dimensional (3D) conductive wrapping" method to design ternary HRG/MnO_2/CNT nanocomposites with improved supercapacitor performance (*cf.* Fig. 15).[238] The nanocomposite was fabricated by wrapping an ultrathin layer of single-wall CNTs or

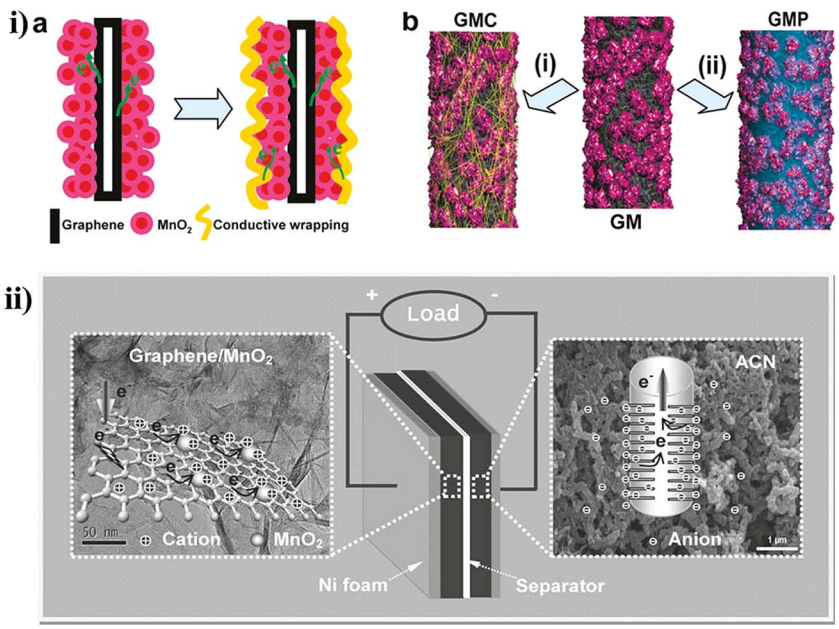

Fig. 15 HRG/MnO_2 nanocomposites as electrode materials. (i-a) Conducting wrapping of graphene/MnO_2 (GM) to introduce an additional electron transport path (in discharge cycle). (i-b) Graphene/MnO_2/CNT (GMC) and graphene/MnO_2/conducting polymer (GMP) formed by wrapping of GM nanostructures with CNTs or conducting polymer. (Black: graphene; rose: MnO_2; yellow: CNTs; blue: conducting polymer). Copyrights reserved to the American Chemical Society.[238] (ii) Fabricated asymmetric supercapacitor device based on graphene/MnO_2 composites as a positive electrode and activated carbon nanofibers as a negative electrode in a neutral aqueous Na_2SO_4 electrolyte. Copyrights reserved to the John Wiley & Sons, Inc.[324]

a conducting polymer around the HRG/MnO_2 hybrids. The three-dimensional wrapping not only provided an additional electron transport path (besides the HRG layer underneath MnO_2 NPs), but also actively participated in the charge storage process. The specific capacitance of the as-prepared composite material could be enhanced significantly (~20%) with values as high as ~380 F g^{-1}. The cycling performance with >95% capacitance retention over 3000 cycles.

Furthermore, HRG/MnO_2 nanocomposites have been applied to develop asymmetric supercapacitors. They make use of different potential windows of the two electrodes in order to increase the maximum operation voltage in the cell system, which may result in an enhanced specific capacitance and improved energy density.[323] In a recent study, an asymmetric supercapacitor with high energy density has been developed using HRG/MnO_2 nanocomposites as a positive electrode and activated carbon nanofibers (ACN) as a negative electrode in a neutral aqueous Na_2SO_4 electrolyte.[324] The composite material exhibits a maximum energy density of 51.1 W h kg^{-1}, in addition to a cycling durability with 97% specific capacitance retained even after 1000 cycles. Graphene has been applied as a negative electrode rather than activated carbon nanofibers. Zilong *et al.* developed a flexible solid-state asymmetric supercapacitor based on two types of electrodes: a MnO_2/ZnO core–shell nanorod array and a hydrogen iodide (HI) reduced graphene oxide assembly.[323]

Apart from MnO_2, electrochemically active Mn_3O_4 NPs and their composites with high power nature have attracted research interest in the field of supercapacitors.[325] Although only a few studies were reported with Mn_3O_4 as the supercapacitor electrode material due to its extremely low electrical conductivity (10^{-7} to 10^{-8} S cm^{-1}), the number is increasing by the encouraging results obtained from combining highly conductive graphene with Mn_3O_4 NPs.[326] Wang *et al.* demonstrated the preparation of HRG/Mn_3O_4 nanocomposites and studied their electrochemical behavior.[242] Densely distributed Mn_3O_4 NPs with diameters of ~10 nm on the surface of graphene sheets played a crucial role in enhancing the electrochemical performance. The nanocomposites exhibited a high specific capacitance of 175 F g^{-1} in a 1 M Na_2SO_4 electrolyte and a 256 F g^{-1} in 6 M KOH electrolyte, respectively. In another example, the rate capability and electrochemical stability of the HRG/Mn_3O_4 electrode could be enhanced by the preparation of porous HRG/Mn_3O_4 nanocomposites *via* a solution-based approach.[327] The HRG/Mn_3O_4 electrode exhibits a much better rate capability compared to the pristine electrode with a maximum specific capacitance of 236.7 F g^{-1} in a 2 M KOH aqueous electrolyte with a current density of 1 A g^{-1} and a voltage window of −0.5 to 0.40 V. More importantly, around 71% of the specific capacitance was retained even after increasing the current density up to 4 A g^{-1}. The measured specific capacitance of 106 F g^{-1} at a high charge–discharge current density of 12 A g^{-1} suggested a good rate capability of as-prepared HRG/Mn_3O_4 nanocomposites. Furthermore, a decrease of 6.32% of the initial capacitance even after 1000 cycles revealed a good electrochemical stability of the HRG/Mn_3O_4 electrode.

For *group 8 metals*, graphene-based iron oxide nanocomposites have attracted attention in supercapacitors. Fe_3O_4 is a promising electrode material due to its high theoretical Li storage capacity, which offers a high pseudocharge capacitance through the associated redox reaction. Mainly, Fe_3O_4 NPs have been combined with graphene to increase and enhance the surface area and electrical conductivity of the material in order to achieve high capacitance in electrical double layer capacitors.[328] Shi *et al.* reported the synthesis of HRG/Fe_3O_4 nanocomposites, which were used to fabricate thin film supercapacitor electrodes by applying a spray deposition technique without the need for adding insulating binders.[329] The composite electrode showed higher specific capacitance than containing pristine Fe_3O_4 NPs, which can be further optimized by tuning the Fe_3O_4 : HRG ratio with a maximum specific capacitance of 480 F g^{-1} at a discharge current density of 5 A g^{-1} obtained at 73.5% Fe_3O_4 NPs. These nanocomposites also showed stable cycling performance without any decrease in the specific capacitance after 10 000 charge–discharge cycles. In another study, Qu *et al.* prepared sandwich-like HRG/Fe_3O_4 nanocomposites by direct growth of FeOOH nanorods on the surface of graphene sheets and the subsequent electrochemical transformation of FeOOH to Fe_3O_4.[330] The hybrid material exhibited a capacitance up to 304 F g^{-1} even at a current density of 10 A g^{-1}, which is much higher than that of many metal oxide based anode materials and comparable to (or even higher than) that of cathode materials such as MnO_2, Co_3O_4, V_2O_5 and MoO_3. The excellent rate capability of the nanocomposite was attributed to the synergistic effect of Fe_3O_4 and graphene. In addition to Fe_3O_4 pristine Fe_2O_3 and FeOOH have been applied as electrode materials in supercapacitors. However, the corresponding HRG/Fe_2O_3 and HRG/FeOOH nanocomposites have been reported only rarely.[331,332]

Besides iron, the applications of graphene-based nanocomposites of ruthenium (Ru) in supercapacitors have been reported in the literature among the elements in group 8.[333,334] In particular, hydrous and amorphous ruthenium oxide (RuO_2) has attracted attention because of its high capacitance, reversible charge–discharge features and good electrical conductivity, despite its high cost.[335] In order to enhance the electrochemical properties of RuO_2 hybrids of RuO_2 with various carbonaceous materials activated carbon, CNTs and exfoliated graphite have been synthesized, which have generated excellent results in the past.[336] Exploiting the distinctive properties of graphene, Wu *et al.* prepared HRG/RuO_2 hydrous nanocomposites by a combination of sol–gel and low-temperature annealing processes. A high performance of HRG/RuO_2-based electrochemical capacitors has been achieved by varying the Ru loading.[337] The nanocomposites delivered a maximum specific capacitance of 570 F g^{-1} with 38.3 wt% Ru, which is much higher than that of pure HRG (148 F g^{-1}) with a good rate capability, electrochemical stability and high energy power density. Wang *et al.* have prepared HRG/RuO_2 nanocomposite capacitors which were coupled with HRG/$Ni(OH)_2$ composite electrodes to fabricate asymmetrical supercapacitors, which exhibited a high specific capacitance and high energy and power densities.[338]

For *group 9 metals*, several reports on the application of graphene-based cobalt oxide nanocomposites in supercapacitors have appeared in the literature.[339] In a recent report, Fan and co-workers have exploited both the electrochemical properties of Co_3O_4 (high theoretical specific capacitance (~3560 F g^{-1}), high redox activity and its good reversibility) and the intriguing properties of graphene (high conductivity) in a HRG/Co_3O_4 electrode for supercapacitors.[340] The as-prepared HRG/Co_3O_4 electrode delivered a maximum specific capacitance of 243.2 F g^{-1} at a scan rate of 10 mV s^{-1} in 6 M KOH aqueous solution with >95% specific capacitance retention even after 2000 cycles. In another report, a HRG/Co_3O_4 electrode was prepared by Zhou *et al.* by a two-step surfactant assisted method, where HRG platelets were incorporated into scrolls of Co_3O_4.[341] The Co_3O_4 scrolls were composed of nanorods, stacked in a parallel fashion, and they were attached to the basal planes and edges of HRG nanosheets by their residual oxygen functional groups. By virtue of the unique scrolled structure of HRG/Co_3O_4 and the synergetic effect between HRG nanosheets and Co_3O_4, the as-prepared electrode exhibited an ~13 times higher specific capacitance than pristine Co_3O_4 NPs (*i.e.*, specific capacitance of 163.8 F g^{-1} at a current density of 1 A g^{-1}).

In addition, Co-based layered materials were utilized as electrodes in supercapacitors.[342] As an example, HRG/Co–Al nanocomposites containing Co–Al layered double hydroxide nanosheets (LDH-NS) as a precursor and their application in a pseudocapacitor were reported by Jin and co-workers.[343,344] In this case, HRG/Co–Al hybrids were fabricated by exploiting the electrostatic interaction between the positively charged layers of Co–Al LDH-NS and the negatively charged graphene sheets to create a layered assembly of two sheets.[344] This kind of face-to-face assembly of Co–Al LDH-NS and HRG facilitated a maximum contact between the layers and graphene sheets, which in turn leads to a fast electron transport through the graphene during the redox reaction. The HRG/Co–Al LDH-NS electrode demonstrated a remarkable performance with a maximum average capacitance of 778 F g^{-1} at a scan rate of 5 mV s^{-1}, and it delivered an energy density of 7.7 W h kg^{-1} at a power density of 4.8 kW kg^{-1}. In an extension of this work Jin and co-workers achieved an improvement of the specific capacitance of the Co-based electrode by preparing HRG/Co–Al LDH-NS multilayer films, which exhibited a high specific capacitance of 1204 F g^{-1} and an areal capacitance of 90 F m^{-2} for a scan rate of 5 mV s^{-1}.[345] Here, the flexible electrode was fabricated by layer-by-layer deposition of a HRG/Co–Al LDH-NS film onto a PET substrate (*cf.* Fig. 16).

From the *metals of group 10*, the majority of the nickel nanocomposites with graphene have found applications in energy storage systems. In particular, their oxides, in particular HRG/NiO and HRG/$Ni(OH)_2$ have been applied as electrode materials in supercapacitors.[346,347] Owing to their high theoretical capacity (2584 F g^{-1} within 0.5 V for NiO), their low price and excellent pseudocapacitive behavior, both NiO and $Ni(OH)_2$ have been considered as suitable replacement for the more expensive amorphous RuO_2.[348,349] However, these materials largely suffer from poor electrical conductivity, low accessible surface areas and volume changes during the cycling process. To address these problems, various strategies were adopted, including the support of graphene to enhance the electrical conductivity and to improve the overall electrochemical performance of the material. Several techniques have been applied to prepare HRG/nickel oxide nanocomposites with different morphologies to minimize particle aggregation and to maintain a high surface area during the charge–discharge process.[350,351]

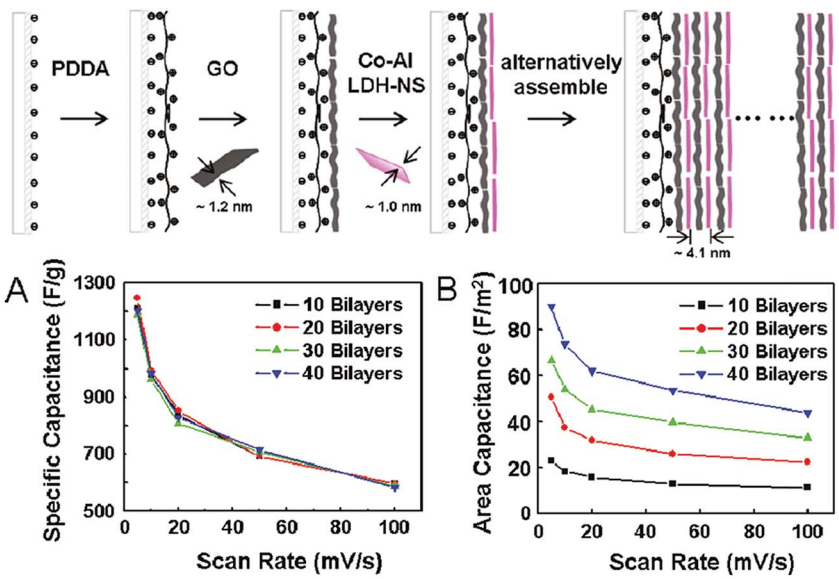

Fig. 16 Schematic illustration of the layer-by-layer assembly process for making multilayer films of positively charged Co–Al LDH-NS and negatively charged HRG sheets. Electrochemical properties of Co Al LDH-NS/GO films after reduction. (A) Specific capacitance of the four films with 10, 20, 30, and 40 bilayers at various scan rates. (B) Areal capacitance of the four films at various scan rates. Copyrights reserved to the American Chemical Society.[345]

In a recent study Lv *et al.* proposed a multi-step strategy to produce sandwich and membrane-like HRG/NiO nanocomposites.[352] The hybrids were comprised of a 3D network of homogeneously distributed NiO NPs tightly fixed on planar graphene nanosheets, which effectively avoid any particle aggregation during charge–discharge cycling and maintain the active surface area. The immobilization of NiO NPs between adjacent graphene nanosheets created ordered channels for ion transport. HRG/NiO sandwich membranes delivered a better capacitive performance. Furthermore, this type of hybrid can be easily manipulated for other energy storage applications due to its membrane-like morphology. Cao *et al.* demonstrated in a recent study the use of HRG/NiO nanocomposites for supercapacitors.[353] The HRG/NiO hybrid exhibited a very high specific capacitance of 816 F g^{-1} at a scan rate of 5 mV s^{-1} with a stable cycling performance even up to 2000 cycles. The good electrochemical properties of the HRG/NiO composite were attributed to its unique 3D network structure with a large specific surface area, which facilitated the rapid transport of electrolyte ions.

Apart from HRG/NiO composites with a 3D network structure, two-dimensional sheets like HRG/NiO nanocomposites have been reported to have excellent electrochemical properties in supercapacitors and deliver a much larger specific capacitance and capacity retention than that of pure NiO (*ca.* 528 F g^{-1} at 200 mA g^{-1} with a capacity retention of 95.4% after 1000 cycles). The hybrids were prepared by self-assembly; the electrostatic interactions of the two species were exploited to create monolayer HRG/NiO sheets with Ni^{2+} ions adsorbed on both sides of HRG sheets.[354] During the process NiO NPs ($\xi \approx 5$–7 nm) were grown densely and homogeneously on a graphene monolayer. The size of the NPs was restricted due to the confining effect of disordered graphene nanosheets. Moreover, the confinement effect of HRG facilitated effective separation of NiO NPs. As a result, the surface area of the material was enhanced significantly, as demonstrated by the specific surface area of the as-prepared hybrid material (134.5 m^2 g^{-1}), which is larger than that of pure NiO (*ca.* 42 m^2 g^{-1}).

The enhanced electrochemical performance of HRG/NiO nanocomposites was demonstrated in another study, where spherical HRG/NiO hybrids showed a superior energy storage performance and an impressive structural stability.[355] The nanocomposites were prepared by spray pyrolysis. Nucleation and growth of NiO nanocrystals occurred predominantly on the surface of GO sheets, which are subsequently reduced to HRG/NiO composites. The globular HRG/NiO nanocomposites were constituted by encapsulation of NiO NPs (~30 nm) in graphene sheets. This encapsulation resulted in the formation of an interconnected 3D network structure, which offers the unique advantage of introducing conductive pathways through the whole structure and improving in parallel the mechanical strength of the resulting composites.

Apart from NiO, $Ni(OH)_2$ has been studied in supercapacitors because of its layered structure and its anion exchange capabilities.[356–359] With the combination of layered $Ni(OH)_2$ and graphene a specific capacitance of 1568 F g^{-1} at a current density of 4 A g^{-1} could be achieved. This is significantly higher than that of bare $Ni(OH)_2$.[360] A HRG/$Ni(OH)_2$ composite electrode with such high capacity was prepared in a mechanically assisted solid-state reaction. Prior to the solid-state reaction, graphene nanosheets were functionalized with benzenesulfonate groups, which play a critical role in forming fine and uniformly distributed $Ni(OH)_2$ NPs and in preventing particle aggregation. In another study, a HRG/$Ni(OH)_2$ composite electrode was synthesized from α-$Ni(OH)_2$ NPs, while most of the studies related to $Ni(OH)_2$ were reported on β-$Ni(OH)_2$ which is easily accessible, but NPs of the α polymorph have superior electrochemical properties compared to their β counterpart.[361] Lee *et al.* have described a template-free method for making HRG/α-$Ni(OH)_2$ nanocomposites in ethylene glycol with a different GO/to $Ni(OH)_2$ mass ratio. The highest capacitance (1215 F g^{-1} at a scan rate of 5 mV s^{-1}) was observed in an electrode prepared in a 1 : 20 mass ratio of GO to $Ni(OH)_2$. Notably, by increasing the mass of $Ni(OH)_2$ NPs the capacitance decreased due to the presence of Ni^{2+} ions around HRG, which induce an aggregation of NPs, thereby leading to poor dispersion and low capacitance.

By virtue of their intercalation properties, metal based layered double hydroxides (LDH) were combined with graphene to fabricate electrodes for supercapacitors.[362] LDHs are well-known anionic or hydrotalcite-like clays. Typically, they contain divalent and trivalent cations and a variety of organic or inorganic anions.[362] Gao *et al.* reported the hydrothermal synthesis of HRG/NiAl LDH nanocomposites, where Ni/Al LDH platelets were formed *in situ* on the graphene surface.[363] The LDA/graphene composite was comprised of thin hexagonal platelets with a diameter of 50 nm, decorated on graphene sheets as a loose lamellar structure. This arrangement prevents restacking of graphene nanosheets and preserves the active surface area. In addition, graphene sheets overlap loosely with each other to afford a three-dimensional conducting network, which facilitates fast electron transfer and enhances the contact between the electrode and the electrolyte. With this electrode a high specific capacitance of 781.5 F g^{-1} at a scan rate of 5 mV s^{-1} with long cycle life was obtained. In more recent studies, nitrogen-doped graphene (NHRG) has been used to further enhance the electrochemical performances of LDH nanocomposites, by improving the access to redox sites, enhancing the structural stability and increasing the conductivity. Hou *et al.* designed a unique composite of Ni and Ni/Co double hydroxide nanoparticles wrapped in nitrogen-doped graphene (NiH@NHRG & NiCoDH@NHRG) sheets.[364] The hybrid materials were prepared hydrothermally and contained a well-defined network of nanostructures confined in NHRG sheets. The crystallinity and well-defined structure of the as-prepared nanocomposites promoted the transfer of electrons from redox sites to the electron collector and *vice versa*, which allowed nickel and cobalt to contribute to the double pseudocapacitance. The electrode material showed a remarkable performance compared to most previously reported graphene-based LDH nanocomposites.

For *group 11*, only a few reports on the application of HRG/Cu_2O nanocomposites in supercapacitors have appeared so far.[365] For group 12 metals applications as HRG/ZnO nanocomposites for energy storage were reported.[366–368] HRG/ZnO

nanocomposites showed enhanced performance compared to pristine ZnO NPs as electrode materials in supercapacitors. HRG/ZnO nanocomposites prepared by spray pyrolysis exhibited a specific capacitance of 61.7 F g^{-1} and a maximum power density of 4.8 kW kg^{-1}. A capacitance of 62.2 F g^{-1} and a maximum power density of 8.1 kW kg^{-1} were achieved for HRG/ZnO nanocomposites prepared by reduction with glucose.[369,370] The electrochemical capacitative performance appeared to depend on the morphology of HRG/ZnO nanocomposites.[371] Chen *et al.* demonstrated a composite material with a low weight percent of HRG to be controlled by the homogeneous incorporation of HRG sheets within the ZnO matrix.[372] A specific capacitance (308 F g^{-1} at 1 A g^{-1} in the potential range of 0.0–1.0 V) and cycling stability (6.5% decay over 1500 cycles) has been achieved for a ZnO to HRG mass ratio of 93.3 : 6.7. The 3D network structure of the hybrid allowed the diffusion of electrolyte ions to the electrochemically active sites. Huang *et al.* used layer-by-layer deposition to fabricate HRG/ZnO nanocomposites with ZnO nanorods vertically aligned on HRG sheets using PET as a flexible substrate.[373]

Clearly, the combination of graphene with various metal oxide NPs leads to a significant improvement as electrode materials in supercapacitors. For instance, these nanocomposites demonstrated enhanced specific surface area, improved electrical and ionic conductivities, good cyclic stability, and excellent specific capacity as well as increased energy and power density. These enhanced properties are mainly attributed to the synergistic effects due to characteristic surface interactions between the components. Despite the great potential of these materials in supercapacitors, several problems remain: (i) the synthesis of electroactive nanocomposites with controlled size, morphology and phases is still challenging. Degradation of the electrode material due to the aggregation of graphene layers during the charge–discharge process is another major problem in this area. (iii) The contamination of the electrode material due to impurities introduced by improper reduction of GRO is a major concern.

3.1.3 Solar cells. Solar cells or photovoltaic cells are the electrical devices that directly convert sunlight energy into electricity by the photovoltaic effect. Graphene-based nanocomposites have potential applications in these devices due to their excellent optical, electronic and electrical properties.[374] Graphene and graphene-based materials have been applied as transparent electrode materials in photoelectrochemical and photovoltaic devices. Graphene can be either a conductive platform or active element such as an electron acceptor in photovoltaic and photoelectrochemical devices, (*e.g.* in dye-sensitized solar cells (DSSCs)), which have gained significant attention due to their moderate light-to-electricity conversion efficiency, easy fabrication and low cost. DSSCs are composed of a photoelectrode, a counter electrode, an electrolyte and a sensitizing dye.

For *group 4 metals*, TiO_2 NPs were commonly applied as photoanodes in DSSCs due to their large surface area, which facilitates anchoring of sensitizing dye molecules. Furthermore, due to their high conductivity and low cost, HRG/TiO_2 nanocomposites have become attractive electrode materials for solar cell, electrochemical sensor and biosensor applications, where TiO_2 NPs exhibit improved electrochemical properties through the support of graphene.[375–377] Recently, dye-sensitized solar cells (DSSCs) were fabricated using HRG/TiO_2 photoanodes, where 0.5 wt% incorporated graphene demonstrated a power conversion efficiency of 4.28%, which is 59% higher than that without graphene. The incorporated graphene, apart from increasing the dye adsorption also enhanced the electron lifetime significantly. In another study, an enhanced power conversion efficiency of 7.25% was obtained in DSSCs by delicately controlling the morphology of TiO_2 NPs on graphene sheets.[378] For this purpose, various HRG/TiO_2 nanocomposites have been synthesized with different nanostructures including ultra-small 2 nm NPs, 12 nm NPs and nanorods. Among them, the photoanode based on the nanocomposites of ultra-small 2 nm TiO_2 NPs exhibited the highest power conversion efficiency. For the electrochemical sensing, a HRG/TiO_2 modified glassy carbon electrode has been prepared, which showed favorable electron transfer kinetics and electrocatalytic activity for the oxidation of dopamine.[379]

Apart from TiO_2 in group 4, HRG/NiO nanocomposites were used to fabricate photoelectrodes in DSSCs. p-semiconducting nickel oxide (NiO) has been considered a potential photocathode material for dye sensitized solar cells (DSSCs) because of its large optical band gap (*ca.* 3.4 eV) and its high ionization potential (5.4 eV *vs.* vacuum). However, it suffers from its intrinsically low charge transfer rate.[380,381] Recently Yang *et al.* synthesized supported NiO by graphene to enhance the charge transport properties of NiO cathodes. Apart from its large surface area and high conductivity, it may serve as a shuttle to enhance electron transport and to suppress the recombination in n-type DSSCs.[382] The novel HRG/NiO composite has doubled its power conversion efficiency when applied as a photoelectrode in p-DSCs. Additionally, the composite photocathode (with an appropriate amount of graphene) offers faster hole transport and larger surface area than bare NiO films.

HRG/Pt nanocomposites were applied as counter electrodes (CEs) in DSSCs.[383] Gong *et al.* prepared ultrathin films of HRG/Pt nanocomposites on conductive glass by layer-by-layer self-assembly using monolayers of PDDA/graphene/PDDA/H_2PtCl_6 as a precursor.[384] The HRG/Pt monolayer as a CE in DSSCs achieved 7.66% power conversion efficiency, which is comparable to 8.16% obtained from sputtered Pt as a CE. Commonly, in Pt based DSSCs the amount of Pt loading determines the catalytic activity and cost of the device. Therefore, the support of graphene in the composite CE reduced the amount of Pt ($\sim$1000 fold) by lowering the cost of CEs without compromising the activity of the device.

p-type semiconducting Cu_2O in *group 11*, which exhibits high solar absorbance, has great potential for photovoltaic device applications.[385] Wu *et al.* prepared conductive and transparent electrodes by electrochemical deposition of crystalline Cu_2O films on a PET (polyethylene terephthalate) substrate that was spincoated before graphene oxide.[386] Electrochemical deposition of Cl-doped n-type Cu_2O was carried out by Wu *et al.* to prepare HRG/Cu_2O–Cl electrodes for photovoltaic applications.[387] Doping with Cl is carried out with carrier

concentrations of up to 1×10^{20} cm^{-3}. The surface coverage of Cl depends on the degree of Cl doping. Cl–Cu_2O deposited by addition of 0.3 mmol or 1 mmol $CuCl_2$ showed a higher light-to-electron/hole conversion efficiency.

From the above results, it is clear that the application of composites from graphene/inorganic NPs as photoelectrode materials have great potential in photovoltaic cells due to ease of processing and flexible substrate compatibility. Besides, graphene offers a broad solar spectrum; therefore, graphene-based materials as transparent electrodes may further improve the quantum efficiency of solar cells. However, in order to utilize the full potential of graphene inorganic nanocomposites in photovoltaic devices, several challenges need to be tackled: (i) the controlled synthesis of graphene, free from other chemical residues, is necessary to achieve the enhanced performance of graphene in solar cells. (ii) Since the defect-induced or doped graphene exhibits higher activity than pristine graphene, the optimization of the defect concentration during the preparation of graphene would be beneficial, which is a rather challenging task.

3.1.4 Fuel cells. A fuel cell utilizes the chemical energy of another fuel, which is chemically stored in electrochemical cells to produce electricity.[388] Unlike batteries or other energy storage devices, it generates electricity through the reaction between a fuel (anode) and an oxidant (cathode), such as hydrogen/oxygen or methanol/oxygen, *etc.* Fuel cells comprised of a cathode, an anode and a separation membrane, where cathodes are the prominent materials, require special attention for the large scale commercial development. Commonly, noble metal NPs such as Pt, Ru, Au, and their hybrid materials are applied as electrocatalysts for the oxygen reduction reaction (ORR). However, the high cost of these nanocatalysts prevents their large scale application in the commercial development. Recently, graphene inorganic nanocomposites have gained prominent significance as a new class of electrocatalysts, due to the outstanding physico-chemical properties of graphene, such as excellent electronic conductivity, huge specific surface area (2600 m^2 g^{-1}) and high stability.[389]

For this purpose, various graphene-based inorganic nanocomposites have been exploited as electrocatalysts in ORR. From *groups 4 to 9*, only a few examples of graphene based Co nanocomposites that have been applied as electrocatalysts in oxygen reductions reactions (ORR) and oxygen evolution reactions (OER) have appeared in the literature.[390] However, the results obtained so far are very encouraging and indicate the significant potential of HRG based Co nanocomposites as electrocatalysts in fuel cells.[391,392] As an example, Liang *et al.* developed a hybrid material consisting of spinel-structured Co_3O_4 nanocrystals (~4–8 nm in size) grown on HRG sheets as a high performance bi-functional catalyst for the ORR and OER.[393] Notably, pure Co_3O_4 NPs exhibit little ORR activity, but, the HRG/Co_3O_4 catalyst prepared *via* a two-step hydrothermal synthesis showed unexpectedly high ORR activities in alkaline solution, comparable to those of currently available commercial Pt/C catalysts. In addition, they also demonstrated a better stability and durability than a Pt/C catalyst. The ORR catalytic activity of the HRG/Co_3O_4 catalyst was further enhanced by nitrogen doping of HRG sheets, where the N-doped hybrid exhibited a similar catalytic activity, but a stability superior to Pt in alkaline solutions.

Moving to *group 10*, HRG/Pd nanocomposites were used as electrocatalysts for the ORR and the oxidation of alcohols in different types of fuel cells, such as DMFCs, DEFCs, and DFAFCs.[394–396] Due to the electrocatalytic activity of Pd NPs, HRG/Pd electrocatalysts have gained attention as a cost-efficient replacement for Pt-based electrocatalysts, which are often poisoned by reaction intermediates like CO in acidic media. Zhao *et al.* applied poly-pyrrole-functionalized graphene as a carbon support for the Pd catalyst, which resulted in a higher electrocatalytic activity and stability for methanol oxidation compared to that of the more expensive Pt-based electrocatalysts.[397] Yang *et al.* exploited HRG/Pd based electrocatalysts for the catalytic oxidation of formic acid in DFAFC.[398] The as-prepared hybrid electrocatalysts have excellent catalytic activities for the electrooxidation of formic acid, which is attributed to the small size and high dispersion of Pd NPs and the stabilizing effect of the graphene support. Similarly, catalytic oxidation of formic acid was carried out with HRG/Pd nanocomposites.[399] However, the hybrid electrocatalyst was prepared by a galvanic displacement process in the absence of surfactants or stabilizers with a copper template. The as-prepared HRG/Pd electrocatalysts obtained by etching the copper template demonstrated higher catalytic activity than conventional Pd/Vulcan electrocatalysts for formic acid oxidation in high performance DFAFCs. Similarly, the catalytic oxidation of ethanol was carried out with HRG/Pd nanocomposites,[400] and graphene-supported ternary nanocomposites have also been applied as electrocatalysts in ORR and for the oxidation of alcohols.[401] For instance, HRG/Pd–MWCNT nanocomposites prepared by Machado *et al.* have shown enhanced ORR activity and excellent durability.[402] Ren *et al.* prepared ternary HRG/Pd–Pt nanocomposites in the absence of stabilizing agents as electrocatalysts for the oxidation of ethanol in alkaline media.[403]

Graphene-based platinum nanocomposites have been applied extensively as cathode and anode materials in several types of fuel cells including DMFCs (Direct Methanol Fuel Cells), DFAFCs (Direct Formic Acid Fuel Cells), PEMFCs (Proton Exchange Membrane Fuel Cells), PEFCs (Polymer Electrolyte Fuel Cells) and so on.[404] A wide application of platinum electrocatalysts in fuel cells has been hampered by their high costs and poor utilization coefficients. This can be overcome by carbon supports, such as SWCNTs, MWCNTs and carbon black (CB).[405] The physicochemical properties of graphene have been exploited in fuel cell applications by combining Pt NPs and graphene. The open and planar structure of graphene allows both sides of the sheet to be utilized for the catalysts. Therefore HRG/Pt nanocomposites can be applied as catalyst supports in fuel cells. Several studies have reported on the properties and application of graphene nanocomposites with platinum and other platinum based materials, such as HRG/Pt, HRG/PtRu, HRG/PtCo, HRG/PtAu, HRG/Pt_3Co and HRG/Pt_3Cr, as catalysts in DMFCs.[156,406–408]

HRG/Pt nanocomposites have been synthesized by direct reduction of Pt ions on Ar–H_2 or N_2-treated graphene sheets at

high temperature or by decoration of Pt NPs in water–ethylene glycol.[409,410] Zhou *et al.* introduced a one-step electrochemical reduction method for the preparation of HRG/Pt nanocomposites, which exhibited a higher catalytic activity and stability compared to the Pt/Vulcan and Pt/graphite, when applied as electrocatalysts for the oxidation of methanol in DMFCs.[411] Qiu *et al.* dispersed Pt NPs with an average size of ~4.6 nm on prefunctionalized graphene nanosheets with PDDA to prepare HRG/Pt nanocomposites.[412] Apart from providing the charged GO surface for the Pt NP deposition, PDDA helps to control the loading density of the NPs. The resultant HRG/Pt nanocomposites exhibit an improved higher electrochemical active surface area and better tolerance toward CO compared to only Pt. Thus the electrocatalytic activity is enhanced for the oxidation of methanol and the reduction of oxygen. Huang *et al.* chemically deposited Pt NPs with an average size of 2.3 nm on graphene nanoplatelets in order to circumvent the oxidation of graphite and subsequent reduction of graphene oxide by reduction or subsequent annealing.[413] The HRG/Pt composites exhibited an electrochemically active surface area (ECSA) of 53.6 $m^2 g^{-1}$, which is much larger than that of XC-72/Pt hybrids (33.7 $m^2 g^{-1}$). This was tested for methanol oxidation under acidic conditions in DMFCs. The nanocomposites exhibit excellent electrocatalytic activity and stability because of the graphene support, which significantly enhances the catalytic properties of Pt NPs and also plays a key role in decreasing the catalyst poisoning.

Platinum, however, has serious drawbacks. Most important are the costs and catalyst poisoning by the adsorption of CO formed during methanol electrooxidation. Thus different kinds of platinum-based alloys together with the graphene support, such as HRG/Pt–Ru and HRG/Pt–Au, have been tested in order to reduce the costs and to enhance the catalytic efficiency of the hybrid material.[414] Lee *et al.* reported the hydrothermal preparation of HRG/Pt–Ru nanocomposites, where PtRu NPs were uniformly dispersed on graphene nanosheets.[415] The surface area of HRG/Pt–Ru, investigated by hydrogen adsorption/desorption from the electrode surface, is 68 $m^2 g^{-1}$ (compared to that of Pt/MWCNT (20 $m^2 g^{-1}$) reported in the same study). Methanol electro-oxidation was carried out with a HRG/Pt–Ru catalyst, by cyclic voltammetry in 0.5 M H_2SO_4/1.0 M CH_3OH solution at 25 °C and showed a peak potential and peak current density of 968 mV and 20.8 mA cm^{-2}. In another study the electrocatalytic activity of HRG/Pt–Ru was tested for the electro-oxidation of both methanol and ethanol.[416] The composite material demonstrated enhanced diffusion efficiency and oxidation potential compared to the widely used Vulcan XC-72R carbon black catalyst support. Similarly, a Pt/Pd alloy on Nafion–graphene exhibited efficient electrocatalytic activity and stability towards ethanol oxidation in alkaline solution.[417] The hybrid anode catalyst showed good tolerance against poisoning by reaction intermediates during the electro-oxidation of ethanol. A hybrid material comprised of graphene supported Pt and Au delivered better electrocatalytic activity and selectivity.[418] The HRG/Pt–Au catalyst was prepared by electrodeposition of Pt–Au NPs on graphene. The morphology and the composition of the nanocatalyst were controlled by adjusting the molar ratio between the Pt and Au precursors. The HRG/Pt–Au electrocatalyst with a Pt/Au molar ratio of 2 : 1 exhibits the highest electrocatalytic activity toward the ORR (Oxygen Reduction Reaction) and methanol oxidation reaction.

Graphene supported bimetallic Pt–Au nanocomposites are important electrocatalysts in DFAFCs fuel cells for formic acid oxidation. The incorporation of Au has an effect on Pt NPs by promoting the direct oxidation of formic acid to CO_2 without pronounced CO intermediates.[419] Several reports appeared on the application of HRG/Pt–Au nanocomposites for the formic acid oxidation (FAO) which suggests that the electrochemical properties of the hybrid material are affected by the preparation method.[420] Zhang *et al.* reported on enhanced FAO activity of HRG/Pt–Au (20 wt%) nanocomposites prepared by $NaBH_4$ reduction.[421] Pt–Au alloy NPs could be dispersed with a polyelectrolyte process. Diallyldimethyl ammonium chloride acts as a nanoreactor for the preparation of the alloy NPs and facilitates the uniform dispersion of NPs on graphene. Rao *et al.* prepared HRG/Pt–Au NPs by polyol reduction and measured the anodic performance and compared it with that of commercial Pt/C (E-TEK) under DFAFC operating conditions.[422] The hybrid anode showed a maximum power density of 185 mW cm^{-2} in DFAFC at 303 and 333 K, which is higher than that of HRG/Pt nanocomposites without Au, measured as a reference. The enhanced electrochemical activity is attributed to the change in electronic structure of Pt by alloying with Au. In addition to the oxidation of alcohol and formic acid in fuel cells, graphene and Pt alloy nanocomposites also find applications in PEMFCs (Proton Exchange Membrane Fuel Cells), which were used as electrocatalysts for the oxygen reduction reaction (ORR).[423] ORR plays an important role in the electrochemistry of fuel cells, particularly in PEMFCs and PEFCs.[424] In a recent study, HRG/Pt nanocomposites prepared with perfluorosulfonic acid (PFSA) as a functionalization and anchoring agent were applied as electrocatalysts for ORR.[425] PFSA not only enhanced the Pt–graphene interactions and the stability of the catalyst, but also provided more channels for H^+ towards Pt surfaces, thereby creating more active catalytic sites (*cf.* Fig. 17). In addition, PFSA facilitates absorption of CO and water on the catalyst and the formation of an active Pt–OH oxy compound which promotes the oxidation of CO to CO_2. Such a PFSA-functionalized HRG/Pt hybrid showed an improved excellent oxidation of CO and lower loss rate of electrochemical active area. In another study, graphene supported Pt_3Co and Pt_3Cr nanocomposites were applied as electrocatalysts for ORR which exhibited a 3–4 times higher activity than HRG/Pt.[426] This enhanced activity is attributed to the inhibition of formation of hydroxyl groups on the Pt surface. Maximum power densities of 875 and 985 mW cm^{-2} were observed with HRG/Pt_3Co and HRG/Pt_3Cr cathodes, respectively.

Apart from graphene-based inorganic nanocomposites, functionalized and doped graphene has also been applied as a metal free catalyst in oxygen reduction reactions in fuel cells.[427] In a recent study, the enhanced electrochemical performance of amino-functionalized graphene as an efficient electrocatalyst in ORR has been demonstrated.[428] The electrocatalyst was obtained solvothermally from GO in the presence of ammonia.

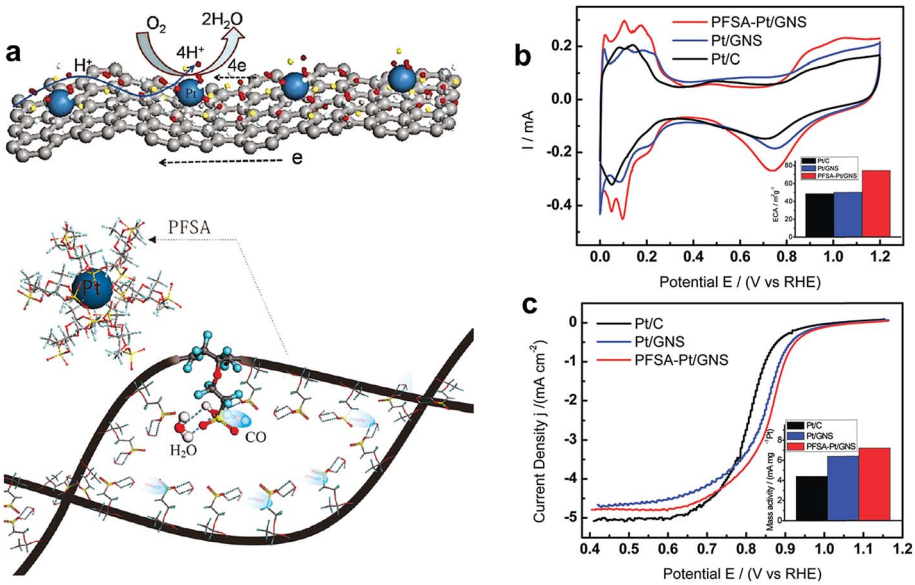

Fig. 17 (a) Schematic illustration of the electrocatalytic reaction and electro oxidation mechanism carried out with HRG/Pt nanocomposites. (b) CV curves of PFSA–Pt/GNS, Pt/GNS, and Pt/C catalysts. (c) Current–potential curves for ORR in O_2-saturated 0.5 mol L^{-1} H_2SO_4 and comparisons of ORR mass activities and specific activity of catalysts. Copyrights reserved to the American Chemical Society.[425]

The results demonstrated that the graphitic and amino-type of nitrogen components determine the onset potential and electron transfer number, while the total content of graphitic and pyridinic nitrogen atoms is the key factor to enhance the current density in the electrocatalytic activity for ORR.

It is clear that graphene-based inorganic nanocomposites show enhanced performance as electrocatalysts in fuel cells compared to cost-inefficient Pt/C commercial electrocatalysts. However, to further improve the performances of these materials and to fully exploit them commercially, extensive research is still required. Among various challenges that occur in this field, maintaining the smaller size of NPs on the surface of graphene is a major problem. Furthermore, the electrocatalytic activity of graphene-based inorganic nanocomposites can be enhanced by controlling the interactions between graphene and the NPs, which often proves to be difficult. Additionally, the stability of the electrocatalyst plays a major role in the efficiency of fuel cells.

3.2 Catalysis

The unique 2D structure of graphene and its physical, chemical and mechanical properties provide an ultimate support for any catalytic activity. Although single layers of graphene have not been used as a catalytic support so far, the application of few-layers of graphene in the field of catalysis has gained significance.[429] Apart from the large theoretical specific surface area, high adsorption capacity and good biocompatibility, graphene based materials have been applied as support materials in catalysis. By the adsorption of metal and metal oxide NPs on the surface of graphene, intriguing properties emerged due to the interactions between the individual components, which have been exploited for catalytic, electro- and photoacatalytic applications.

3.2.1 Photocatalysis. Due to its sp^2-hybridized two-dimensional structure and the associated electrical conductivity, and large surface area, graphene has received much greater attention in photocatalysis than most other carbonaceous materials.[430] Moreover, the recent development of a wide range of sequential oxidation–reduction methods for the large scale synthesis of graphene makes it an attractive support for anchoring inorganic nanomaterials such as TiO_2 for photocatalytic applications.

Titanium dioxide (TiO_2) is an attractive semiconductor material from *group 4* metals that has been used in many fields including photochromic devices and sensors. It is used in particular as a photocatalyst to decompose organic contaminants in water and air.[431] A popular pathway for enhancing the photocatalytic activity of TiO_2 is the formulation of carbon–TiO_2 nanocomposites by incorporating carbon nanomaterials (including graphene).[432] Significant work has been done on HRG/TiO_2, where the photocatalytic activities of TiO_2 NPs have been reported to be enhanced by the inclusion of graphene.[433,434] The catalytic application of HRG/TiO_2 nanocomposites is largely dependent on the crystal morphology of TiO_2 NPs as well as their density on HRG sheets.[435,436] Recently, Wang *et al.* reported the synthesis of HRG/TiO_2 nanocomposites, where monodisperse anatase TiO_2 NPs were deposited on the surface of HRG sheets without agglomeration.[437] The NPs exhibited a tetragonal *cuboid-morphology* with square crystal facets and a side length ranging from 250 to 300 nm, and they were enclosed by the {001} and {100} crystal facets (*cf.* Fig. 18). HRG/TiO_2 nanocomposites with controlled exposed crystal facets were obtained by varying the concentration of the starting precursor solutions and the reaction time. The as-prepared HRG/TiO_2 nanocomposite exhibited enhanced photocatalytic activities compared to the reported HRG/P25

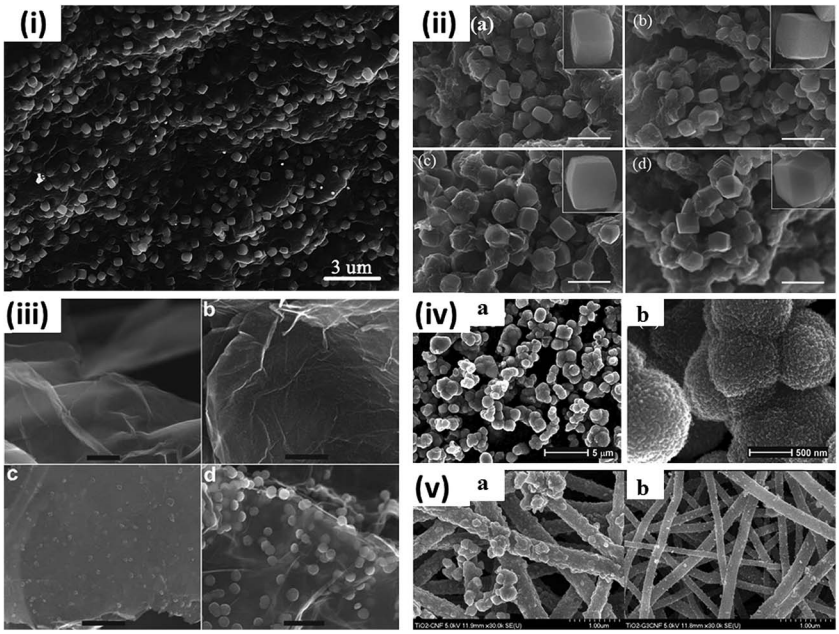

Fig. 18 SEM images of various HRG/TiO_2 nanocomposites. (i) As-prepared HRG/TiO_2 nanocomposites synthesized *via* hydrothermal reaction with aqueous solutions containing $(NH_4)_2TiF_6$ (0.03 M) and GO at 160 °C for 4 h. (ii) Illustrates the gradual change of the morphology of TiO_2 NPs with the increase of time (ii-a) cuboid-like morphology of anatase TiO_2 NPs obtained in 2 h reaction time. (ii-b) After 8 h, the NPs grow fatter and the four lateral facets of the cuboid-like particles rose in the waist. (ii-c) After 12 h (ii-d) after 24 h, the NPs turned into truncated octahedral morphologies. The inset shows the corresponding magnified SEM images. Copyrights reserved to the RSC publishing.[437] (iii) SEM images of HRG treated in the sulfuric acid reaction solution containing titanium sulfate at 100 C (a) pristine graphene sheets (b) after 1 h (c) after 4 h (d) after 6 h. Scale bar in (a–d) 400 nm. Copyrights reserved to the John Wiley & Sons, Inc.[220] (iv-a and b) SEM images of pristine TiO_2. Copyrights reserved to the Elsevier Ltd.[441] (v) SEM images of (a) TiO_2–CNF (carbon nanofibers) (b) TiO_2–CCNF (carbon composite nanofibers). Copyrights reserved to the Elsevier Ltd.[442]

samples in both photocatalytic H_2 evolution from a methanol solution and degradation of methylene blue.[438]

The improved reactivity of HRG/TiO_2 nanocomposites was attributed to the extended optical absorption resulting from surface impurity doping (defects) and increased lifetime of TiO_2-confined holes due to the injection of photoexcited electrons into the carbon nanomaterials.[439] Recently, Liang *et al.* demonstrated the role of defects in photocatalytic activities of HRG/TiO_2 nanocomposites. They prepared HRG/TiO_2 nanocomposites with low defect density using SEG (Solvent Exfoliated Graphene) as a precursor that exhibited a significantly larger enhancement in the photo-oxidation of CH_3CHO and photoreduction of CO_2.[375] Notably, in contrast to the conventional role of defects in catalysis, the less defective SEG based TiO_2 nanocomposite was shown to possess a higher photocatalytic activity than the graphene-based nanocomposite (graphene has a significantly higher defect density than SEG). Furthermore, due to a variation of the graphene processing and nanocomposite loading, the optimized nanocomposites showed an improvement of their catalytic activities. In another study, Fan *et al.* prepared HRG/TiO_2 nanocomposites by UV-assisted photocatalytic reduction, hydrazine reduction or hydrothermal reduction and compared their photocatalytic activities for H_2 evolution from alcohol under UV irradiation.[440] The HRG/TiO_2 nanocomposite prepared by a hydrothermal method turned out to be the most efficient photocatalyst that exhibited stronger interactions between TiO_2 and graphene sheets. Such strong interactions accelerated the transfer of photogenerated electrons on TiO_2 to graphene, suppressed the recombination of charge carriers thereby increasing the photocatalytic performance. The HRG/TiO_2 ratio in the composite determined the photocatalytic performance, and the optimum mass ratio was found to be 1/0.2.

Nanocomposites of the *group 5* elements niobium and tantalum have been rarely reported in the literature.[443,444] However, in some cases they have been used as photocatalytic materials. In a very recent example, Qi *et al.* reported a novel HRG/Nb_2O_5 nanocomposite, which exhibited excellent visible light photocatalytic performance.[445] In addition, these transition metals have also been incorporated into graphene-based mixed metal oxides of indium (In) and tantalum (Ta) composites, respectively.[446,447] The composite of HRG/$InNbO_4$ was prepared hydrothermally and shown to improve the photocatalytic activity of $InNbO_4$, a visible-light driven photocatalyst.[446] Particles of monoclinic $InNbO_4$ uniformly dispersed on the surface of HRG sheets provided a sufficient contact surface between the HRG and $InNbO_4$ particles and thus facilitated the carrier transport. The kinetic constant of methylene blue (MB) removal with the HRG/$InNbO_4$ composite was slightly higher (0.0346 min^{-1}) than that of pristine $InNbO_4$ (0.0185 min^{-1}). Furthermore, the ability of graphene to act as an electron transfer highway was demonstrated by the preparation of

nitrogen-doped HRG/$Sr_2Ta_2O_{7-x}N_x$ composites by *in situ* photo-induced reduction of GRO.[447] During the reaction under visible-light, tantalum oxide accelerated the reduction process by potentially injecting electrons into the GRO conduction band and reducing more functional groups. In addition, to carry out photocatalytic efficiency measurements with HRG/$Sr_2Ta_2O_{7-x}$-N_x composites, platinum was loaded onto graphene sheets. The HRG/$Sr_2Ta_2O_{7-x}N_x$ composites containing platinum demonstrated an additional ~80% increase in hydrogen formation and a quantum efficiency of 6.45% (177% increase compared to pristine undoped $Sr_2Ta_2O_7$) due to the efficient charge carrier separation on the photocatalyst.

In *group 11*, photocatalytic applications have been reported for graphene supported silver and silver based binary and/or ternary nanocomposites, containing silver halides and other metallic NPs, such as graphene oxide/Ag/AgX (X = Cl, Br) and HRG/Ag/TiO_2.[448,449] Silver and silver halide based nanomaterials display plasmon resonance in the visible region, due to the presence of metallic Ag NPs. Therefore, they can be applied as photocatalysts for the degradation of pollutants under visible light. The intrinsic catalytic properties of such silver based materials have been boosted by a graphene support which acts as an ideal catalyst carrier, due to its large surface area, and the locally conjugated aromatic system. Graphene oxide/Ag/AgX hybrid composites prepared in oil/water microemulsions were used for the plasmonic photocatalytic degradation of methyl orange in sunlight.[450] Finally HRG/Ag and HRG/Ag/TiO_2 nanocomposites were applied for the catalytic reduction of 2-nitroaniline to 1,2-benzenediamine and *p*-nitrophenol to *p*-aminophenol.[451]

Semiconducting ZnO finds technological applications in several fields, including photocatalysis.[452,453] HRG/ZnO nanocomposites have shown enhanced photocatalytic performance in the reduction of Cr(VI) compared to pure ZnO with a maximum removal rate of 96% (under UV light irradiation).[454] Furthermore, the photocatalytic degradation of dyes for waste water purification was carried out using a HRG/ZnO hybrid semiconductor photocatalyst.[455] Xu *et al.* reported the photocatalytic performance of HRG/ZnO nanocomposites, which were prepared by reducing the surface bound GO on ZnO NPs with hydrazine for the degradation of organic dyes.[456] The hybridization of graphene and ZnO increased the photocatalytic efficiency of ZnO by a factor of ~5 (with 2.0 wt% of graphene).

In another study, the photocatalytic decomposition of rhodamine 6G under UV light was carried out with a HRG/ZnO hybrid photocatalyst, which was prepared with PVP (poly vinyl pyrrolidone) functionalized graphene and the $Zn(NH_3)_4CO_3$ precursor.[457] GRO was used for the preparation of photocatalysts, because the oxygen containing functional groups proved useful for the functionalization and formation of dense, homogeneous dispersions of NPs. A high-performance photocatalyst based on GRO (GRO/ZnO) was used for the degradation of methylene blue from water under visible light.[458] Besides ZnO, other ternary structures incorporated with graphene were used for photocatalysis. As an example, hydrothermally prepared HRG/$ZnFe_2O_4$ nanocomposites were applied for the photocatalytic degradation of methylene blue in the presence of H_2O_2.[459]

3.2.2 Conventional catalysis. Graphene and graphene based materials have been used for conventional catalysis.[460] Beginning from *group 4 to group 9*, only a few examples of graphene nanocomposites occurred in the literature that were applied as catalysts. Chandra *et al.* reported the preparation of HRG/Rh nanocomposites by sonochemical reduction of Rh^{3+} using borohydride.[461,462] During this process, Rh NPs with an average size of 1–3 nm were distributed homogeneously on stabilized graphene sheets. The stabilization of graphene sheets was carried out by pre-functionalizing GRO sheets with either poly(ethylene oxide)/poly(propylene oxide)/poly(ethylene oxide) (PEO/PPO/PEO) triblock copolymers or pluronic F68.[461] Notably, the pluronic-stabilized HRG/Rh composites exhibited a porous structure with a surface area of 285 $m^2\ g^{-1}$ and a pore volume of 0.164 $cm^3\ g^{-1}$, which allowed their application as a catalyst for the hydrogenation of arenes. However, examples of graphene-based materials comprising elements of group 10 of the periodic table appeared in the literature, including HRG/Ni, HRG/Pd and HRG/Pt. In one such study, the catalytic properties of HRG/Ni nanocomposites were used for the reduction of *p*-nitrophenol into *p*-aminophenol.[463] The stable magnetic behavior of HRG/Ni nanocomposites has been utilized for the removal of adsorbed organic dyes from water.[464]

HRG/Pd nanocomposites were applied as chemical catalysts for organic reactions.[465] The large surface area of graphene and the presence of functional groups (although in minor quantity) in HRG, which facilitate the sorption and intercalation of ions and molecules and the intrinsic catalytic properties of Pd, collectively contribute to the enhancement of the catalytic properties of the hybrid nanocatalysts.[466] In particular, HRG/Pd-catalyzed C–C cross-coupling reactions have been used for industrial chemical and pharmaceutical synthesis. Scheuermann *et al.* demonstrated the excellent catalytic properties of HRG/Pd nanocomposites for Suzuki–Miyaura coupling reactions,[467] where the immobilization of Pd^{2+} on graphite oxide *via* cation exchange and subsequent chemical reduction afforded a composite nanocatalyst. The heterogeneous catalysts have high activities with turnover frequencies of up to 39 000/h with very low Pd leaching (<1 ppm). Additionally, the as-prepared nanocatalysts were air stable, readily available and easy to handle. Therefore they are promising alternatives to commercially available Pd catalysts, (*e.g.* Pd on charcoal).

The catalytic properties of hybrid catalysts were demonstrated as well for other carbon–carbon coupling (Suzuki, Heck) reactions. The hybrid catalysts were prepared by microwave-assisted chemical reduction, which were applied for a broad range of reactions under ligand-free ambient conditions in mixtures of ethanol/deionized water.[468] The advantage of these catalysts compared to commercial systems is their easy recovery with minimal loss, excellent re-usability and better performance. Apart from coupling reactions, graphene supported Pd-based binary and ternary nanocatalysts have been applied in hydrogenation reactions.[469] The hydrogenation of vinyl acetate was carried out using HRG/Pd–Fe_3O_4 ternary nanocomposites, where the hybrid catalyst was prepared solvothermally and the

presence of Pd^{2+} ions assisted the formation of magnetite NPs on the surface of graphene sheets (*cf.* Fig. 19).[470]

Several examples, where multicomponent graphene/Pt based nanocomposites were applied as chemical catalysts, have been reported. HRG/Pt/TiO_2 was applied as a conventional catalyst for the hydrogenation of nitrobenzene (NB).[471] The catalytic hydrogenation of NB is used for the synthesis of amines on an industrial scale. The nanocomposite is comprised of TiO_2 NPs (ξ(~ 10 nm, where almost each TiO2 particle adheres to a Pt NP) uniformly distributed on the HRG sheets. The composite exhibited high activity with a turnover frequency of 59 ,000 h−11 and some selectivity to aniline, and it could be reused six times without any loss of activity.

In *group 11*, conventional catalytic applications of graphene-supported silver and gold NP based hybrids as well as their respective binary and/or ternary nanocomposites were reported.[472,473] For instance, HRG/Ag and HRG/Ag/TiO_2 nanocomposites were applied for the catalytic reduction of 2-nitroaniline to 1,2-benzenediamine and *p*-nitrophenol to *p*-aminophenol.[451] HRG/Au hybrids catalyze the conversion of graphene into CNTs without applying additional hydrocarbons.[474] Here, graphene is assumed to enhance the catalytic activity of Au NPs, thereby facilitating the conversion of graphene into CNTs at 500 °C. It has been speculated that Au NPs create small defects in the graphitic structure of graphene layers, which initiate subsequently the formation of CNTs in the catalytic reaction. Graphene/inorganic nanocomposites may have a promising future in conventional catalysis, but the success of these materials on the industrial scale critically depends on the large scale synthesis of high quality graphene with controllable layer thickness at low cost.

3.3 Sensing

Recently, the trend of applying graphene and graphene-based materials for the fabrication of electrochemical sensors and biosensors has gained importance.[475] The electrical and electronic properties of graphene have significant importance in electroanalysis. For instance, the wide electrochemical potential window, excellent charge transfer resistance and highly efficient electron transfer behavior of graphene have been successfully exploited in various analytical sensing systems.[476] Additionally, due to the high electrocatalytic activity and its excellent electrochemical performance towards glucose oxidase graphene has potential applications for biosensors.

3.3.1 Chemical sensors. So far, several graphene based nanocomposites have been applied as electrochemical sensors for the detection of various chemicals. *In group 4*, zirconia (ZrO_2) is a non-toxic, thermally stable inorganic oxide, which has a strong affinity to phosphoric moieties, and it has been commonly used for the detection of phosphopeptide enrichment, phosphoprotein capture and organophosphorus (OP) agents.[477,478] Recently, to further enhance the electrochemical and detection properties of zirconia, Du *et al.* prepared HRG/ZrO_2 nanocomposites, where ZrO_2 NPs were used as selective sorbents for solid-phase extraction (SPE) and detection of OP pesticides and nitroaromatic OP pesticides such as methyl parathion (MP). HRG/ZrO_2 nanocomposites were fabricated by electrochemical deposition, which exhibited fast electron-transfer kinetics and excellent electrocatalytic activity for the electroactive species. Due to its strong affinity to phosphorus moieties the HRG/ZrO_2 electrochemical sensor facilitated the fast extraction of the target analyte. The combination of SPE and stripping voltammetric analysis allows a fast, sensitive and selective determination of MP in garlic samples.[477] More recently, Gong *et al.* applied HRG/ZrO_2 nanocomposites as SPE for the enzymeless detection of methyl parathion (0.6 ng mL^{-1} ($S/N = 3$)).[479]

For *group 6* metals, only graphene-supported nanocomposites of WO_3 have been reported.[480] WO_3 is an n-type semiconductor that shows efficient photocatalysis under UV light irradiation, and it has attracted great attention due to its

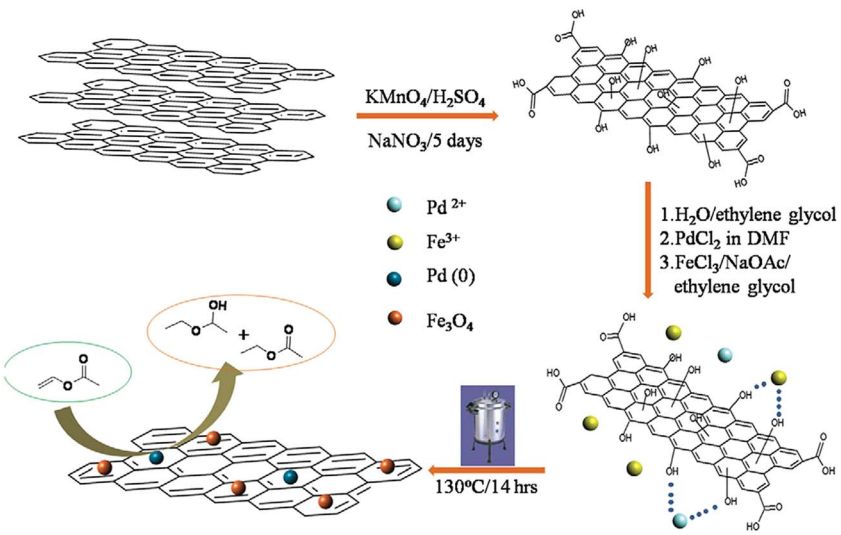

Fig. 19 Schematic representation of the synthesis of HRG/Pd/Fe_3O_4 nanocomposites and their application for hydrogenation reactions. Copyrights reserved to the Elsevier Ltd.[470]

distinctive sensing properties towards numerous gases.[481] The intrinsic conductivity of WO_3 plays an important role in its sensing performance; however, it is expected to be improved greatly by the effect of graphene sheets in the composite materials.[482] Qin *et al.* reported the synthesis of HRG/WO_3 nanocomposites by a multi-step process *via* UV-assisted photoreduction in water at room temperature.[483] In the as-prepared nanocomposites graphene sheets are decorated with a dispersion of WO_3 nanoplatelets with lengths of 50–200 nm, where some of the WO_3 nanoplatelets were oriented perpendicular to graphene sheets. HRG/WO_3 nanocomposites showed an enhanced electrical conductivity compared to pristine WO_3. As a result, the gas response of the nanocomposites was considerably better than that of WO_3 NPs.

In *group 10*, HRG/$Ni(OH)_2$ has been applied as an electrochemical sensor because Ni-based materials possess an excellent catalytic activity towards electrocatalytic molecules such as H_2O_2, ethanol and glucose.[484] Subramanian *et al.* described a non-enzymatic glucose sensor based on a HRG/$Ni(OH)_2$ composite, which was used for the detection of glucose.[485] The nanocomposite is comprised of leaf-shaped $Ni(OH)_2$ nanoplates with a diameter of ~150 nm, homogeneously dispersed between the graphene nanosheets. The dispersion could be dropped onto a glassy carbon electrode to demonstrate the non-enzymatic glucose sensor properties. In this way a low detection limit of 0.6 mM with a wide linear range from 2 mM to 3.1 mM could be obtained.

Furthermore, the intrinsic sensing ability of Pd NPs and the excellent sensing properties of graphene have been exploited for various sensing applications.[486] The enhanced properties of HRG/Pd nanocomposites arise from a change in the electrical conductivity of graphene by charge transfer from molecules adsorbed on its surface. Recently, Johnson *et al.* applied HRG/Pd nanocomposites for the detection of hydrogen in fuel cells.[487] For this purpose, multi-layer graphene nanoribbon networks were prepared by dispersing expanded graphite flakes, which were functionalized with Pd NPs in a water/surfactant water solution. The porous structure of the nanoribbon network provided a high specific surface area, which enabled efficient functionalization and high sensitivity for the adsorbed gas. The as-prepared composite gas sensor exhibited high sensitivity towards hydrogen at room temperature with a fast response, recovery time and good repeatability. An increase in the operating temperature leads to increased sensitivity, faster response and recovery time. At low concentrations, the sensing response showed a linear behavior as a function of H_2 concentration, and the sensor resistance fully recovered upon exposure to air. Similarly, Lange *et al.* reported the detection of hydrogen at a level from 0.5 to 1% in synthetic air.[488] The sensor composite was prepared by layer-by-layer deposition on gold electrodes. The poor hydrogen sensitivity of graphene could be enhanced by one order of magnitude by incorporating Pd NPs. HRG/Pd nanocomposites, which were prepared by sonoelectrochemistry in ionic liquids, were applied as sensors for the detection of chlorophenols.[489] The formation of the nanocomposites was assumed to be driven by the electric and ultrasonic pulses. The hybrid nanocatalysts showed a remarkable current enhancement and good stability. The large electrochemical surface area led to good electrocatalytic activity, and the ionic liquid further enhanced the catalytic activity of Pd–graphene for chlorophenol. The results showed that the peak current is linear with the concentration of phenol in the range from 4 to 800 $\mu mol\ L^{-1}$, with a detection limit of 1.5 $\mu mol\ L^{-1}$.

In *group 11*, HRG/Au nanocomposites have been applied as electrode materials in conventional electrochemical sensors, which were applied for the detection of chemicals, organic molecules, and metallic ions, such as organophosphate pesticides, hydroquinone, or lead.[490,491] The quenching ability of Au NPs was used to prepare a chemosensor for a "turn-on" fluorescence sensing of lead ions (Pb^{2+}), *e.g.* for the detection of organophosphate pesticides. Here, the hybrid electrode was deposited with acetylcholinesterase, which was stabilized by a water soluble polyelectrolye (poly(diallyldimethylammonium chloride (PDDA))).[492] An ionic liquid 1-ethyl-3-methylimidazolium tetrafluoroborate [(EMIM)BF_4] modified carbon paste electrode in combination with a HRG/Au nanocomposite hybrid film was used to detect hydroquinone.[493]

In *group 12*, the combined action of the electronic and semiconducting properties of graphene and ZnO has been exploited for the preparation of highly sensitive photosensors.[494] ZnO NPs were incorporated into graphene to fabricate HRG/ZnO composite visible-blind UV photosensors, where the ZnO nanorods act as UV absorbing and charge carrier generating materials, and graphene serves as a conductive matrix.[495] The thin-film photoconductor based on HRG/ZnO nanocomposites showed a photoresponse up to 22.7 $A\ W^{-1}$ at 20 V (45 000 fold higher than that of single graphene sheet based photodetectors, ~0.1–0.5 $mA\ W^{-1}$).

Tian *et al.* prepared HRG/ZnO nanocomposites by ultrasonicating Zn plates in a GO solution with ammonia at room temperature.[496] This hybrid was modified with zinc porphyrin (ZnP), which acts as a photosensitizer for photocurrent generation in the visible range. The HRG/ZnO/ZnP modified ITO electrodes exhibit a prompt photocurrent response and enhanced photocurrent compared to ZnP modified electrodes. Ding *et al.* demonstrated the field emission and photoluminescence properties of HRG/ZnO nanocomposites, prepared on n-Si (100) substrates by using an electrophoretic deposition and magnetron sputtering technique.[497] This hybrid exhibited excellent emission behavior, which may potentially be exploited in field emission displays.

The photoluminescence (PL) properties of HRG/ZnO nanocomposites have been explored for gas sensing.[498] HRG/ZnO nanocomposites showed semiconducting behavior and optoelectronic properties, in the near UV to blue PL.[499] The luminescent ZnO NPs not only act as spacers between the graphene sheets but also serve as sensing transducers for gases like CO, NH_3 and NO. Apart from this, sensors based on HRG/SnO_2 nanocomposites also showed good sensitivity and selectivity.[500] A HRG/SnO_2 based gas sensor showed good sensitivity towards propanol, an important volatile aldehyde used in chemical and medical industries.[501] Sensors based on HRG/SnO_2 nanocomposites were applied for the detection of H_2S, NH_3, and NO_2.[502,503]

3.3.2 Biosensors. Several graphene-based inorganic nanocomposites have been reported as enzyme-free biosensors for glucose and other biomolecules.[504] They exhibited improved sensitivity and selectivity during the oxidation of target molecules.[505] Lu *et al.* reported an electrochemical biosensor based on a HRG/Pd modified electrode for the detection of glucose.[506] The biosensor has enhanced the electrocatalytic oxidation of glucose in alkaline solution, and it can be applied for the quantification of glucose over a wide range (from 10 μM to 5 mM) with a detection limit of 1 μM. In another study, water-soluble HRG/Pd nanocomposites were applied for the preparation of a glucose biosensor.[507] Here, graphene was functionalized covalently with chitosan, which improved the biocompatibility and hydrophilicity of the hybrid material. The hybrid biosensor was prepared subsequently by immobilization of glucose oxidase on a HRG/Pd modified glassy carbon electrode, and it showed good electrocatalytical activity, high sensitivity and good reproducibility.

By virtue of their good electrical conductivity and biocompatibility, HRG/Pt nanocomposites have also found applications as sensors and biosensors.[508–510] Dey *et al.* developed a HRG/Pt amperometric biosensor for the detection of H_2O_2 and cholesterol.[511] The electrode material contained randomly deposited Pt NPs on HRG. The graphene support of Pt catalyst particles facilitated the electron transfer and catalyzed the electrochemical oxidation of H_2O_2. In addition, a cholesterol biosensor was fabricated with the same composite by immobilization of cholesterol oxidase and cholesterol esterase on its surface. Similarly Gao *et al.* utilized NiPt alloy NPs to synthesize a HRG/NiPt composite biosensor for non-enzymatic glucose detection.[512] The material was synthesized by an ultrasonication-assisted electrochemical method, which demonstrated high NP loading and effective graphene oxide reduction. The resulting electrocatalyst exhibited enhanced electrochemical performance for glucose detection, and showed good selectivity, stability, and a low detection limit and superior resistance to poisoning.

In the *group 11* HRG/Cu, HRG/CuO and HRG/Cu_2O nanocomposites have been widely applied as biosensors. HRG/Cu nanocomposites were used for electrochemical sensing of biomolecules such as carbohydrates. HRG/Cu composites were prepared by reduction of $CuCl_2$–graphite intercalation compounds and deposition of Cu NPs with a reducing flame technique.[513,514] Very recently, HRG/Cu nanocomposites were prepared by *in situ* chemical reduction of GO in the presence of copper(II) ions with potassium borohydride, which was used subsequently to fabricate electrodes for carbohydrate sensing.[515] The analytical performance of these hybrid electrodes was demonstrated by a combination of cyclic voltammetry and capillary electrophoresis for electrochemical sensing of five different carbohydrates, including mannitol, sucrose, lactose, glucose and fructose. The peak current for the oxidation of glucose on a HRG/Cu electrode was much higher than that on a pure copper electrode, which occurred in the 0.40–0.80 V potential range (Fig. 15). The catalytic oxidation was assisted by copper ions, whereas the electrocatalytic activity was enhanced by the gradual support, which improved the electron transduction. Furthermore, the synergetic effect between Cu NPs and graphene sheets significantly enhanced the current response of carbohydrates (Fig. 20).

In another study, the HRG/Cu electrode for non-enzymatic glucose detection was prepared by potentiostatic electrodeposition of Cu NPs on graphene sheets.[516] For instance, the HRG/Cu electrode sensor presented a wide linear range up to 4.5 mM glucose with a detection limit of 0.5 mM, at a detection potential of 500 mV. Furthermore, the as-prepared HRG/Cu composite electrode was used to detect glucose in a simulated serum sample, where the successful detection of glucose in the presence of other electrochemically active components such as ascorbic acid and uric acid demonstrated the application potential of the HRG/Cu based biosensor in routine blood glucose sensing. Copper oxide nanomaterials have been used in combination with graphene in biosensor applications. HRG/CuO nanocomposites were used for glucose detection and cuprous oxide based HRG/Cu_2O hybrids were applied for the detection of dopamine.[517,518] Both composites displayed high electrocatalytic activity for the oxidative sensing of the respective materials compared to the glassy carbon electrode (GCE).

HRG/Ag nanocomposites were also applied in sensing applications, particularly for the detection of H_2O_2, glucose and nitroaromatic compounds.[519–522] HRG/Ag nanocomposites were applied as catalysts for the reduction and detection of H_2O_2, as a sensor to detect glucose, and also as a SERS substrate.[523] As an enzymeless H_2O_2 sensor, the composite material has a fast amperometric response time of less than 2 s, with an estimated detection limit of 7×10^{-6} M.

From *group 11*, nanocomposites of graphene-supported Au NPs have been reported for biosensing and immunosensing applications.[524,525] Gold NPs have unique properties including strong adsorption ability, excellent compatibility and good conductivity.[526] The ability of Au NPs to provide a suitable microenvironment for the immobilization of biomolecules has been exploited for the fabrication of biosensors.[527] Because of its charge transfer properties at room temperature, extremely

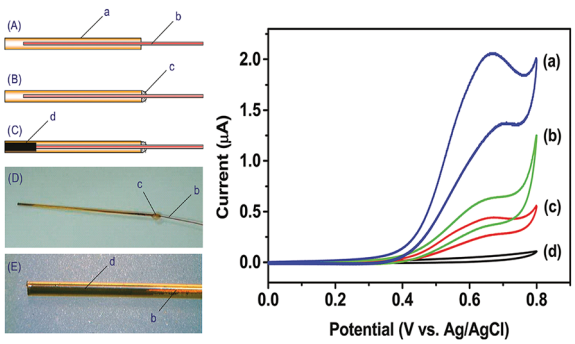

Fig. 20 HRG/Cu nanocomposite and its application. (A–E) Fabrication process of a HRG/Cu composite paste electrode. (a–d) Cyclic voltammograms at (a) a HRG/Cu composite paste electrode (b) a Cu NP paste electrode (c) a graphite–Cu composite paste electrode (d) a graphene paste electrode. Copyrights reserved to the American Chemical Society.[515]

high specific surface area and superb charge storage properties, graphene has been applied as a support material for Au-based electrochemical biosensors.[528] Zhang *et al.* constructed an electrochemical sensor based on a GRO/Au composite, which was synthesized by a redox reaction between $AuCl_4^-$ and GO for the detection of H_2O_2 in food.[529] The electrocatalytic efficiency of the composite biosensor was demonstrated by the reduction of H_2O_2 in buffered solution (pH 5.8), where it showed a dynamic response towards H_2O_2 in the range of 0.1 mM and 2.3 mM with a detection limit of 0.01 mM at 3 s. Chen *et al.* applied a carboxylate functionalized HRG/Au composite for the detection of glucose, where glucose oxidase (GOD) was surface bound by conjugation of terminal amino groups of its lysine residues and the carboxyl groups on Au NPs.[530] The glucose biosensor demonstrated good stability and efficiently measured the blood sugar concentrations in human serum. Apart from carbohydrates, the electrochemical detection of amino acids has been reported with HRG/Au biosensors. A sensitive aptasensor for the detection of L-histidine, based on switching-structure DNAzymes and HRG/Au nanocomposites was reported by Liang *et al.*[531]

Graphene-supported electrochemical sensors have shown potential for the detection of dopamine.[532] Multilayer film electrodes based on HRG/Au nanocomposites, which were made of polymer functionalized graphene and polyamidoamine dendrimer functionalized Au NPs by layer-by-layer self-assembly, exhibited good sensing performance for the detection of dopamine between 1 μM and 60 μM with a detection limit of 0.02 μM. Furthermore, HRG/Au based nanocomposites have been applied as FET (field effect transistor) biosensors for the detection of proteins.[533,534] The FET biosensor was fabricated by suspending thermally reduced graphene oxide (TRG) sheets above the substrates across the gold electrode. When the protein was introduced, it induced changes in the electrical characteristics of the device, which were investigated by FET and direct current measurements. In other applications, apart from the detection of proteins, the HRG/Au nanocomposite biosensor has been applied for the detection of DNA and determination of the specific sequence of DNA.[535,536]

Other typical applications of HRG/Au based biosensors include the electrochemical detection of β-NADH (nicotinamide adenine dinucleotide), a coenzyme involved in the redox reactions of cellular respiration. The ability of Au NPs for the catalytic oxidation and determination of β-NADH could be incorporation of graphene.[537] The presence of several electrochemical reaction sites, such as oxygen containing functional groups on the edges of the graphene layer, and the synergetic effects of Au NPs with graphene in the HRG/Au composites enhanced the electron transfer between the enzyme and electrode. In another study, an electroactive epinephrine (EP), which is an important neurotransmitter in the mammalian central nervous system, was detected with high sensitivity using a HRG/Au modified GCE electrode.[538] Furthermore, HRG/ZnO nanocomposites were applied as non-enzymatic amperometric sensors for the detection of H_2O_2 and glucose.[539,540] For instance, electrochemically prepared HRG/ZnO GCE electrodes towards H_2O_2 at −0.38 V in the concentration range of 0.02 to 22.48 μM showed a linear and fast response (<5 s).[539]

So far, the results suggested that graphene-based materials have excellent potential in analytical and bioanalytical applications, and they may be promising options for various sensing applications. However, there is still a long way to go for a commercial exploitation of these materials on a large scale, which greatly requires further property improvements, including detection sensitivity, shelf life, selectivity, linear range and so on. One of the greatest challenges in this field is the determination of the biocompatibility of these materials, which is crucial for the *in vivo* detection of bioanalytes. Furthermore, the binding of non-specific substances is a major concern, which seriously affects bimolecular interactions. Therefore, in order to detect the analyte with high specificity, the selectivity of the graphene based biosensor needs to be enhanced, which requires great efforts.

3.4 Applications of HRG as a support material

3.4.1 Adsorbent materials. Apart from the applications discussed above, graphene-based inorganic nanocomposites have been applied for other applications including waste water treatment or gas sorption.[541] For example, graphene-based manganese oxide composites were applied as adsorbent materials.[542] The combination of graphene sheets and MnO_2 NPs serves the purpose of water purification. Recently, metal ion scavenging applications of HRG/MnO_2 nanocomposites have been demonstrated by Sreeprasad *et al.* taking Hg(II) as a model pollutant.[543] The composite material has a high distribution coefficient (K_d), which is one order of magnitude higher compared to that of the parent materials (>10 L g^{-1}) for Hg(II) uptake. The as-prepared nanocomposites were immobilized on river sand using chitosan as a binder and found to be efficient adsorbent candidates for field applications. Furthermore, the HRG/Mn_3O_4 hybrid exhibited excellent catalytic activity towards thermal decomposition of ammonium perchlorate, due to the synergistic effect of Mn_3O_4 and graphene.[544]

In recent years, HRG/Fe_3O_4 nanocomposites have attracted much interest and have been used as adsorbents for the removal of heavy metals and other contaminants from the environment using their magnetic properties, high surface-to-volume ratio and short diffusion rate by the support of graphene.[545,546] Several studies have been published in this regard, including a report of Zhang *et al.* on the synthesis of HRG/Fe_3O_4 nanocomposites and their application in the removal of tetracycline.[547] Chandra *et al.* described the synthesis of HRG/Fe_3O_4 nanocomposites consisting of Fe_3O_4 NPs ($\xi \sim 10$ nm), which showed a high binding capacity for As(III) and As(V) in drinking water.[548] The composites are superparamagnetic at room temperature and can easily be separated by an external magnetic field. This suppresses any chance of creating secondary waste involving the remaining composite material. Besides heavy metals removal, HRG/Fe_3O_4 nanocomposites were used for the separation of various dye pollutants from water resources. A HRG/Fe_3O_4 hybrid prepared by Geng *et al.* demonstrated excellent adsorption performance for a series of dyes, such as RhB, R6G, AB92, OII, MG and NC.[549] In addition, the material could easily and rapidly be separated from water

due to the presence of magnetic Fe_3O_4 NPs, and efficiently regenerated and utilized *via* simple annealing treatment under moderate conditions. Moreover, graphene-based iron oxide nanocomposites including HRG/Fe_3O_4 and HRG/Fe_2O_3 have demonstrated excellent adsorption ability to bind other heavy metals and organic dyes such as chromium, lead, cobalt, neutral red, methylene blue and so on.[550–553] More recently, a ternary composite of HRG/Fe_3O_4/TiO_2 has been reported, which exhibited high selectivity and capacity in capturing phosphopeptides.[554] In another study, zinc hydroxide ($Zn(OH)_2$) was incorporated into graphene for hydrogen sulfide (H_2S) removal.[555] Among the two types of nanocomposites with $Zn(OH)_2$, composites of $Zn(OH)_2$ with GO (GO/$Zn(OH)_2$) exhibited better adsorption of H_2S than HRG/$Zn(OH)_2$ nanocomposites or pristine $Zn(OH)_2$.

3.4.2 Surface-enhanced Raman scattering substrates. Graphene-based nanocomposites of metallic nanoparticles (NPs) combining the properties of both the components in a synergistic manner have been used for surface enhanced Raman scattering (SERS).[556] SERS enhances the signal intensity by orders of magnitudes, and it has been potentially exploited for the ultra-sensitive detection of various analytes, including a number of chemical and biological molecules.[557] Among the precious metal NPs, which are available with good control on size and morphology, silver (Ag) NPs have high SERS activity. Significant efforts have been made to prepare graphene silver (Ag) nanocomposites (HRG/Ag), combining the properties of Ag and graphene, *e.g.* high SERS activity of silver and large specific surface area of graphene.[558–560] Recently, Khan *et al.* have described the synthesis of HRG/Ag nanocomposites using a *Pulicaria glutinosa* plant extract as a reducing agent (*cf.* Fig. 21). The plant extract functionalizes the surfaces of HRG which helps conjugating the Ag NPs to HRG. The as-prepared PE–HRG–Ag nanocomposites display excellent SERS activity, and significantly enhanced the intensities of the Raman signal of graphene.[561]

SERS is a powerful and reliable analytical tool for the ultra-sensitive detection of analytes even at the single molecule level.[562,563] SERS is attributed to an electromagnetic mechanism (EM) based on surface plasmon resonance (SPR) and/or a chemical mechanism (CM) based on charge transfer.[564] SERS substrates often suffer from a lack of adsorption of molecules.[565] Due to its flexible and smooth 2D honeycomb structure, graphene shows adsorption for many molecules, especially for aromatic ones.[566] Moreover, an enhanced chemical mechanism has also been proposed for graphene, due to its high surface plasma frequency in the terahertz range.[567] Therefore, graphene has been extensively applied as a support material to prepare HRG/Ag nanocomposites to obtain high SERS activity, good and efficient plasmonic and chemiluminescence properties, which facilitate the detection of molecules even at low concentrations.[568,569]

Ag NP decorated single-layer HRG films on a silicon surface showed Raman enhancement and adsorption of aromatic molecules (rhodamine 6G, methyl violet, rhodamine B and methylene blue).[570] The hybrid material was used as an SERS substrate to detect the adsorbed molecules with a detection limit at the nanomolar level. Sun *et al.* prepared HRG/Ag nanocomposites as SERS substrates to detect 4-aminobenzenethiol, nile blue and rhodamine 6G, which have different coupling abilities to graphene sheets.[571] The hybrid material was also used as a SERS substrate to demonstrate the combined SERS effect, and it was shown that both EM and CM effects coexist for Ag NPs, graphene sheets, and the absorbed analytes. The combined and competitive SERS effect between the adsorbed probe molecules and the graphene sheets varies depending on the species and concentration of the adsorbed probe molecules.

The morphologies of metal NPs, such as Ag or Au on pristine *n*-layer graphenes, depend on the number of graphene layers.[572] A study of the thickness-dependent morphologies and the SERS effect of HRG/Ag nanocomposites, where 2 or 5 nm silver films were deposited onto *n*-layer graphenes, showed that with increasing sample temperature the thickness-dependent Ag morphologies become more pronounced due to the changes of the temperature-dependent surface diffusion coefficient of *n*-

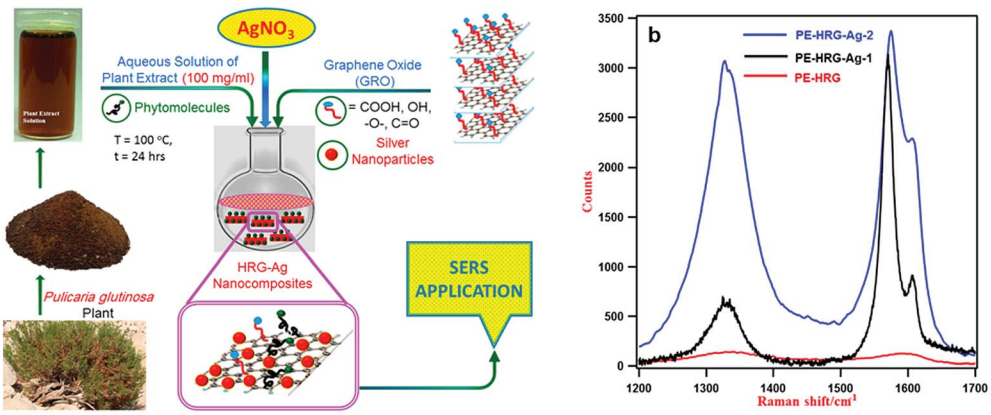

Fig. 21 Schematic illustration of the green synthesis of graphene/silver nanocomposites using an aqueous extract of *Pulicaria glutinosa* plant. (b) Raman spectra of HRG, HRG/Ag-1 and HRG/Ag-2 with 50 and 75 wt% of Ag respectively. With increasing the concentration of Ag NPs the intensities of the Raman signals also increase. Copyrights reserved to the MDPI.[561]

layer graphenes.[573] The SERS effect was enhanced after thermal deposition of Ag films, and the enhancement factors were dependent on the number of graphene layers. A single layer showed the biggest SERS enhancement, which was attributed to the coupled surface plasmon resonance (SPR) of Ag NPs (*cf.* Fig. 22).

The aggregation of graphene sheets due to π–π stacking interactions leads to a decrease of the SERS enhancement factor with increasing number of graphene layers. This problem can be overcome by prefunctionalization of graphene sheets. High quality single-layer HRG/Ag nanocomposites, which were used as SERS substrates for the detection of 4-aminothiophenol in liquid, were obtained using poly-vinyl-2-pyrrolidone (PVP) as the reductant and stabilizer.[574] Similarly, poly(diallyldimethyl ammonium chloride (PDDA)) was used as a stabilizer for preparing cationic polyelectrolyte functionalized graphene oxide and as a support for Ag NPs for detecting folic acid by SERS.[575]

Apart from silver, Au NPs (like Ag NPs) induce a large enhancement of the Raman signal when deposited on graphene. Several studies have been conducted on the enhanced SERS activity of the analytes with HRG/Au hybrids. Au NPs deposited on the surface of graphene have enhanced the Raman signal by a factor of 2.5.[576–578] An enhancement of 60 has been achieved with Au nanodiscs, which were deposited on mechanically exfoliated single-layer graphene.[579] An even larger

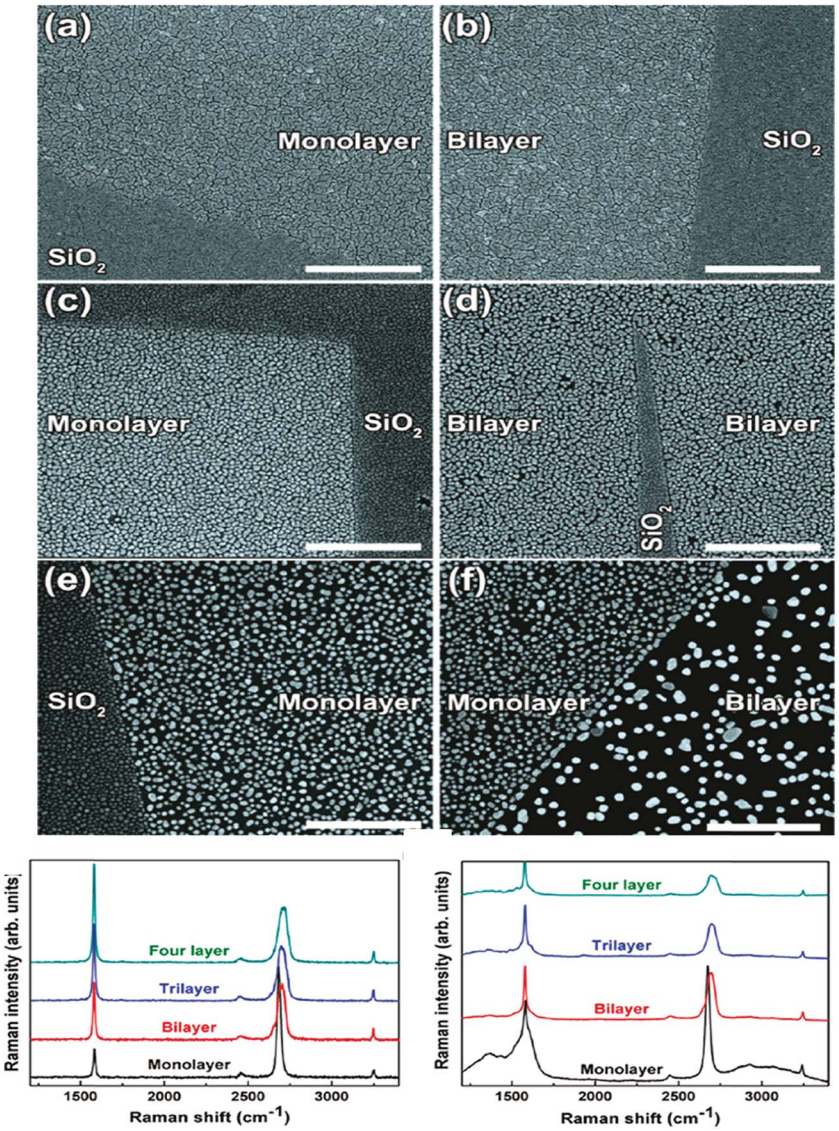

Fig. 22 Schematic representation and SEM images of graphene-supported Ag-based nanocomposites. Thickness-dependent morphologies of 5 nm Ag on *n*-layer graphenes with samples kept at a controlled temperature and Raman spectra of pristine and 5 nm Ag-covered *n*-layer graphenes. Scale bar: 1 μm. (a and b) Ag morphologies deposited on monolayer and bilayer graphene at 298 K. (c and d) Silver morphologies on monolayer and bilayer graphene at 333 K. (e and f) Ag morphologies on monolayer and bilayer graphene at 373 K. Raman spectra of pristine (a) and 5 nm Ag-covered (b) *n*-layer graphenes. From the intensities and shapes of the G (~1580 cm^{-1}) and 2D (~2700 cm^{-1}) peaks, SERS of *n*-layer graphenes can be observed obviously, which is dependent on the layer number. Copyrights reserved to the American Chemical Society.[573]

enhancement (×120) could be achieved by depositing Au NPs on single-layer graphene (at excitation 633 nm).[580] The SERS enhancement of single-layer graphene is much larger compared to graphene, and the enhancement of the G band was larger than that of the D band.

3.5 Biological applications

Graphene and graphene-based materials have great potential in various biomedical applications,[581] as indicated by the number of publications in this area. Several studies have been carried out on biomedical applications of graphene, including drug/gene delivery, imaging, antibacterial and anti-cancer activities and so on.[582,583] Superparamagnetic Fe_2O_3 NPs were applied in magnetic resonance imaging (MRI), biological separation, and hyperthermia therapy. In this regard, HRG/Fe_3O_4 nanocomposites have attracted attention to achieve enhanced MRI contrast, improved biocompatibility and physiological stability.[584–586] The synthesis of dextran-coated HRG/Fe_3O_4 nanocomposites and their application as T_2-weighted contrast agents for cellular magnetic resonance imaging (MRI) have been reported recently.[587] The as-prepared nanocomposites exhibit improved T_2-weighted MRI contrast due to the formation of Fe_3O_4 NP aggregates on HRG sheets, resulting in an enhanced T_2 relaxivity. Some other applications of HRG/Fe_2O_3 and HRG/Fe_3O_4 nanocomposites for magnetically targeted drug delivery, bioseparation and other biological applications have been reported as well.[588–591]

Ag NPs are known to exhibit the highest bactericidal activity and biocompatibility among all antibacterial nanomaterials. They have been applied as antiseptic, disinfectant and pharmaceutical agents.[592] The toxicity of Ag is strongly dependent on the size and morphology of the NPs where high surface area and easy cell penetration with small Ag NPs lead to high antibacterial activity. Macromolecules, photo-catalytic, and other carbonaceous materials, have been used as supports for monodisperse and stable Ag NPs with excellent antibacterial, optical and electronic properties.[593] However, due the low solubility in water, graphene or HRG has rarely been used as an anti-bacterial agent.[594,595] Graphene oxide with oxygen-containing functional groups is water soluble and therefore more biocompatible than graphene; as a result, Ag-based graphene oxide nanocomposites may be used as anti-bacterial agents.[596]

Oleylamine-capped Ag NPs have been anchored on graphene oxide sheets in a phase transfer system.[597] The resulting graphene oxide/Ag nanocomposite revealed enhanced antibacterial properties against Gram-negative bacteria compared to pristine Ag NPs. Ma *et al.* showed the synergetic effect of Ag NPs and graphene oxide to be responsible for the enhanced anti-bacterial activity.[598] The anti-bacterial mechanism of graphene oxide/Ag nanocomposites on *E. coli* bacteria appears to depend on hydrogen bonding between graphene oxide and lipopolysaccharide strings of the cell membrane, where graphene oxide sheets adhere to *E. coli*. This blocks the cells from taking up nutrients, which ultimately leads to cell death.

4 Conclusion and future perspective

The current developments in the synthesis of graphene, graphene-based metal and metal oxide nanocomposites with a special focus on their synthesis by a top-down approach and properties characterized by various techniques were discussed in detail. The exceptional electronic, electrical, and mechanical properties of free standing single layer graphene obtained from graphite by micromechanical cleavage have attracted the attention of the scientific community. As a result, the number of publications related to graphene and graphene-based materials has increased exponentially in recent years. The improved knowledge on graphene surface chemistry, methods of surface functionalization, preparation of stable and homogeneous dispersions of graphene in large quantities and progress in the colloidal synthesis of inorganic nanomaterials has provided a wide range of possibilities for the preparation of graphene-based inorganic nanocomposites by incorporating various functional nanomaterials. The cooperative effects between graphene, metal and metal oxide materials in these nanocomposites have paved the way to design and explore a variety of new applications ranging from the medical to the energy sector (*cf.* Fig. 23).

So far, tremendous progress has been made in the chemical preparation of graphene and graphene-based materials by methods broadly classified as *top-down* and *bottom-up* approaches. Although *bottom-up* strategies can yield single layer, defect free graphene, they are not suitable presently for a bulk synthesis of graphene, generally required for large scale production of graphene-based materials. Therefore, considering the great demand for the bulk production of graphene, *top-down* approaches have gained attention. These techniques typically involve the sequential oxidation and reduction of graphite, which is a low cost commodity material that offers economic advantages. Furthermore, *top-down* approaches have become more attractive due to the recent advancements in the methods of direct exfoliation of graphite in various solvents in

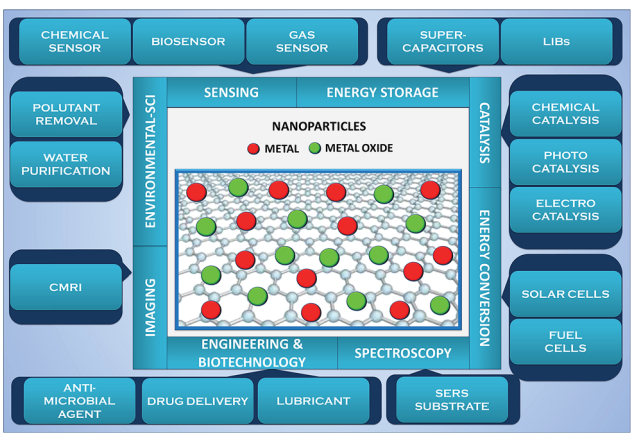

Fig. 23 Graphical illustration of the wide range of applications of graphene inorganic nanoparticles (NPs), including metal and metal oxide NP based nanocomposites.

the absence of any reducing or stabilizing agents. Hence, for the synthesis of graphene based materials required for the potential industrial applications, graphite based *top-down* approaches are more suitable and economically viable.

Still, there is plenty of scope to explore new protocols for *top-down* approaches to synthesize bulk quantities, which are cost effective, environmentally friendly and yield *defect free* graphene. Most of the currently available synthetic methods lack control over size, shape, edge and thickness (number of layers) of graphene due to random exfoliation, growth and assembly processes. Despite the considerable progress in the synthesis of graphene-based inorganic nanocomposites, challenges exist in the application on an industrial scale. For instance, advanced applications of graphene-based metal and metal oxide nanocomposites require extensive research to understand the interactions between nanomaterials and the graphene surface, which will have direct impact on the properties of these nanocomposites. A proper understanding of these interactions will surely enhance the application potential of the nanocomposites in various fields, including biosensing, catalysis drug delivery, imaging and so on. Furthermore, to improve the processability of these nanocomposites, a work needs to be done towards the enhancement of dispersion quality. Although considerable success has been achieved in obtaining homogeneous dispersions of graphene in various organic solvents, efforts must be directed towards the prevention of restacking graphene and the improvement of the dispersion quality of graphene-based inorganic nanocomposites. Several methods have been applied to synthesize homogeneously dispersed nanocomposites by various reduction and functionalization techniques. However, many reported reductants and surfactants may have adverse effects on the potential applications of these nanocomposites. Particularly, it is important to understand the biocompatibility and toxicity of these reductants and surfactants to make the resulting nanocomposites safe for biomedical applications.

Nevertheless, graphene is a novel 2D support for the growth, assembly and nucleation of metal and metal oxide nanoparticles, and the integration and synergistic effects of these nanoparticles with graphene greatly enhance the performance of the composite materials. Therefore, graphene based metal and metal oxide composites with anchored, encapsulated, wrapped, layered and mixed structures have enormous potential for many industrial applications, and they are commercially feasible compared to nanocomposites using other carbonaceous materials. The controlled synthesis of these nanocomposites, with well-defined size, shape and crystallinity of nanomaterials, not only prevents the restacking of graphene nanosheets, but also provides excellent templates for the preparation of 3D porous networks with enhanced electrical and electronic properties. Moreover, improvements in the quality of graphene will ultimately lead to the synthesis of uniform nanocomposites, which can be fine-tuned for various potential applications. Therefore a multidisciplinary approach must be used to improve the protocols for the bulk production of graphene to achieve the mature form of nanotechnology to build devices.

Abbreviations

HRG	Highly reduced graphene oxide
GO	Graphite oxide
CNTs	Carbon nanotubes
0D	Zero-dimensional
CVD	Chemical vapor deposition
CMG	Chemically modified graphene
NMP	*N*-Methyl pyrrolidone
HR-TEM	High resolution-transmission electron microscopy
TRG	Thermally reduced graphene oxide
KMG	KOH-modified graphene oxide
hKMG	Hydrazine-reduced KMG
PEM	Proton exchange membrane
AFM	Atomic force microscopy
HRG	Highly reduced graphene oxide
rGO	Reduced graphene oxide
CReGO	Chemically reduced graphene oxide
CCG	Chemically converted graphene
PE	Plant extracts
Mtr/Ornc	Outer membrane c-type cytochromes
SERS	Surface enhanced Raman scattering
DI	Deionized water
SEM	Scanning electron microscopy
XRD	X-ray diffraction
XPS	X-ray photoelectron spectroscopy
MWI	Microwave irradiation
EG	Exfoliated graphite
GICs	Graphite intercalation compounds
IL	Ionic liquid
SC	Supercritical
[BMIM]	1-Butyl-3-methylimidazolium
[PF_6]	hexafluorophosphate
DSSC	Dye-sensitized solar cells
SPE	Solid-phase extraction
MP	Methyl parathion
LIBs	Lithium-ion batteries
MB	Methylene blue
2D	Two-dimensional
3D	Three-dimensional
ACN	Activated carbon nanofibers
0D	Zero-dimensional
MRI	Magnetic resonance imaging
QDs	Quantum dots
LDH-NS	Layered double hydroxide nanosheets
ORR	Oxygen reduction reaction
DMFC	Direct methanol fuel cell
CB	Carbon black
ECSA	Electrochemically active surface area
MWCNT	Multi-walled carbon nanotubes
FAO	Formic acid oxidation
NB	Nitrobenzene
GCE	Glassy carbon electrode
EM	Electromagnetic mechanism
SPR	Surface plasmon resonance
CM	Chemical mechanism
PVP	Poly-vinyl-2-pyrrolidone

GOD	Glucose oxidase
FET	Field effect transistor
EP	Electroactive epinephrine
ZnP	Zinc porphyrin

Acknowledgements

This project was funded by National Plan for Science, Technology and Innovation (MAARIFAH), King Abdulaziz City for Science and Technology, Kingdom of Saudi Arabia, Award Number (11NAN-1860-02).

References

1 K. Geim and K. S. Novoselov, *Nat. Mater.*, 2007, **6**, 183–191.
2 C. N. R. Rao, A. K. Sood, K. S. Subrahmanyam and A. Govindaraj, *Angew. Chem., Int. Ed.*, 2009, **48**, 7752–7777.
3 M. J. Allen, V. C. Tung and R. B. Kaner, *Chem. Rev.*, 2010, **110**, 132–145.
4 J. Wu, W. Pisula and K. Müllen, *Chem. Rev.*, 2007, **107**, 718–747.
5 X. Huang, Z. Yin, S. Wu, X. Qi, Q. He and Q. Zhang, *Small*, 2011, **7**, 1876–1902.
6 X. Wan, Y. Huang and Y. Chen, *Acc. Chem. Res.*, 2012, **45**, 598–607.
7 O. C. Compton and S. B. Nguyen, *Small*, 2010, **6**, 711–723.
8 R. Denk, M. Hohage, P. Zeppenfeld, J. Cai, C. A. Pignedoli, H. Söde, R. Fasel, X. Feng, K. Müllen, S. Wang, D. Prezzi, A. Ferretti, A. Ruini, E. Molinari and P. Ruffieux, *Nat. Commun.*, 2014, **5**, 4253.
9 H.-W. Liang, X. Zhuang, S. Brüller, X. Feng and K. Müllen, *Nat. Commun.*, 2014, **5**, 4973.
10 H. W. Kroto, J. R. Heath, S. C. Obrien, R. F. Curl and R. E. Smalley, *Nature*, 1985, **318**, 162–163.
11 S. Lijima, *Nature*, 1991, **354**, 56–58.
12 D. R. Kaufmann and A. Star, *Analyst*, 2010, **135**, 2790–2797.
13 A. Fasolino, J. H. Los and M. I. Katsnelson, *Nat. Mater.*, 2007, **6**, 858–861.
14 M. Antonietti and K. Müllen, *Adv. Mater.*, 2010, **22**, 787.
15 A. Lax and R. Maxwell, *National Trust Annual Archaeological Review*, 1998–1999, 18–23.
16 M. Eizenberg and J. M. Blakely, *Surf. Sci.*, 1970, **82**, 228–236.
17 K. S. Novoselov, K. S. Geim, S. V. Morozov, D. Jiang, Y. Zhang, S. V. Dubonos, I. V. Grigorieval and A. A. Firsov, *Science*, 2004, **306**, 666–669.
18 D. Mermin, *Phys. Rev.*, 1968, **176**, 250–254.
19 M. Ortila, C. Faugeras, P. Plochocka, P. Neugebauer, G. Martinez, D. K. Maude, A.-L. Barra, M. Sprinkle, C. Berger, W. A. de Heer and M. Potemski, *Phys. Rev. Lett.*, 2008, **101**, 267601.
20 A. A. Balandin, S. Ghosh, W. Bao, I. Calizo, D. Teweldebrhan, F. Miao and C. N. Lau, *Nano Lett.*, 2008, **8**, 902–907.
21 X. Du, I. Skachko, A. Barker and E. Y. Andrei, *Nat. Nanotechnol.*, 2008, **3**, 491–495.
22 Y. Zhu, S. Murali, W. Cai, X. Li, J. W. Suk and J. R. Potts, *Adv. Mater.*, 2010, **22**, 3906–3924.
23 C. M. Weber, D. M. Eisele, J. P. Rabe, Y. Liang, X. Feng, L. Zhi, K. Müllen, J. L. Lyon, R. Williams, D. A. V. Bout and K. J. Stevenson, *Small*, 2011, **6**, 184–189.
24 S. Pang, Y. Hernandez, X. Feng and K. Müllen, *Adv. Mater.*, 2011, **23**, 2779–2795.
25 C. Lee, X. Wei, J. W. Kysar and J. Hone, *Science*, 2008, **321**, 385–388.
26 J. C. Slonczewski and P. R. Weiss, *Phys. Rev.*, 1958, **109**, 272–279.
27 S. Park and R. S. Ruoff, *Nat. Nanotechnol.*, 2009, **4**, 217–224.
28 L. Dössel, L. Gherghel, X. Feng and K. Müllen, *Angew. Chem., Int. Ed.*, 2011, **50**, 2540–2543.
29 H. Kim, A. A. Abdala and C. W. Macosko, *Macromolecules*, 2010, **43**, 6515–6530.
30 J. Luo, J. Kim and J. Huang, *Acc. Chem. Res.*, 2013, **46**, 2225–2234.
31 S. Bai and X. Shen, *RSC Adv.*, 2012, **2**, 64–98.
32 X. Huang, X. Qi, F. Boey and H. Zhang, *Chem. Soc. Rev.*, 2012, **41**, 666–686.
33 C. Zhang, R. Hao, H. Yin, F. Liu and Y. Hou, *Nanoscale*, 2012, **4**, 7326–7329.
34 K. Müllen, *ACS Nano*, 2014, **8**, 6531–6541.
35 Y. Liu, X. Dong and P. Chen, *Chem. Soc. Rev.*, 2012, **41**, 2283–2307.
36 A. H. C. Neto, F. Guines, N. M. R. Peren, K. S. Novoselov and A. K. Geim, *Rev. Mod. Phys.*, 2009, **81**, 109–162.
37 Y. Zhang, L. Zhang and C. Zhou, *Acc. Chem. Res.*, 2013, **46**, 2329–2339.
38 W. Pisula, X. Feng and K. Müllen, *Chem. Mater.*, 2011, **23**, 554–567.
39 V. Singh, D. Joung, L. Zhai, S. Das, S. I. Khondaker and S. Seal, *Prog. Mater. Sci.*, 2011, **56**, 1178–1271.
40 C. A. Coulson and R. Taylor, *Proc. Phys. Soc., London, Sect. A*, 1952, **65**, 815–825.
41 K. S. Novoselov, D. Jiang, F. Schedin, T. J. Booth, V. V. Khotkevich, S. V. Morozov and A. K. Geim, *Proc. Natl. Acad. Sci. U. S. A.*, 2005, **102**, 10451–10453.
42 S. Park, J. H. An, R. D. Piner, I. W. Jung, D. Yang, A. Velamakanni, S. T. Nguyen and R. S. Ruoff, *Chem. Mater.*, 2008, **20**, 6592–6594.
43 L. Chen, Y. Hernandez, X. Feng and K. Müllen, *Angew. Chem., Int. Ed.*, 2012, **51**, 7640–7654.
44 J. Cai, P. Ruffieux, R. Jaafar, M. Bieri, T. Braun, S. Blankenburg, M. Muoth, A. Seitsonen, M. Saleh, X. Feng, K. Müllen and R. Fasel, *Nature*, 2010, **466**, 470–473.
45 Y. Ito, C. Christodoulou, M. V. Nardi, N. Koch, H. Sachdev and K. Müllen, *ACS Nano*, 2014, **8**, 3337–3346.
46 Z. Yan, Z. Peng and J. M. Tour, *Acc. Chem. Res.*, 2014, **47**, 1327–1337.
47 B. Shen, J. Ding, X. Yan, W. Feng, J. Li and Q. Xue, *Appl. Surf. Sci.*, 2012, **258**, 4523–4531.
48 Q. Huang, J. J. Kim, G. Ali and S. O. Cho, *Adv. Mater.*, 2013, **25**, 1144–1148.
49 A. Narita, X. Feng, Y. Hernandez, S. A. Jensen, M. Bonn, H. Yang, I. A. Verzhbitskiy, C. Casiraghi, M. R. Hansen, A. H. R. Koch, G. Fytas, O. Ivasenko, B. Li, K. S. Mali,

T. Balandina, S. Mahesh, S. D. Feyter and K. Müllen, *Nat. Chem.*, 2014, **6**, 126–132.
50 L. Zhi and K. Mullen, *J. Mater. Chem.*, 2008, **18**, 1472–1484.
51 E. Castillo-Martínez, J. Carretero-González, J. Sovich and M. D. Lima, *J. Mater. Chem. A*, 2014, **2**, 221–228.
52 D. Wei, L. Xie, K. K. Lee, Z. Hu, S. Tan, W. Chen, C. H. Sow, K. Chen, Y. Liu and A. T. S. Wee, *Nat. Commun.*, 2013, **4**, 1–9.
53 W. Zhang, J. Cui, C. A. Tao, Y. Wu, Z. Li, L. Ma, Y. Wen and G. Li, *Angew. Chem., Int. Ed.*, 2009, **48**, 5864–5868.
54 L. Talirz, H. Söde, J. Cai, P. Ruffieux, S. Blankenburg, R. Jafaar, R. Berger, X. Feng, K. Müllen, D. Passerone, R. Fasel and C. A. Pignedoli, *J. Am. Chem. Soc.*, 2013, **135**, 2060–2063.
55 W. Bin, G. Dechao and G. Yunlong, *Adv. Mater.*, 2011, **23**, 3522–3525.
56 A. N. Obraztsov, *Nat. Nanotechnol.*, 2009, **4**, 212–213.
57 I. Salzmann, A. Moser, M. Oehzelt, T. Breuer, X. Feng, Z. Y. Juang, D. Nabok, R. G. D. Valle, S. Duhm, G. Heimel, A. Brillante, E. Venuti, I. Bilotti, C. Christodoulou, J. Frisch, P. Puschnig, C. Draxl, G. Witte, K. Müllen and N. Koch, *ACS Nano*, 2012, **6**, 10874–10883.
58 Y.-Z. Tan, B. Yang, K. Parvez, A. Narita, S. Osella, D. Beljonne, X. Feng and K. Müllen, *Nat. Commun.*, 2013, **4**, 2646.
59 M. G. Schwab, A. Narita, Y. Hernandez, T. Balandin, K. S. Mali, S. D. Feyter, X. Feng and K. Müllen, *J. Am. Chem. Soc.*, 2012, **134**, 18169–18172.
60 A. Hamwi and V. Marchand, *J. Phys. Chem. Solids*, 1996, **57**, 867–872.
61 A. V. Okotrub, P. Asanovl, N. F. Yudanov, K. S. Babin, A. V. Guselnikov, T. I. Nedoseikina and P. N. Gevko, *Phys. Status Solidi B*, 2009, **246**, 2545–2548.
62 J. L. Sznopet and D. W. Olson, U. S Geological Survey Data Series, 2010, p. 140.
63 D. Li, M. B. Muller, S. Gilje, R. B. Kaner and G. G. Wallace, *Nat. Nanotechnol.*, 2008, **3**, 101–105.
64 I. K. Moon and J. Lee, *Chem. Commun.*, 2011, **47**, 9681–9683.
65 C. K. Chua and M. Pumera, *Chem. Soc. Rev.*, 2014, **43**, 291–312.
66 L. Chen, Y. Hernandez, X. Feng and K. Müllen, *Angew. Chem., Int. Ed.*, 2012, **51**, 7640–7654.
67 S. Barg, F. M. Perez, N. Ni, P. V. Pereira, R. C. Maher, E. Garcia-Tuñon, S. Eslava, S. Agnoli, C. Mattevi and E. Saiz, *Nat. Commun.*, 2014, **5**, 4328.
68 T. S. Sreeprasad and V. Berry, *Small*, 2013, **9**, 341–350.
69 J. N. Coleman, M. Lotya, A. O'Neill, S. D. Bergin, P. J. King, U. Khan, K. Young, A. Gaucher, S. De, R. J. Smith, I. V. Shvets, S. K. Arora, G. Stanton, H.-Y. Kim, K. Lee, G. T. Kim, G. S. Duesberg, T. Hallam, J. J. Boland, J. J. Wang, J. F. Donegan, J. C. Grunlan, G. Moriarty, A. Shmeliov, R. J. Nicholls, J. M. Perkins, E. M. Grieveson, K. Theuwissen, D. W. McComb, P. D. Nellist and V. Nicolosi, *Science*, 2011, **331**, 568–571.
70 K. Parvez, Z.-S. Wu, R. Li, X. Liu, R. Graf, X. Feng and K. Müllen, *J. Am. Chem. Soc.*, 2014, **136**, 6083–6091.
71 A. B. Bourlinos, V. Georgakilas, R. Zboril, T. A. Steriotis and A. Stubos, *Small*, 2009, **5**, 1841–1845.
72 S. Sampath, A. N. Basuray, K. J. Hartlieb, T. Aytun, S. I. Stupp and J. F. Stoddart, *Adv. Mater.*, 2013, **25**, 2740–2745.
73 N. Liu, F. Luo, H. Wu, Y. Liu, C. Zhang and J. Chen, *Adv. Funct. Mater.*, 2008, **18**, 1518–1525.
74 N. Behabtu, J. R. Lomeda, M. J. Green, A. L. Higginbotham, A. Sinitskii, D. V. Kosynkin, D. Tsentalovich, A. N. G. Parra-Vasquez, J. Schmidt, E. Kesselman, Y. Cohen, Y. Talmon, J. M. Tour and M. Pasquali, *Nat. Nanotechnol.*, 2010, **5**, 406–411.
75 H. Xu and K. Suslick, *J. Am. Chem. Soc.*, 2011, **133**, 9148–9151.
76 D. Rangappa, K. Sone, M. Wang, U. K. Gautam, D. Golberg, H. Itoh, M. Ichihara and I. Honma, *Chem.–Eur. J.*, 2010, **16**, 6488–6494.
77 A. Ciesielski and P. Samori, *Chem. Soc. Rev.*, 2014, **43**, 381–398.
78 U. Khan, A. O'Neill, M. Loty, S. De and J. N. Coleman, *Small*, 2010, **6**, 864–871.
79 M. Lotva, P. J. King, U. Khan, S. De and J. N. Coleman, *ACS Nano*, 2010, **4**, 3155–3162.
80 A. Ghosh, K. V. Rao, S. J. George and C. N. Rao, *Chem.–Eur. J.*, 2010, **16**, 2700–2704.
81 X. An, T. Simmons, R. Shah, C. Wolfe, K. M. Lewis, M. Washington, S. K. Nayak, S. Talapatra and S. Kar, *Nano Lett.*, 2010, **10**, 4295–4301.
82 S. Yang, R. E. Bachman, X. Feng and K. Müllen, *Acc. Chem. Res.*, 2013, **46**, 116–128.
83 R. Kabe, X. Feng, C. Adachi and K. Müllen, *Chem.–Asian J.*, 2014, **9**, 3125–3129.
84 M. Zhang, R. R. Parajuli, D. Mastrogiovanni, B. Dai, P. Lo, W. Cheung, R. Brukh, P. L. Chiu, T. Zhou, Z. Liu, E. Garfunkel and H. He, *Small*, 2010, **6**, 1100–1107.
85 C.-J. Shih, A. Vijayaraghavan, R. Krishnan, R. Sharma, H. J.-H. Han, M.-H. Ham, Z. Jin, S. Lin, G. L. C. Paulus, N. F. Reuel, Q. H. Wang, D. Blankschtein and M. S. Strano, *Nat. Nanotechnol.*, 2011, **6**, 439–445.
86 K. S. Rao, J. Sentilnathan, H. W. Cho, J. J. Wu and M. Yoshimura, *Adv. Funct. Mater.*, 2015, **25**, 298–305.
87 K. R. Paton, E. Varrla, C. Backes, R. J. Smith, U. Khan, A. O'Neill, C. Boland, M. Lotya, O. M. Istrate, P. King, T. Higgins, S. Barwich, P. May, P. Puczkarski, I. Ahmed, M. Moebius, H. Pettersson, E. Long, J. Coelho, S. E. O'Brien, E. K. McGuire, B. M. Sanchez, G. S. Duesberg, N. McEvoy, T. J. Pennycook, *et al.*, *Nat. Mater.*, 2014, **13**, 624–630.
88 H. P. Boehm and E. Stumpp, *Carbon*, 2007, **45**, 1381–1383.
89 C. Schafheutl, *Philos. Mag.*, 1840, **16**, 570–590.
90 B. C. Brodie, *Philos. Trans. R. Soc. London*, 1859, **149**, 249–259.
91 B. C. Brodie, *Ann. Chim. Phys.*, 1860, **59**, 466–472.
92 L. Staudenmaier, *Ber. Dtsch. Chem. Ges.*, 1898, **31**, 1481–1487.
93 W. S. Hummers and R. E. Offeman, *J. Am. Chem. Soc.*, 1958, **80**, 1339.
94 D. R. Dreyer, S. Park, C. W. Bielawski and R. S. Ruoff, *Chem. Soc. Rev.*, 2010, **39**, 228–240.

95 S. Pan and I. A. Aksay, *ACS Nano*, 2011, **5**, 4073–4083.
96 C. Botas, P. Álvarez, C. Blanco, R. Santamaría, M. Granda, P. Ares, F. Rodríguez-Reinosoc and R. Menéndeza, *Carbon*, 2012, **50**, 275–282.
97 K. Krishnamoorthy, M. Veerapandian, K. Yun and S.-J. Kim, *Carbon*, 2013, **53**, 38–49.
98 D. R. Dreyer, A. D. Todd and C. W. Bielawski, *Chem. Soc. Rev.*, 2014, **43**, 5288–5301.
99 G. Ruess, *Monatsh. Chem.*, 1946, **76**, 381–417.
100 W. Scholz and H. P. Boehm, *Z. Anorg. Allg. Chem.*, 1969, **369**, 327–340.
101 T. Nakajima and Y. Matsuo, *Carbon*, 1994, **32**, 469–475.
102 A. Lerf, M. Forster and J. Klinowski, *J. Phys. Chem. B*, 1998, **102**, 4477–4482.
103 T. Szabó, O. Berkesi, P. Forgó, K. Josepovits, Y. Sanakis, D. Petridis and I. Dékány, *Chem. Mater.*, 2006, **16**, 2740–2749.
104 A. Lerf, H. He, T. Riedl, M. Foster and J. Klinowski, *Solid State Ionics*, 1997, **101–103**, 857–862.
105 J. L. Li, K. N. Kundin, M. J. McAllister, R. K. Prud'homme, I. A. Aksay and R. Car, *Phys. Rev. Lett.*, 2006, **96**, 176101-1–4.
106 K. N. Kundin, B. Ozbas, H. C. Schniepp, R. K. Prudhumme, I. A. Aksay and R. Car, *Nano Lett.*, 2008, **8**, 36–41.
107 D. W. Boukhvalov and M. I. Katsnelson, *J. Am. Chem. Soc.*, 2008, **130**, 10697–10701.
108 S. Stankovich, R. D. Piner, X. Chen, N. Wu, S. T. Nguyen and R. S. Ruoff, *J. Mater. Chem.*, 2006, **16**, 155–158.
109 J. Barkauskas, I. Stankeviciene, J. Daksevic and A. Padarauskas, *Carbon*, 2011, **49**, 5373–5381.
110 S. Stankovich, R. Piner, S. T. Nguyen and R. S. Ruoff, *Carbon*, 2006, **44**, 3342–3347.
111 J. Liu, J. Tang and J. J. Gooding, *J. Mater. Chem.*, 2012, **22**, 12435–12452.
112 J. I. Paredes, S. Villar-Rodil, A. Martinez-Alonso and J. M. D. Tascon, *Langmuir*, 2008, **2**, 10560–10564.
113 R. Jalili, S. H. Aboutalebi, D. Esrafilzadeh, K. Konstantinov, S. E. Moulton, J. M. Razal and G. G. Wallace, *ACS Nano*, 2013, **7**, 3981–3990.
114 X. Shen, X. Lin, N. Yousefi, J. Jia and J.-K. Kim, *Carbon*, 2014, **66**, 84–92.
115 R. K. Joshi, P. Carbone, F. C. Wang, V. G. Kravets, Y. Su, I. V. Grigorieva, H. A. Wu, A. K. Geim and R. R. Nair, *Science*, 2014, **343**, 752–754.
116 K. Cui, O. Ivasenko, K. S. Mali, D. Du, X. Feng, K. Müllen, S. D. Feyter and S. F. L. Mertens, *Chem. Commun.*, 2014, **50**, 10376–10378.
117 S. Yang, Y. Sun, L. Chen, Y. Hernandez, X. Feng and K. Müllen, *Sci. Rep.*, 2012, **2**, 427.
118 W. Gao, M. Majumder, L. B. Alemany, T. N. Narayanan, M. A. Ibarra, B. K. Pradhan and M. M. Ajayan, *ACS Appl. Mater. Interfaces*, 2011, **3**, 1821–1826.
119 C. K. Chua and M. Pumera, *Chem. Soc. Rev.*, 2014, **43**, 291–312.
120 P. V. Kumar, N. M. Bardhan, S. Tongay, J. Wu, A. M. Belcher and J. C. Grossmann, *Nat. Chem.*, 2014, **6**, 151–158.
121 B. Wang, Q. Liu, J. Han, X. Zhang, J. Wang, Z. Li, H. Yan and L. Liu, *J. Mater. Chem. A*, 2014, **2**, 1137–1143.
122 G.-H. Moon, H. Kim, Y. Shin and W. Choi, *RSC Adv.*, 2012, **2**, 2205–2207.
123 P. Gong, Z. Wang, Z. Li, Y. Mi, J. Sun, L. Niu, H. Wang, J. Wang and S. Yang, *RSC Adv.*, 2013, **3**, 6327–6330.
124 S. Stankovich, D. A. Dinkin, R. D. Piner, K. A. Kohlhaas, A. Kleinhammes, Y. Jia, Y. Wu, S. T. Nguyen and R. S. Ruoff, *Carbon*, 2007, **45**, 1558–1565.
125 H. J. Shin, K. K. Kim, A. Benayad, S. M. Yoon, H. K. Park, I. S. Jung, M. H. Jin, H.-K. Jeong, J. M. Kim, J.-Y. Choi and Y. H. Lee, *Adv. Funct. Mater.*, 2009, **19**, 1987–1992.
126 V. H. Pham, T. T. Dang, K. Singh, S. H. Hur, E. W. Shin, J. S. Kim, M. A. Lee, S. H. Baeck and J. S. Chung, *J. Mater. Chem. A*, 2013, **1**, 1070–1077.
127 A. N. Abbas, G. Liu, A. Narita, M. Orosco, X. Feng, K. Müllen and C. Zhou, *J. Am. Chem. Soc.*, 2014, **136**, 7555–7558.
128 M. J. Fernandez-Merino, L. Guardia, J. I. Paredes, S. Villar-Rodil, P. Solis-Fernandez and A. Martinez-Alonso, *J. Phys. Chem. C*, 2010, **114**, 6426–6432.
129 I. K. Moon, J. Lee, R. S. Ruoff and H. Lee, *Nat. Commun.*, 2010, **1**, 73–78.
130 H. A. Becerril, J. Mao, Z. Liu, R. M. Stoltenberg, Z. Bao and Y. Chen, *ACS Nano*, 2008, **2**, 463–470.
131 H. Feng, R. Cheng, X. Zhao, X. Duan and J. Li, *Nat. Commun.*, 2012, **4**, 1539, 1–7.
132 T. Kuila, A. K. Mishra, P. Khanra, N. H. Kim and J. H. Lee, *Nanoscale*, 2013, **5**, 52–71.
133 S. Pei and H.-M. Cheng, *Carbon*, 2011, **50**, 3210–3228.
134 A. Esfandial, O. Akhavan and A. Irajizad, *J. Mater. Chem.*, 2011, **21**, 10907–10914.
135 Q. Zhuo, J. Gao, M. Peng, L. Bai, J. Deng, Y. Xia, Y. Ma, J. Zhong and X. Sun, *Carbon*, 2013, **52**, 559–564.
136 Z. Fan, K. Wang, T. Wei, J. Yan, L. Song and B. Shao, *Carbon*, 2010, **48**, 1686–1689.
137 X. Mei and J. Ouyang, *Carbon*, 2011, **49**, 5389–5397.
138 Z. J. Fan, W. Kai, J. Yan, T. Wei, L. J. Zhi and J. Feng, *ACS Nano*, 2011, **5**, 191–198.
139 M. S. Akther, J. Panwar and Y.-S. Yun, *ACS Sustainable Chem. Eng.*, 2013, **1**, 591–602.
140 S. F. Adil, M. E. Assal, M. Khan, A. Al-Warthan, M. R. H. Siddiqui and L. M. Liz-Marzán, *Dalton Trans.*, 2015, **44**, 9709–9717.
141 M. Khan, M. Khan, S. F. Adil, M. N. Tahir, W. Tremel, H. Z. Alkhathlan, A. Al-Warthan and M. R. H. Siddiqui, *Int. J. Nanomed.*, 2013, **8**, 1507–1516.
142 M. Khan, M. Khan, M. Kuniyil, S. F. Adil, A. Al-Warthan, H. Z. Alkhathlan, W. Tremel, M. N. Tahir and M. R. H. Siddiqui, *Dalton Trans.*, 2014, **43**, 9026–9033.
143 M. Khan, A. H. Al-Marri, M. Khan, N. Mohri, S. F. Adil, A. Al-Warthan, M. R. H. Siddiqui, H. Z. Alkhathlan, R. Berger, W. Tremel and M. N. Tahir, *RSC Adv.*, 2014, **4**, 24119–24125.
144 J. Li, G. Xiao, C. Chen, R. Li and D. Yan, *J. Mater. Chem. A*, 2013, **1**, 1481–1487.
145 A. Nandgaonkar, Q.-Q. Wang, K. Fu, W. E. Krause, Q. Wei, R. Gorga and L. Lucia, *Green Chem.*, 2014, **16**, 3195–3201.
146 M. Fan, C. Zhu, Z.-Q. Feng, J. Yang, L. Liu and D. Sun, *Nanoscale*, 2014, **6**, 4882–4888.

147 T. Kuila, S. Bose, P. Khanra, K. A. Mishra, N. H. Kim and J. H. Lee, *Carbon*, 2012, **50**, 914–921.
148 G. Wang, F. Qian, C. W. Saltikov, Y. Jiao and Y. Li, *Nano Res.*, 2011, **4**, 563–570.
149 M. J. McAllister, J. Li, D. H. Adamson, H. C. Schniepp, A. A. Abdala, J. Liu, M. Herrera-Alonso, D. L. Milius, R. Car, R. K. Prud'homme and I. A. Aksay, *Chem. Mater.*, 2007, **19**, 4396–4404.
150 C. J. Kim, W. Khan and S. Y. Park, *Chem. Phys. Lett.*, 2011, **511**, 110–115.
151 L. Song, F. Khoerunnisa, W. Gao, W. Dou and T. Hayashi, *Carbon*, 2013, **52**, 608–612.
152 B. Shen, D. Lu, W. Zhai and W. Zheng, *J. Mater. Chem. C*, 2013, **1**, 50–53.
153 W. Lv, D. M. Tang, Y. B. He, C. H. You, Z. Q. Shi, X. C. Chen, C.-M. Chen, P.-X. Hou, C. Liu and Q.-H. Yang, *ACS Nano*, 2009, **3**, 3730–3736.
154 H.-B. Zhang, J.-W. Wang, Q. Yan, W.-G. Zheng, C. Chen and Z.-Z. Yu, *J. Mater. Chem.*, 2011, **21**, 5392–5397.
155 K. H. Liao, A. Mittal, S. Bose, C. Leighton, A. Mkhovan and W. W. Macosko, *ACS Nano*, 2011, **5**, 1253–1258.
156 S. M. Choi, M. H. Seo, H. J. Kim and W. B. Kim, *Carbon*, 2011, **49**, 904–909.
157 Z.-L. Wang, D. Xu, Y. Huang, Z. Wu, L.-M. Wang and X.-B. Zhang, *Chem. Commun.*, 2012, **48**, 976–978.
158 J. Yang, M. R. Jo, M. Kang, Y. S. Huh, H. Jung and Y. M. Kang, *Carbon*, 2014, **53**, 106–113.
159 J. A. Gerbec, D. Magana, A. Washington and G. F. Strouse, *J. Am. Chem. Soc.*, 2005, **127**, 15791–15800.
160 H. Hu, X. Wang, F. Liu, J. Wang and C. Xu, *Synth. Met.*, 2011, **161**, 404–410.
161 B. Tryba, A. W. Morawski and M. Inagaki, *Carbon*, 2005, **43**, 2417–2419.
162 T. Wei, Z. J. Fan, J. L. Luo, C. Zheng and D. S. Xie, *Carbon*, 2009, **47**, 337–339.
163 Z. Li, Y. Yao, Z. Lin, K. S. Moon, W. Lin and C. Wong, *J. Mater. Chem.*, 2010, **20**, 4781–4783.
164 G. Demazeau, *J. Mater. Chem.*, 1999, **9**, 15–18.
165 H. Wang, J. T. Robinson, X. Li and H. Dia, *J. Am. Chem. Soc.*, 2009, **131**, 9910–9911.
166 Y. Zhou, Q. Bao, L. A. L. Tang, Y. Zhong and K. P. Loh, *Chem. Mater.*, 2009, **21**, 2950–2956.
167 R. Wang, Y. Wang, C. Xu, J. Sun and L. Gao, *RSC Adv.*, 2013, **3**, 1194–1200.
168 S. Dubin, S. Gilje, K. Wang, V. C. Tung, K. Cha and A. S. Hall, *ACS Nano*, 2010, **4**, 3845–3852.
169 D. Zhou, Q.-Y. Cheng and B.-H. Han, *Carbon*, 2011, **49**, 3920–3927.
170 R. Larciprete, S. Fabris, T. Sun, P. Lacovig, A. Baralidi and S. Lizzit, *J. Am. Chem. Soc.*, 2011, **133**, 17315–17321.
171 D. Yang, A. Velamakanni, G. L. Bozoklu, S. Park, M. Stroller and R. D. Piner, *Carbon*, 2009, **47**, 145–152.
172 H. K. Jeong, Y. P. Lee, M. H. Jin, E. S. Kim, J. J. Bae and Y. H. Lee, *Chem. Phys. Lett.*, 2009, **470**, 255–258.
173 X. Gao, J. Jang and S. Nagase, *J. Phys. Chem. C*, 2010, **114**, 832–842.
174 A. Ganguly, S. Sharma, P. Papakontantino and J. Hamilton, *J. Phys. Chem. C*, 2011, **115**, 17009–17019.
175 M. Acik, G. Lee, C. Mattevi, A. Pirkle, R. M. Wallace, M. Chhowalla, K. Cho and Y. Chabal, *J. Phys. Chem. C*, 2011, **115**, 19761–19781.
176 X. Fan, W. Peng, Y. Li, X. Li, S. Wang, G. Zhang and F. Zhang, *Adv. Mater.*, 2008, **20**, 4490–4493.
177 T. Kuila, S. Bose, A. K. Mishra, P. Kharna, N. H. Kim and J. H. Lee, *Prog. Mater. Sci.*, 2012, **57**, 1061–1105.
178 K. P. Loh, Q. Bao, K. P. Ang and J. Yang, *J. Mater. Chem.*, 2012, **20**, 2277–2289.
179 H. Bai, C. Li and G. Shi, *Adv. Mater.*, 2011, **23**, 1089–1115.
180 P. E. Solon and N. Tagmatarchis, *Chem.–Eur. J.*, 2013, **19**, 12930–12936.
181 T. S. Sreeprasad and V. Berry, *Small*, 2013, **9**, 341–350.
182 E. Nossol, A. B. S. Nossol, S.-X. Guo, J. Zhang, X.-Y. Fang, A. G. J. Zarbin and A. M. Bond, *J. Mater. Chem. C*, 2014, **2**, 870–878.
183 R. Muszynski, B. Seger and P. V. Kamat, *J. Phys. Chem. C*, 2008, **112**, 5263–5266.
184 S. Guo, S. Dong and E. Wang, *ACS Nano*, 2009, **4**, 547–555.
185 Z. Ji, X. Shen, Y. Song and G. Zhu, *Mater. Sci. Eng.*, 2011, **176**, 711–715.
186 Y. Zhang, S. Liu, L. Wang, X. Qin, J. Tian, W. Lu, G. Chang and X. Sun, *RSC Adv.*, 2012, **2**, 538–545.
187 Z. Ji, X. Shen, Y. Xu, H. Zhou, S. Bai and G. Zhu, *RSC Adv.*, 2014, **4**, 13601–13609.
188 K. D. J. I. Jayawardena, R. Rhodes, K. K. Gandhi, M. R. R. Prabhath, G. D. M. R. Dabera, M. J. Beliatis, L. J. Rozanski, S. J. Henley and S. R. P. Silva, *J. Mater. Chem. A*, 2013, **1**, 9922–9927.
189 H. Kim, D. H. Seo, S. W. Kim, J. Kim and K. Kang, *Carbon*, 2011, **49**, 326–332.
190 J. Zhang, X. Liu, L. Wang, T. Yang, X. Guo and S. Wu, *Carbon*, 2011, **49**, 3538–3543.
191 J. Li, Z. Yang, H. Qiu, Y. Dai, Q. Zheng, G.-P. Zheng and J. Yang, *J. Mater. Chem. A*, 2013, **1**, 11451–11456.
192 X. Huang, X. Qi, F. Boey and H. Zhang, *Chem. Soc. Rev.*, 2012, **41**, 666–686.
193 H. M. A. Hassan, V. Abdelsayed, R. A. E. Khder, K. M. AbouZeid, J. Terner, M. S. El-Shall, S. I. Al-Resayes and A. A. El-Azhary, *J. Mater. Chem.*, 2009, **19**, 3832–3837.
194 X. Liu, L. Pan, T. Lv, T. Lu, G. Zhu, Z. Sun and C. Sun, *Catal. Sci. Technol.*, 2011, **1**, 1189–1193.
195 M. Li, X. Bo, Y. Zhang, C. Han and L. Guo, *Biosens. Bioelectron.*, 2014, **56**, 223–230.
196 T. Li, J. R. Hauptmann, Z. Wei, S. Petersen, N. Bovet, T. Vosch, J. Nygård, W. Hu, Y. Liu, T. Bjørnholm, K. Nørgaard and B. W. Laursen, *Adv. Mater.*, 2012, **24**, 1333–1339.
197 P. Chen, T. Y. Xiao, H. H. Li, J. J. Yang, Z. Wang, H. B. Yao and S. H. Yu, *ACS Nano*, 2012, **6**, 712–719.
198 L. Ye, J. Fu, Z. Xu, R. Yuan and Z. Li, *ACS Appl. Mater. Interfaces*, 2014, **6**, 3483–3490.
199 J. Shen, M. Shi, H. Ma, B. Yan, N. Li and M. Ye, *Mater. Res. Bull.*, 2011, **46**, 2077–2083.

200 B. Li, H. Cao, J. Shao, M. Qu and J. H. Warner, *J. Mater. Chem.*, 2011, **21**, 5069–5075.
201 J. Shen, M. Shi, B. Yan, H. Ma, N. Li and M. Ye, *Nano Res.*, 2011, **4**, 795–806.
202 W. Gao, B. Alemany, L. Ci and P. M. Ajayan, *Nat. Chem.*, 2009, **1**, 403–408.
203 H. Chang and H. Wu, *Energy Environ. Sci.*, 2013, **6**, 3483–3507.
204 K. Hu, D. D. Kulkarni, I. Choi and V. V. Tsukruk, *Prog. Polym. Sci.*, 2014, **39**, 1934–1972.
205 M. Terrones, O. Martin, M. Gonzalez, J. Pozuelo, B. Serrano, J. C. Cabanelas, S. M. Vega-Diaz and J. Baselga, *Adv. Mater.*, 2011, **23**, 5302–5310.
206 Z.-S. Wu, K. Parvez, A. Winter, H. Vieker, X. Liu, S. Han, A. Turchanin, X. Feng and K. Müllen, *Adv. Mater.*, 2014, **26**, 4552–4558.
207 R. Chen, D. Sun and W. P. Sung, *Adv. Mater.*, 2012, **430**, 79–82.
208 N. Mahmood, C. Zhang, H. Yin and Y. Hou, *J. Mater. Chem. A*, 2014, **2**, 15–32.
209 Q. Li, N. Mahmood, J. Zhu, Y. Hou and S. Sun, *Nano Today*, 2014, **9**, 668–683.
210 F. Bonaccorso, L. Colombo, G. Yu, M. Stoller, V. Tozzini, A. C. Ferrari, R. S. Ruoff and V. Pellegrini, *Science*, 2015, **347**, 6217.
211 D. P. Dubal, O. Ayyad, V. Ruiz and P. Gómez-Romero, *Chem. Soc. Rev.*, 2015, **44**, 1777–1790.
212 C. Hu, L. Song, Z. Zhang, N. Chen, Z. Feng and L. Qu, *Energy Environ. Sci.*, 2015, **8**, 31–54.
213 N. Mahmood and Y. Hou, *Advanced Science*, 2014, **1**, 1–20.
214 Y. Huang, H. Liu, Y. Lu, Y. Hou and Q. Li, *J. Power Sources*, 2015, **284**, 236–244.
215 B. Oschmann, D. Bresser, M. N. Tahir, K. Fischer, W. Tremel, S. Passerini and R. Zentel, *Macromol. Rapid Commun.*, 2013, **34**, 1693.
216 D. Bresser, B. Oschmann, M. N. Tahir, W. Tremel, R. Zentel and S. Passerini, *J. Power Sources*, 2014, **248**, 852.
217 J. Wang, L. Shen, P. Nie, G. Xu, B. Ding, S. Fang, H. Dou and X. Zhang, *J. Mater. Chem. A*, 2014, **2**, 9150–9155.
218 B. Qiu, M. Xing and J. Zhang, *J. Am. Chem. Soc.*, 2014, **136**, 5852–5855.
219 V. Etacheri, J. E. Yourey and B. M. Bartlett, *ACS Nano*, 2014, **8**, 1491–1499.
220 N. Li, G. Liu, C. Zhen, F. Li, L. Zhang and H. M. Cheng, *Adv. Funct. Mater.*, 2011, **21**, 1717–1722.
221 M. S. Whittingham, *Chem. Rev.*, 2004, **104**, 4271–4301.
222 Z.-S. Wu, G. Zhou, L.-C. Yin, W. Ren and F. Li, *Nano Energy*, 2012, **1**, 107–131.
223 M. Lee, S. K. Balasingam, H. Y. Jeong, W. G. Hong, H.-B. R. Lee, B. H. Kim and Y. Jun, *Sci. Rep.*, 2015, **5**, 8151.
224 M. Li, G. Sun, P. Yin, C. Ruan and K. Ai, *ACS Appl. Mater. Interfaces*, 2013, **5**, 11462–11470.
225 J. Cheng, B. Wang, H. L. Xin, G. Yang, H. Cai, F. Nie and H. Huang, *J. Mater. Chem. A*, 2013, **1**, 10814–10820.
226 H. Liu and W. Yang, *Energy Environ. Sci.*, 2011, **4**, 4000–4008.
227 G. Du, K. H. Seng, Z. Guo, J. Liu, W. Li, D. Jai, C. Cook, Z. Liu and H. Liu, *RSC Adv.*, 2011, **1**, 690–697.
228 X. Yang, H. Ding, D. Zhang, X. Yan, C. Lu, J. Qin, R. Zhang, H. Tang and H. Song, *Cryst. Res. Technol.*, 2011, **46**, 1195–1201.
229 P. Lu, J. Liu and M. Lei, *CrystEngComm*, 2014, **16**, 6745–6755.
230 K. Chang, Z. Mei, T. Wang, Q. Kang, S. Ouyang and J. Ye, *ACS Nano*, 2014, **8**, 7078–7087.
231 K. Chang and W. Chen, *J. Mater. Chem.*, 2011, **21**, 17175–17184.
232 K. Chang and W. Chen, *ACS Nano*, 2011, **65**, 4720–4728.
233 D. H. Youn, S. Han, J. Y. Kim, J. Y. Kim, H. Park, S. H. Choi and J. S. Lee, *ACS Nano*, 2014, **8**, 5164–5173.
234 Z. X. Huang, Y. Wang, Y. G. Zhu, Y. Shi, J. I. Wong and H. Y. Yang, *Nanoscale*, 2014, **6**, 9839–9845.
235 U. Maitra, U. Gupta, M. De, R. Datta, A. Govindaraj and C. N. R. Rao, *Angew. Chem., Int. Ed.*, 2013, **52**, 13057–13061.
236 L. Liao, J. Zhu, X. Bian, L. Zhu, M. D. Scanlon, H. H. Girault and B. Liu, *Adv. Funct. Mater.*, 2013, **23**, 5326–5333.
237 Y. Cao, X. Lin, C. Zhang, C. Yang, Q. Zhang, W. Hu, M. Zheng and Q. Dong, *RSC Adv.*, 2014, **4**, 30150–30155.
238 A. Yu, H. W. Park, A. Davies, D. C. Higgins, Z. Chen and X. Xiao, *J. Phys. Chem. Lett.*, 2011, **2**, 1855–1860.
239 C. Chen, H. Jian, X. Fu, Z. Ren, M. Yan, G. Qian and Z. Wang, *RSC Adv.*, 2014, **4**, 5367–5370.
240 L. Li, Z. Guo, A. Du and H. Liu, *J. Mater. Chem.*, 2012, **22**, 3600–3605.
241 H. Huang, L. Zhang, Y. Xia, Y. Gan, X. Tao, C. Liang and W. Zhang, *New J. Chem.*, 2014, **38**, 4743–4747.
242 B. Wang, J. Park, C. Wang, H. Ahn and G. Wang, *Electrochim. Acta*, 2010, **55**, 6812–6817.
243 B. Sun, Z. X. Chen, H. S. Kim, H. Ahn and G. X. Wang, *J. Power Sources*, 2011, **196**, 3346–3349.
244 L. Xiao, M. Schroeder, S. Kluge, A. Balducci, U. Hagemann, C. Schulz and H. Wiggers, *J. Mater. Chem. A*, 2015, DOI: 10.1039/c5ta02549d.
245 Y. Chen, Z. Lei, H. Wu, C. Zhu, P. Gao, Q. Ouyanga, L.-H. Qia and W. Qin, *Mater. Res. Bull.*, 2013, **48**, 3362–3366.
246 P. Guo, G. Zhu, H. Song, X. Chen and S. Zhang, *Phys. Chem. Chem. Phys.*, 2011, **13**, 17818–17824.
247 B. Jang, O. B. Chae, S.-K. Park, J. Ha, S. M. Oh, H. B. Na and Y. Piao, *J. Mater. Chem. A*, 2013, **1**, 15442–15446.
248 X. Huang, B. Sun, S. Chen and G. Wang, *Chem.–Asian J.*, 2014, **9**, 206–211.
249 D. Chen, G. Ji, Y. Ma, J. Y. Lee and J. Lu, *ACS Appl. Mater. Interfaces*, 2011, **3**, 3078–3083.
250 C. Liang, T. Zhai, W. Wang, J. Chen, W. Zhao, X. Lu and Y. Tong, *J. Mater. Chem. A*, 2014, **2**, 7214–7220.
251 S. H. Lee, S.-H. Yu, J. E. Lee, A. Jin, D. J. Lee, N. Lee, H. Jo, K. Shin, T.-Y. Ahn, Y.-W. Kim, H. Choe, Y.-E. Sung and T. Hyeon, *Nano Lett.*, 2013, **13**, 4249–4256.
252 J. Su, M. Cao, L. Ren and C. Hu, *J. Phys. Chem. C*, 2011, **115**, 14469–14477.
253 S. K. Behera, *Chem. Commun.*, 2011, **47**, 10371–10373.
254 G. Wang, T. Liu, X. Xie, Z. Ren, J. Bai and H. Wang, *Mater. Chem. Phys.*, 2011, **128**, 336–340.

255 X. Li, X. Huang, D. Liu, X. Wang, S. Song, L. Zhou and H. Zhang, *J. Phys. Chem. C*, 2011, **115**, 21567–21573.
256 J. Lin, A.-R. Raji, K. Nan, Z. Peng and Z. Yan, *Adv. Funct. Mater.*, 2014, **24**, 2044–2048.
257 X. Zhu, X. Song, X. Ma and G. Ning, *ACS Appl. Mater. Interfaces*, 2014, **6**, 7189–7197.
258 W. Zhou, J. Zhu, C. Cheng, J. Liu, H. Yang, C. Cong, C. Guan, X. Jia, H. J. Fan, Q. Yan, C. M. Li and T. Yu, *Energy Environ. Sci.*, 2011, **4**, 4954–4961.
259 Y. Zou, J. Kan and Y. Wang, *J. Phys. Chem. C*, 2011, **115**, 20747–20753.
260 X. Zhu, Y. Zhu, S. Murali, M. D. Stoller and R. S. Ruoff, *ACS Nano*, 2011, **5**, 3333–3338.
261 J. Yang, J. Wang, Y. Tang, D. Wang, X. Li, Y. Hu, R. Li, G. Liang, T.-K. Sham and X. Sun, *Energy Environ. Sci.*, 2013, **6**, 1521–1528.
262 W. K. Kim, W. H. Ryu, D. W. Han, S. J. Lim, J. Y. Eom and H. S. Kwon, *ACS Appl. Mater. Interfaces*, 2014, **6**, 4731–4736.
263 X. Zhou, F. Wang, Y. Zhu and Z. Liu, *J. Mater. Chem.*, 2011, **21**, 3353–3358.
264 X. L. Huang, X. Zhao, Z. L. Wang, L. M. Wang and X. B. Zhang, *J. Mater. Chem.*, 2012, **22**, 3764–3769.
265 Y. Lou, J. Liang, Y. Peng and J. Chen, *Phys. Chem. Chem. Phys.*, 2015, **17**, 8885–8893.
266 B. Li, H. Cao, J. Shao, G. Li, M. Qu and G. Yin, *Inorg. Chem.*, 2011, 1628–1632.
267 C. Sun, F. Li, C. Ma, Y. Wang, Y. Ren, W. Wang, Z. Ma, J. Li, Y. Chen, Y. Kim and L. Chen, *J. Mater. Chem. A*, 2014, **2**, 7188–7196.
268 S. Yang, G. Cui, S. Pang, Q. Cao, U. Kolb, X. Feng, J. Maier and K. Mullen, *ChemSusChem*, 2010, **3**, 236–239.
269 Z.-S. Wu, W. Ren, L. Wen, L. Gao, J. Zhao, Z. Chen, G. hou, F. Li and H.-M. Cheng, *ACS Nano*, 2010, **4**, 3187–3194.
270 L. Tao, J. Zai, K. Wang, H. Zhang, M. Xu, J. Shen, Y. Su and X. Qian, *J. Power Sources*, 2012, **202**, 230–235.
271 G. Wang, J. Liu, S. Tang, H. Li and D. Cao, *J. Solid State Electrochem.*, 2011, **15**, 2587–2592.
272 S. Q. Chen and Y. Wang, *J. Mater. Chem.*, 2010, **20**, 9735–9739.
273 J. Zhu, Y. K. Sharma, Z. Zeng, X. Zhang, M. Srinivasan, S. Mhaisalkar, H. Zhang, H. H. Hng and Q. Yan, *J. Phys. Chem. C*, 2011, **115**, 8400–8406.
274 F. D. Wu and Y. Wang, *J. Mater. Chem.*, 2011, **21**, 6636–6641.
275 Y. Qi, H. Zhang, N. Du and D. Yang, *J. Mater. Chem. A*, 2013, **1**, 2337–2342.
276 C. Peng, B. Chen, Y. Qin, S. Yang, C. Li, Y. Zuo, S. Liu and J. Yang, *ACS Nano*, 2012, **6**, 1074–1081.
277 Y. Wang, W. Yang, C. Chen and D. G. Evans, *J. Power Sources*, 2008, **184**, 682–690.
278 S. Chen, J. Zhu and X. Wang, *J. Phys. Chem. C*, 2010, **114**, 11829–11834.
279 X. L. Huang, J. Chai, T. Jiang, Y. J. Wei, G. Chen, W. G. Liu, D. Han, L. Niu, L. Wang and X.-B. Zhang, *J. Mater. Chem.*, 2012, **22**, 3404–3410.
280 W. Sun and Y. Wang, *Nanoscale*, 2014, **6**, 11528–11552.
281 S. Yang, P. Gao, D. Bao, Y. Chen, L. Wang, P. Yang, G. Li and Y. Sun, *J. Mater. Chem. A*, 2013, **1**, 6731–6735.
282 J. H. Warner, M. H. Rummeli, A. Bachmatiuk, M. Wilson and B. Buchner, *ACS Nano*, 2010, **4**, 470–476.
283 Y. Yao, C. Xu, S. Miao, H. Sun and S. Wang, *J. Colloid Interface Sci.*, 2014, **402**, 230–236.
284 N. Mahmood, C. Zhang, J. Jiang, F. Liu and Y. Hou, *Chem.–Eur. J.*, 2013, **19**, 5183–5190.
285 W. Liu, C. Lu, X. Wang, K. Liang and B. K. Tay, *J. Mater. Chem. A*, 2015, **3**, 624–633.
286 J. Zai, C. Yu, L. Tao, M. Xu, Y. Xiao, B. Li, Q. Han, K. Wang and X. Qian, *CrystEngComm*, 2013, **15**, 6663–6671.
287 Y. Zou and Y. Wang, *Nanoscale*, 2011, **3**, 2615–2620.
288 L. Tao, J. Zai, K. Wang, Y. Wan, H. Zhang, C. Yu, Y. Xiao and X. Qian, *RSC Adv.*, 2012, **2**, 3410–3415.
289 Y. J. Mai, S. J. Shi, D. Zhang, Y. Lu, C. D. Gu and J. P. Tu, *J. Power Sources*, 2012, **204**, 155–161.
290 B. Li, H. Cao, J. Shao, H. Zheng, Y. Lu, J. Yin and M. Qu, *Chem.Commun.*, 2011, **47**, 3159–3161.
291 M. Xu, F. Wang, B. Ding, X. Song and J. Fang, *RSC Adv.*, 2012, **2**, 2240–2243.
292 X. Zhou, J. Zhang, Q. Su, J. Shi, Y. Liu and G. Du, *Electrochim. Acta*, 2014, **125**, 615–621.
293 Y. J. Mai, X. L. Wang, J. Y. Xiang, Y. Q. Qiao, D. Zhang, C. D. Gu and J. P. Tu, *Electrochim. Acta*, 2011, **56**, 2306–2311.
294 J. Zhu, D. Yang, Z. Yin, Q. Yan and H. Zhang, *Small*, 2014, **10**, 3480–3498.
295 L. Q. Lu and Y. Wang, *Electrochem. Commun.*, 2012, **14**, 82–85.
296 B. Wang, X.-L. Wu, C.-Y. Shu, Y.-G. Guo and C.-R. Wang, *J. Mater. Chem.*, 2010, **20**, 10661–10664.
297 S. Sun, X. Zhang, X. Song, S. Liang, L. Wang and Z. Yang, *CrystEngComm*, 2012, **14**, 3545–3553.
298 N. Li, Y. Xiao, C. Hu and M. Cao, *Chem.–Asian J.*, 2013, **8**, 1960–1965.
299 Y. Zhang, X. Wang, L. Zeng, S. Song and D. Liu, *Dalton Trans.*, 2012, **41**, 4316–4319.
300 X. Wang, X. Cao, L. Bourgeois, H. Guan, S. Chen, Y. Zhong, D.-M. Tang, H. Li, T. Zhai, L. Li, Y. Bando and D. Golberg, *Adv. Funct. Mater.*, 2012, **2**, 2682–2690.
301 H. Wang, F. Fu, F. Zhang, H.-E. Wang, S. V. Kershaw, J. Xu, S.-G. Sun and A. L. Rogach, *J. Mater. Chem.*, 2012, **22**, 2140–2148.
302 R. Thomas, *J. Mater. Chem. A*, 2015, **3**, 274–280.
303 J. Liang, W. Wei, D. Zhong, Q. Yang, L. Li and L. Guo, *ACS Appl. Mater. Interfaces*, 2012, **4**, 454–459.
304 X. Huang, X. Zhou, L. Zhou, K. Qian, Y. Wang, Z. Liu and C. Yu, *ChemPhysChem*, 2011, **12**, 278–281.
305 P. Lian, X. Zhu, S. Liang, Z. Li, W. Yang and H. Wang, *Electrochim. Acta*, 2011, **56**, 4532–4539.
306 J. Jiang, Y. Feng, N. Mahmood, F. Liu and Y. Hou, *Sci. Adv. Mater.*, 2013, **5**, 1667–1675.
307 C. Zhang, N. Mahmood, H. Yin, F. Liu and Y. Hou, *Adv. Mater.*, 2013, **25**, 4932–4937.
308 J. Hou, C. Cao, F. Idrees and X. Ma, *ACS Nano*, 2015, **9**, 2556–2564.
309 N. Mahmood, C. Zhang and Y. Hou, *Small*, 2013, **9**, 1321–1328.

310 N. Mahmood, C. Zhang, F. Liu, J. Zhu and Y. Hou, *ACS Nano*, 2013, **7**, 10307–10318.
311 X. Cao, Z. Yin and H. Zhang, *Energy Environ. Sci.*, 2014, **7**, 1850–1865.
312 J. Han, L. L. Zhang, S. Lee, J. Oh, K.-S. Lee, J. R. Potts, J. Ji, X. Zhao, R. S. Ruoff and S. Park, *ACS Nano*, 2013, **7**, 19–26.
313 Y. Liang, Z. Wang, J. Huang, H. Cheng, F. Zhao, Y. Hu, L. Jiang and L. Qu, *J. Mater. Chem. A*, 2015, **3**, 2547–2551.
314 J. L. Xia, F. Chen, J. H. Li and N. J. Tao, *Nat. Nanotechnol.*, 2009, **4**, 505.
315 S. Giri, D. Ghosh and C. K. Das, *Adv. Funct. Mater.*, 2013, **24**, 1312–1324.
316 S. D. Perera, A. D. Liyanage, N. Nijem, J. P. Ferraris, Y. J. Chabal and K. J. Balkus, *J. Power Sources*, 2013, **230**, 130–137.
317 X. Feng, N. Chen, Y. Zhang, Z. Yan, X. Liu, Q. Shen, Y. Ma, L. Wang and W. Huang, *J. Mater. Chem. A*, 2014, **2**, 9178–9184.
318 G. Hag, Y. Liu, E. Kan, J. Tang, L. Zhang, H. Wang and W. Tang, *RSC Adv.*, 2014, **4**, 9898–9904.
319 Z.-S. Wu, K. Parvez, X. Feng and K. Müllen, *Nat. Commun.*, 2013, **4**, 2487.
320 G. Han, Y. Liu, E. Kan, J. Tang, L. Zhang, H. Wang and W. Tang, *RSC Adv.*, 2014, **4**, 9898–9904.
321 J. Yan, Z. Fan, T. Wei, W. Qian, M. Zhang and F. Wei, *Carbon*, 2010, **48**, 3825–3833.
322 Q. Cheng, J. Tang, J. Ma, H. Zhang, N. Shinya and L. C. Qin, *Carbon*, 2011, **49**, 2917–2925.
323 W. Zilong, Z. Zhu, J. Qiu and S. Yang, *J. Mater. Chem. C*, 2014, **2**, 1331–1336.
324 Z. Fan, J. Yan, T. Wei, L. Zhi, G. Ning, T. Li and F. Wei, *Adv. Funct. Mater.*, 2011, **21**, 2366–2375.
325 W. Qian, Z. Chen, S. Cottingham, W. A. Merill, N. A. Swartz, A. M. Goforth, T. L. Clarec and J. Jiao, *Green Chem.*, 2012, **14**, 371–377.
326 A. T. Chidembo, S. H. Aboutalebi, K. Konstantinov, C. J. Jafta, H. K. Liu and K. I. Ozoemena, *RSC Adv.*, 2014, **4**, 886–892.
327 D. Wang, Y. Li, Q. Wang and T. Wang, *Eur. J. Inorg. Chem.*, 2012, 628–635.
328 C. Long, T. Wei, J. Yan, L. Jiang and Z. Fan, *ACS Nano*, 2013, **7**, 11325–11332.
329 W. Shi, J. Zhu, D. H. Sim, Y. Y. Tay, Z. Lu, X. Zhang, Y. Sharma, M. Srinivasan, H. Zhang, H. H. Hng and Q. Yan, *J. Mater. Chem.*, 2011, **21**, 3422–3427.
330 Q. Qu, S. Yang and X. Feng, *Adv. Mater.*, 2011, **23**, 5574–5580.
331 Z. Ma, X. Huang, S. Dou, J. Wu and S. Wang, *J. Phys. Chem. C*, 2014, **118**, 17231–17239.
332 H. Xu, Z. Hu, A. Lu, Y. Hu, L. Li, Y. Yang, Z. Zhang and H. Wu, *Mater. Chem. Phys.*, 2013, **141**, 310–317.
333 X. Liu, K. X. Yao, C. Meng and Y. Han, *Dalton Trans.*, 2012, **41**, 1289–1296.
334 S.-J. Kim, H. Jung, C. Lee, M. H. Kim and Y. Lee, *Sens. Actuators, B*, 2014, **191**, 298–304.
335 P. Bharali, K. Kuratani, T. Takeuchi, T. Kiyobayashi and N. Kuriyama, *J. Power Sources*, 2011, **196**, 7878–7881.
336 R. Vellacheri, V. K. Pillai and S. Kurungot, *Nanoscale*, 2012, **4**, 890–896.
337 Z.-S. Wu, D.-W. Wang, W. Ren, J. Zhao and G. Zhou, *Adv. Funct. Mater.*, 2010, **20**, 3595–3602.
338 H. Wang, Y. Liang, T. Mirfakhrai, Z. Chen, H. S. Casalongue and H. Dai, *Nano Res.*, 2011, **4**, 729–736.
339 Q. Liao, N. Li, S. Jin, G. Yang and C. Wang, *ACS Nano*, 2015, **9**, 5310–5317.
340 J. Yan, T. Wei, W. Qiao, B. Shao, Q. Zhao, L. Zhang and Z. Fan, *Electrochim. Acta*, 2010, **55**, 6973–6978.
341 W. Zhou, J. Liu, T. Chen, K. S. Tan, X. Jia, Z. Luo, C. Cong, H. Yang, C. M. Li and T. Yu, *Phys. Chem. Chem. Phys.*, 2011, **13**, 14462–14465.
342 T. A. Mahmood, J. Zhu, C. Cao and Y. Hou, *Nano Energy*, 2015, **11**, 267–276.
343 J. Hao, W. Yang, Z. Zhang, B. Lu, X. Ke and B. Zhang, *J. Colloid Interface Sci.*, 2014, **426**, 131–136.
344 L. Wang, D. Wang, X. Y. Dong, Z. J. Zhang, X. F. Pei, X. J. Chen, B. Chen and J. Jin, *Chem. Commun.*, 2011, **47**, 3556–3558.
345 X. Dong, L. Wang, D. Wang, C. Li and J. Jin, *Langmuir*, 2012, **28**, 293–298.
346 M.-S. Wu, Y.-P. Lin, C.-H. Lin and J.-T. Lee, *J. Mater. Chem.*, 2012, **22**, 2442–2448.
347 W. Zhou, M. L. Tan and X. S. Zhou, *Adv. Mater. Res.*, 2012, **345**, 75–78.
348 Z.-S. Wu, Y. Sun, Y.-Z. Tan, S. Yang, X. Feng and K. Müllen, *J. Am. Chem. Soc.*, 2012, **134**, 19532–19535.
349 Y.-M. Wang, D.-D. Zhao, Y.-Q. Zhao, C.-L. Xu and H.-L. Li, *RSC Adv.*, 2012, **2**, 1074–1082.
350 Y.-Y. Yang, Z. A. Hu, Z.-Y. Zhang, F.-H. Zhang, P.-J. Liang, H.-Y. Zhang and H.-Y. Lu, *Mater. Chem. Phys.*, 2012, **133**, 363–368.
351 Z. Ji, J. Wu, X. Shen, H. Zhou and H. Xi, *J. Mater. Sci.*, 2011, **46**, 1190–1195.
352 W. Lv, F. Sun, D. M. Tang, H. T. Fang, C. Liu, Q. H. Yang and H.-M. Cheng, *J. Mater. Chem.*, 2011, **21**, 9014–9019.
353 X. Cao, Y. Shi, W. Shi, G. Lu, X. Huang and Q. Yan, *Small*, 2011, **7**, 3163–3168.
354 B. Zhao, J. Song, P. Liu, W. Zu, T. Fang, Z. Jiao, H. Zhang and Y. Jiang, *J. Mater. Chem.*, 2011, **21**, 18729–18798.
355 A. Chidembo, S. H. Aboutalebi, K. Konstantinov, M. Salari, B. Winton, S. A. Yamini, I. P. Nevirkovets and H. K. Liu, *Energy Environ. Sci.*, 2012, **5**, 5236–5240.
356 J. Zhu, S. Chen, H. Zhou and X. Wang, *Nano Res.*, 2012, **5**, 11–19.
357 J. Xie, X. Sun, N. Zhang, K. Xu, M. Zhou and Y. Xie, *Nano Energy*, 2013, **2**, 65–74.
358 J. T. Zhang, S. Liu, G. L. Pan, G. R. Li and X. P. Gao, *J. Mater. Chem. A*, 2014, **2**, 1524–1529.
359 W. Yang, Z. Gao, J. Wang, J. Ma, M. Zhang and L. Liu, *ACS Appl. Mater. Interfaces*, 2013, **5**, 5443–5454.
360 Z. Sun and X. Lu, *Ind. Eng. Chem. Res.*, 2012, **51**, 9973–9979.
361 J. W. Lee, T. Ahn, D. Soundarajan, J. M. Ko and J. D. Kim, *Chem. Commun.*, 2011, **47**, 6305–6307.

362 T.-H. Gu, J. L. Gunjakar, I. Y. Kim, S. B. Patil, J. M. Lee, X. Jin, N.-S. Lee and S.-J. Hwang, *Small*, 2015, DOI: 10.1002/smll.201500286.

363 Z. Gao, J. Wang, Z. Li, W. Yang, B. Wang, M. Hou, Y. He, Q. Liu, T. Mann, P. Yang, M. Zhang and L. Liu, *Chem. Mater.*, 2011, **23**, 3509–3516.

364 N. Mahmood, M. Tahir, A. Mahmood, W. Yang, X. Gu, C. Cao, Y. Zhang and Y. Hou, *Science China Materials*, 2015, **58**, 114–125.

365 K. Wang, X. Dong, C. Zhao, X. Qian and Y. Xu, *Electrochim. Acta*, 2015, **152**, 433–442.

366 P. Yang, X. Xiao, Y. Li, Y. Ding, P. Qiang, X. Tan, W. Mai, Z. Lin, W. Wu, T. Li, H. Jin, P. Liu, J. Zhou, C. P. Wong and Z. L. Wang, *ACS Nano*, 2013, **7**, 2617–2626.

367 J. Chen, C. Li, G. Eda, Y. Zhang, W. Lei, M. Chowalla, W. I. Milne and W.-Q. Deng, *Chem. Commun.*, 2011, **47**, 6084–6086.

368 T. Lu, L. Pan, H. Li, G. Zhu, T. Lv, X. Liu, Z. Sun, T. Chen and D. H. C. Chu, *J. Alloys Compd.*, 2011, **509**, 5488–5492.

369 T. Lu, Y. Zhang, H. Li, L. Pan, Y. Li and Z. Sun, *Electrochim. Acta*, 2010, **55**, 4170–4173.

370 J. Wang, Z. Gao, Z. Li, B. Wang, Y. Yan, Q. Liu, T. Mann, M. Zhang and Z. Jiang, *J. Solid State Chem.*, 2011, **184**, 1421–1427.

371 A. Prakash and D. Bahadur, *ACS Appl. Mater. Interfaces*, 2014, **6**, 1394–1405.

372 Y.-L. Chen, Z.-A. Hu, Y.-Q. Chang, H.-W. Wang, Z.-Y. Zhang, Y.-Y. Yang and H.-Y. Wu, *J. Phys. Chem. C*, 2011, **115**, 2563–2571.

373 L. Huang, G. Guo, Y. Liu, Q. Chang and Y. Xie, *J. Disp. Technol.*, 2012, **8**, 1–4.

374 V.-D. Dao, Y. Choi, K. Yong, L. L. Larina and H.-S. Choi, *Carbon*, 2015, **84**, 383–389.

375 Y. T. Liang, B. K. Vijayan, K. A. Gray and M. C. Hersam, *Nano Lett.*, 2011, **11**, 2865–2870.

376 J. D. Roy-Mayhew and I. A. Aksay, *Chem. Rev.*, 2014, **114**, 6323–6348.

377 G. Cheng, M. S. Akther, O.-B. Yang and F. J. Stadler, *ACS Appl. Mater. Interfaces*, 2013, **5**, 6635–6642.

378 Z. He, G. Guai, J. Liu, C. Guo, J. S. C. Loo, C. M. Li and Y. T. T. Tan, *Nanoscale*, 2011, **3**, 4613–4616.

379 Y. Fan, H. T. Lu, J. H. Liu, C. P. Yang, Q. S. Jing, Y. X. Zhang, X. K. Yang and K. J. Huang, *Colloids Surf., B*, 2011, **83**, 78–82.

380 G. Natu, Z. Huang, Z. Ji and Y. Wu, *Langmuir*, 2012, **28**, 950–956.

381 R. Bajpai, S. Roy, N. Koratkar and D. S. Misra, *Carbon*, 2013, **56**, 56–63.

382 H. Yang, G. H. Guai, C. Guo, Q. Song, S. P. Jiang, Y. Wang, W. Zhang and C. M. Li, *J. Phys. Chem. C*, 2011, **115**, 12209–12215.

383 M.-H. Yeh, L.-Y. Lin, J.-S. Su, Y.-A. Leu, R. Vittal, C.-L. Sun and K.-C. Ho, *ChemElectroChem*, 2014, **1**, 416–425.

384 F. Gong, H. Wang and Z. S. Wang, *Phys. Chem. Chem. Phys.*, 2011, **13**, 17676–17682.

385 K. P. Musselman, A. Marin, L. Schmidt-Mende and J. L. MacManus-Driscoll, *Adv. Funct. Mater.*, 2012, **22**, 2202–2208.

386 S. Wu, Z. Yin, Q. He, X. Huang, X. Zhou and H. Zhang, *J. Phys. Chem. C*, 2010, **114**, 11816–11821.

387 S. Wu, Z. Yin, Q. He, G. Lu, X. Zhou and H. Zhang, *J. Mater. Chem.*, 2011, **21**, 3467–3470.

388 B. Stambouli, *Renewable Sustainable Energy Rev.*, 2011, **15**, 4507–4520.

389 F. Perreault, A. F. de Faria and M. Elimelech, *Chem. Soc. Rev.*, 2015, DOI: 10.1039/c5cs00021a.

390 B. Zheng, J. Wang, F.-B. Wang and X. Xia, *J. Mater. Chem. A*, 2014, **2**, 9079–9084.

391 Z.-S. Wu, L. Chen, J. Liu, K. Parvez, H. Liang, J. Shu, H. Sachdev, R. Graf, X. Feng and K. Müllen, *Adv. Mater.*, 2014, **26**, 1450–1455.

392 M. Liu, R. Zhang and W. Chen, *Chem. Rev.*, 2014, **114**, 5117–5160.

393 Y. Liang, Y. Li, H. Wang, J. Zhou, J. Wang, T. Regier and H. Dai, *Nat. Mater.*, 2011, **10**, 780–786.

394 H.-W. Liang, W. Wei, Z.-S. Wu, X. Feng and K. Müllen, *J. Am. Chem. Soc.*, 2013, **135**, 16002–16005.

395 M. Liu, R. Zhang and W. Chen, *Chem. Rev.*, 2014, **114**, 5117–5160.

396 R. N. Singh and R. Awasthi, *Catal. Sci. Technol.*, 2011, **1**, 778–783.

397 Y. Zhao, L. Zhan, J. Tian, S. Nie and Z. Ning, *Electrochim. Acta*, 2011, **56**, 1967–1972.

398 J. Yang, C. Tian, L. Wang and H. Fu, *J. Mater. Chem.*, 2011, **21**, 3384–3390.

399 H. Zhao, J. Yang, L. Wang, C. Tian, B. Jiang and H. Fu, *Chem. Commun.*, 2011, **47**, 2014–2016.

400 M. Sawangphruk, A. Krittayavathananon and N. Chinwipas, *J. Mater. Chem. A*, 2013, **1**, 1030–1034.

401 L. Gao, W. Yue, S. Tao and L. Fan, *Langmuir*, 2013, **29**, 957–964.

402 B. F. Machado and P. Serp, *Catal. Sci. Technol.*, 2012, **2**, 54–75.

403 F. Ren, H. Wang, C. Zhai, M. Zhu, R. Yue, Y. Du, P. Yang, J. Xu and W. Lu, *ACS Appl. Mater. Interfaces*, 2014, **6**, 3607–3614.

404 Z. Luo, L. Yuwen, B. Bao, J. Tian, X. Zhu, L. Weng and L. Weng, *J. Mater. Chem.*, 2012, **22**, 7791–7796.

405 W. Wei, H. Liang, K. Parvez, X. Zhuang, X. Feng and K. Müllen, *Angew. Chem., Int. Ed.*, 2014, **53**, 1570–1574.

406 Y. Xin, J.-G. Liu, Y. Zhou, W. Liu, J. Gao and Y. Xie, *J. Power Sources*, 2011, **196**, 1012–1018.

407 Y. Qian, C. Wang and Z.-G. Le, *Appl. Surf. Sci.*, 2011, **257**, 10758–10762.

408 P. Kannan, T. Maiyalagan, N. G. Sahoo and M. Opallo, *J. Mater. Chem. B*, 2013, **1**, 4655–4666.

409 E. J. Yoo, T. Okata, T. Akita, M. Kohyama and J. Honma, *Nano Lett.*, 2009, **9**, 2255–2259.

410 Y. Li, L. Tang and J. Li, *Electrochem. Commun.*, 2009, **11**, 846–849.

411 Y.-G. Zhou, J.-J. Chen, F.-B. Wang, Z.-H. Sheng and X.-H. Xia, *Chem. Commun.*, 2010, **46**, 5951–5953.

412 J.-D. Qiu, G.-C. Wang, R.-P. Liang, X.-H. Xia and H.-W. Yu, *J. Phys. Chem. C*, 2011, **115**, 15639–15645.

413 H. Huang, H. Chen, D. Sun and X. Wang, *J. Power Sources*, 2012, **204**, 46–52.

414 C. Nethravathi, E. A. Anumol, M. Rajamathi and N. Ravishankar, *Nanoscale*, 2011, **3**, 569–571.
415 S. H. Lee, N. Kakati, S. H. Jee, J. Maiti and Y.-S. Yoon, *Mater. Lett.*, 2011, **65**, 3281–3284.
416 L. Dong, R. R. S. Gari, Z. Li, M. M. Craig and S. Hou, *Carbon*, 2010, **48**, 781–787.
417 X. Yang, Q. Yang, J. Xu and C.-S. Lee, *J. Mater. Chem.*, 2012, **22**, 8057–8062.
418 Y. Hu, H. Zhang, P. Wu, H. Zhang, B. Zhou and C. Cai, *Phys. Chem. Chem. Phys.*, 2011, **13**, 4083–4094.
419 S. Zhang, Y. Shao, G. Yin and Y. Lin, *Angew. Chem., Int. Ed.*, 2010, **49**, 2211–2214.
420 S. Wang, X. Wang and S. P. Jiang, *Phys. Chem. Chem. Phys.*, 2011, **13**, 6883–6891.
421 S. Zhang, Y. Shao, H.-G. Liao, J. Liu, I. A. Aksay, G. Yin and Y. Lin, *Chem. Mater.*, 2011, **23**, 1079–1081.
422 C. V. Rao, C. R. Cabrera and Y. Ishikawa, *J. Phys. Chem. C*, 2011, **115**, 21963–21970.
423 Q. Yue, K. Zhang, X. Chen, L. Wang, J. Zhao, J. Liu and J. Jia, *Chem. Commun.*, 2010, **46**, 3369–3371.
424 E. Yoo, T. Okada, T. Akita, M. Kohyama, I. Honma and J. Nakamura, *J. Power Sources*, 2011, **196**, 110–115.
425 D. He, K. Cheng, H. Li, T. Peng, F. Xu, S. Mu and M. Pan, *Langmuir*, 2012, **28**, 3979–3986.
426 C. V. Rao, A. L. M. Reddy, Y. Ishikawa and P. M. Ajayan, *Carbon*, 2011, **49**, 931–936.
427 L. Dai, *Acc. Chem. Res.*, 2013, **46**, 31–42.
428 C. Zhang, R. Hao, H. Liao and Y. Hou, *Nano Energy*, 2013, **2**, 88–97.
429 D. R. Haag and H. H. Kung, *Top. Catal.*, 2014, **57**, 762–773.
430 H. Pan, S. Zhu, X. Lou, L. Mao, J. Lin, F. Tian and D. Zhang, *RSC Adv.*, 2015, **5**, 6543–6552.
431 J. Zhang, Z. Zhu, Y. Tang, K. Müllen and X. Feng, *Adv. Mater.*, 2014, **26**, 734–738.
432 X. An and J. C. Yu, *RSC Adv.*, 2011, **1**, 1426–1434.
433 S. Pang, S. Yang, X. Feng and K. Müllen, *Adv. Mater.*, 2012, **24**, 1566–1570.
434 J. T. Wang, J. M. Ball, E. M. Barea, A. Abate, J. A. Alexander-Webber, J. Huang, M. Saliba, I. Mora-Sero, J. Bisquert, H. J. Snaith and R. J. Nicholas, *Nano Lett.*, 2014, **14**, 724–730.
435 L. Sun, Z. Zhao, Y. Zhou and L. Liu, *Nanoscale*, 2012, **4**, 613–620.
436 S. Dutta, R. Sahoo, C. Ray, S. Sarkar, J. Jana, Y. Negishi and T. Pal, *Dalton Trans.*, 2015, **44**, 193–201.
437 Z. Wang, B. Huang, Y. Dai, Y. Liu, X. Zhang, X. Qin, J. Wang, Z. Zheng and H. Cheng, *CrystEngComm*, 2012, **14**, 1687–1692.
438 Y. Zhang, Z.-R. Tang, X. Fu and Y.-J. Xu, *ACS Nano*, 2010, **4**, 7303–7314.
439 S. A. Jensen, R. Ulbricht, A. Narita, X. Feng, K. Müllen, T. Hertel, D. Turchinovich and M. Bonn, *Nano Lett.*, 2013, **13**, 5925–5930.
440 W. Fan, Q. Lai, Q. Zhang and Y. Wang, *J. Phys. Chem. C*, 2011, **115**, 10694–10701.
441 G. D. Jiang, Z. F. Lin, C. Chen, L. H. Zhu, Q. Chang and N. Wang, *Carbon*, 2011, **49**, 2693–2701.
442 C. H. Kim, B. H. Kim and K. S. Yang, *Carbon*, 2012, **50**, 2472–2481.
443 F. Hoshyargar, J. K. Sahoo, M. N. Tahir, A. Yella, M. Dietzsch, F. Natalio, R. Branscheid, U. Kolb, M. Panthöfera and W. Tremel, *Dalton Trans.*, 2013, **42**, 5292–5297.
444 S. Qi, L. Fei, R. Zuo, Y. Wang and Y. Wu, *J. Mater. Chem. A*, 2014, **2**, 8190–8195.
445 Q. Wua, L. Liao, Q. Zhang, Y. Nie, J. Xiao, S. Wang, S. Dai, Q. Gao, Y. Zhang, X. Sun, B. Liu and Y. Tang, *Electrochim. Acta*, 2015, **158**, 42–48.
446 X. Zhang, X. Quan, S. Chen and H. Yu, *Appl. Catal., B*, 2011, **105**, 237–242.
447 A. Mukherji, B. Seger, G. Q. Lu and L. Wang, *ACS Nano*, 2011, **5**, 3483–3492.
448 Z. Ji, X. Shen, J. Yang, G. Zhu and K. Chen, *Appl. Catal., B*, 2014, **144**, 454–461.
449 M. Zhu, P. Chen and M. Liu, *ACS Nano*, 2011, **5**, 4529–4536.
450 M. Zhu, P. Chen and M. Liu, *Langmuir*, 2012, **28**, 3385–3390.
451 Y. Zhang, X. Yuan, Y. Wang and Y. Chen, *J. Mater. Chem.*, 2012, **22**, 7245–7251.
452 W. Xitao, L. Rong and W. Kang, *J. Mater. Chem. A*, 2014, **2**, 8304–8313.
453 S. Dong, J. Sun, Y. Li, C. Yu, Y. Li and J. Sun, *Appl. Catal., B*, 2014, **144**, 386–393.
454 X. Liu, L. Pan, Q. Zhao, T. Lv, G. Zhu, T. Chen, T. Lu, Z. Sun and C. Sun, *Chem. Eng. J.*, 2012, **183**, 238–243.
455 B. Li and H. Cao, *J. Mater. Chem.*, 2011, **21**, 3346–3349.
456 T. Xu, L. Zhang, H. Cheng and Y. Zhu, *Appl. Catal., B*, 2011, **101**, 382–387.
457 Y. Yang, L. Ren, C. Zhang, S. Huang and T. Liu, *ACS Appl. Mater. Interfaces*, 2011, **3**, 2779–2785.
458 B. Li, T. Liu, Y. Wang and Z. Wang, *J. Colloid Interface Sci.*, 2012, **377**, 114–121.
459 Y. Fu and X. Wang, *Ind. Eng. Chem. Res.*, 2011, **1**, 7210–7218.
460 H. Hu, J. H. Xin, H. Hu, X. Wang and Y. Kong, *Appl. Catal., A*, 2015, **492**, 1–9.
461 S. Chandra, S. Bag, R. Bhar and P. Pramanik, *J. Nanopart. Res.*, 2011, **13**, 2769–2777.
462 Y. Ren, G. Fan and C. Wang, *J. Hazard. Mater.*, 2014, **274**, 32–40.
463 Z. Ji, X. Shen, G. Zhu, H. Zhou and A. Yuan, *J. Mater. Chem.*, 2012, **22**, 3471–3477.
464 N. Li, M. Cao, Q. Wu and C. Hu, *CrystEngComm*, 2012, **14**, 428–434.
465 J. Sun, Y. Fu, G. He, X. Sun and X. Wang, *Catal. Sci. Technol.*, 2014, **4**, 1742–1748.
466 K. Qu, L. Wu, J. Ren and X. Qu, *ACS Appl. Mater. Interfaces*, 2012, **4**, 5001–5009.
467 G. M. Scheuermann, L. Rumi, P. Steurer, W. Bannwarth and R. Mülhaupt, *J. Am. Chem. Soc.*, 2009, **131**, 8262–8270.
468 A. R. Siamaki, A. R. S. Khder, V. Abdelsayed, S. El-Shall and B. F. Gupton, *J. Catal.*, 2011, **279**, 1–11.
469 J.-H. Yang and D. Ma, *RSC Adv.*, 2013, **3**, 10131–10134.
470 S. Chandra, S. Bag, P. Das, D. Bhattacharya and P. Pramanik, *Chem. Phys. Lett.*, 2012, **519–520**, 59–63.

471 Y. Zhao, H. Zhang, C. Huang, S. Chen and Z. Liu, *J. Colloid Interface Sci.*, 2012, **374**, 83–88.
472 S. K. Movahed, M. Fakharian, M. Dabiri and A. Bazgir, *RSC Adv.*, 2014, **4**, 5243–5247.
473 Y. Li, Y. Cao, J. Xie, D. Jia, H. Qin and Z. Liang, *Catal. Commun.*, 2015, **58**, 21–25.
474 E. Dervishi, S. Bourdo, J. A. Driver, F. Watanabe, A. R. Biris, A. Ghosh, B. Berry, V. Saini and A. S. Biris, *ACS Nano*, 2012, **6**, 501–511.
475 S. S. Varghese, S. Lonkar, K. K. Singh, S. Swaminathan and A. Abdala, *Sens. Actuators, B*, 2015, DOI: 10.1016/j.snb.2015.04.062.
476 S. K. Vashist and J. H. T. Luong, *Carbon*, 2015, **84**, 519–550.
477 D. Du, J. Liu, X. Zhang, X. Cui and Y. Lin, *J. Mater. Chem.*, 2011, **21**, 8032–8037.
478 H. Teymouriana, A. Salimia, S. Firoozia, A. Korania and S. Soltanianc, *Electrochim. Acta*, 2014, **143**, 196–206.
479 J. Gong, X. Miao, H. Wan and D. Song, *Sens. Actuators, B*, 2012, **162**, 341–347.
480 Y. Wu, D. Chu, P. Yang, Y. Du and C. Lu, *Catal. Sci. Technol.*, 2015, **5**, 3375–3382.
481 T. Kida, A. Nishiyama, Z. Hua, K. Suematsu, M. Yuasa and K. Shimanoe, *Langmuir*, 2014, **30**, 2571–2579.
482 B. Weng, J. Wu, N. Zhang and Y.-J. Xu, *Langmuir*, 2014, **30**, 5574–5584.
483 J. Qin, M. Cao, N. Li and C. Hu, *J. Mater. Chem.*, 2011, **21**, 17167–17174.
484 Y. Mu, D. Jia, Y. He, Y. Miao and H.-L. Wu, *Biosens. Bioelectron.*, 2011, **26**, 2948–2952.
485 P. Subramanian, J. Niedziolka-Jonsson, A. Lesniewski, Q. Wang, M. Li, R. Boukherroub and S. Szunerits, *J. Mater. Chem. A*, 2014, **2**, 5525–5533.
486 L. Fu, S. Yu, L. Thompson and A. Yu, *RSC Adv.*, 2015, **5**, 40111–40116.
487 J. L. Johnson, A. Behnam, S. J. Pearton and A. Ural, *Adv. Mater.*, 2010, **22**, 4877–4880.
488 U. Lange, T. Hirsch, V. M. Mirsky and O. S. Wolfbeis, *Electrochim. Acta*, 2011, **56**, 3707–3712.
489 J. J. Shi and J. J. Zhu, *Electrochim. Acta*, 2011, **56**, 6008–6013.
490 X. Fu, T. Lou, Z. Chen, M. Lin, W. Feng and L. Chen, *ACS Appl. Mater. Interfaces*, 2012, **4**, 1080–1086.
491 F. Wang, L. Zhu and J. Zhang, *Sens. Actuators, B*, 2014, **192**, 642–647.
492 Y. Wang, S. Zhang, D. Du, Y. Shao, Z. Li, J. Wang, M. H. Engelhard, J. Li and Y. Lin, *J. Mater. Chem.*, 2011, **21**, 5319–5325.
493 J. Hu, F. Li, K. Wang, D. Han, Q. Zhang, J. Yuan and L. Niu, *Talanta*, 2012, **93**, 345–349.
494 X. Liu, H. Du and X. W. Sun, *RSC Adv.*, 2014, **4**, 5136–5140.
495 H. Chang, Z. Sun, K. Y. F. Ho, X. Tao, F. Yan, W. M. Kwok and Z. Zheng, *Nanoscale*, 2011, **3**, 258–264.
496 J. Tian, S. Liu, H. Li, L. Wang, Y. Zhang, Y. Luo, A. M. Asiri, A. O. Al-Youbi and X. Sun, *RSC Adv.*, 2012, **2**, 1318–1321.
497 J. Ding, X. Yan and Q. Xue, *Mater. Chem. Phys.*, 2012, **133**, 405–409.
498 K. Anand, O. Singh, M. P. Singh, J. Kaur and R. C. Singh, *Sens. Actuators, B*, 2014, **195**, 409–415.
499 N. Singh, A. Choudhary, D. Haranath, A. G. Joshi, N. Singh, S. Singh, S. Singh and R. Pasricha, *Carbon*, 2012, **50**, 385–394.
500 C. Zhu, Y. Fang, D. Wen and S. Dong, *J. Mater. Chem.*, 2011, **21**, 16911–16917.
501 H. Song, L. Zhang, C. He, Y. Qu, Y. Tian and Y. Lv, *J. Mater. Chem.*, 2011, **21**, 5972–5977.
502 S. Mao, S. Cui, G. Lu, K. Yu, Z. Wen and J. Chen, *J. Mater. Chem.*, 2012, **22**, 11009–11013.
503 Z. Zhang, R. Zou, G. Song, L. Yu, Z. Chen and J. Hu, *J. Mater. Chem.*, 2011, **21**, 17360–17365.
504 L. Long, Y. Luo, B. Liu, D. Du and Y. Lin, *RSC Adv.*, 2015, **5**, 4894–4897.
505 Q. Wang, X. Cui, J. Chen, X. Zheng, C. Liu, T. Xue, H. Wang, Z. Jin, L. Qiao and W. Zheng, *RSC Adv.*, 2012, **2**, 6245–6249.
506 L. M. Lu, H. B. Li, F. Qu, X. B. Zhang, G. L. Shen and R. Q. Yu, *Biosens. Bioelectron.*, 2011, **26**, 3500–3504.
507 Q. Zeng, J. S. Cheng, X. F. Liu, H. T. Bai and J. H. Jiang, *Biosens. Bioelectron.*, 2011, **26**, 3456–3463.
508 X. Feng, R. Li, C. Hu and W. Hou, *J. Electroanal. Chem.*, 2011, **657**, 28–33.
509 S. G. Leonardi, D. Aloisio, N. Donato, P. A. Russo, M. C. Ferro, N. Pinna and G. Neri, *ChemElectroChem*, 2014, **1**, 617–624.
510 V. Mani, B. Dinesh, S. M. Chen and R. Saraswathi, *Biosens. Bioelectron.*, 2014, **53**, 420–427.
511 R. S. Dey and C. R. Raj, *J. Phys. Chem. C*, 2010, **114**, 21427–21433.
512 H. Gao, F. Xiao, C. B. Ching and H. Duan, *ACS Appl. Mater. Interfaces*, 2011, **3**, 3049–3057.
513 X. Bin, J. Chen, H. Cao, L. Chen and J. Yuan, *J. Phys. Chem. Solids*, 2009, **70**, 1–7.
514 N. A. Luechinger, E. K. Athanassiou and W. J. Stark, *Nanotechnology*, 2008, **19**, 445201.
515 Q. Chen, L. Zhang and G. Chen, *Anal. Chem.*, 2012, **84**, 171–178.
516 J. Luo, S. Jiang, H. Zhang, J. Jiang and X. Liu, *Anal. Chim. Acta*, 2012, **709**, 47–53.
517 F. Zhang, Y. Li, Y. Gu, Z. Wang and C. Wang, *Microchim. Acta*, 2011, **173**, 103–109.
518 Y. W. Hsu, T. K. Hsu, C. L. Sun, Y. T. Nien, N. W. Pu and M. D. Ger, *Electrochim. Acta*, 2012, **82**, 152–157.
519 X. Lu, H. Qi, X. Zhang, Z. Xue, J. Jin, X. Zhou, J. Jin, X. Zhou and X. Liu, *Chem. Commun.*, 2011, **47**, 12494–12496.
520 S. Liu, J. Tian, L. Wang and X. Sun, *J. Nanopart. Res.*, 2011, **13**, 4539–4548.
521 B. Zhao, Z. Liu, W. Fu and H. Yang, *Electrochem. Commun.*, 2013, **27**, 1–4.
522 K.-J. Huang, Y.-J. Liu, H.-B. Wang and Y.-Y. Wang, *Electrochim. Acta*, 2014, **118**, 130–137.
523 Y. Zhang, S. Liu, L. Wang, X. Qin, J. Tian, W. Lu, G. Chang and X. Sun, *RSC Adv.*, 2012, **2**, 538–545.
524 Z. G. Le, Z. Liu, Y. Qian and C. Wang, *Appl. Surf. Sci.*, 2012, **258**, 5348–5353.
525 X. Sun, F. Li, G. Shen, J. Huang and X. Wang, *Analyst*, 2014, **139**, 299–308.

526 Y.-C. Yeh, B. Creran and V. M. Rotello, *Nanoscale*, 2012, **4**, 1871–1880.
527 E. E. Bedford, J. Spadavecchia, C. M. Pradier and F. X. Gu, *Macromol. Biosci.*, 2012, **12**, 724–739.
528 K. Jayakumar, R. Rajesh, V. Dharuman, R. Venkatasan, J. H. Hahn and S. K. Pandian, *Biosens. Bioelectron.*, 2012, **31**, 406–412.
529 B. Zhang, Y. Cui, H. Chen, B. Liu, G. Chen and D. Tang, *Electroanalysis*, 2011, **23**, 1821–1829.
530 Y. Chen, Y. Li, D. Sun, D. Tian, J. Zhang and J. J. Zhu, *J. Mater. Chem.*, 2011, **21**, 7604–7611.
531 J. Liang, Z. Chen, L. Guo and L. Li, *Chem. Commun.*, 2010, **47**, 5476–5478.
532 Y. Yang, A. M. Asiri, D. Du and Y. Lin, *Analyst*, 2014, **139**, 3055–3060.
533 S. Liu, G. Yan, G. He, D. Zhong, J. Chen, L. Shi, X. Zhou and H. Jiang, *J. Electroanal. Chem.*, 2012, **672**, 40–44.
534 S. Mao, G. Lu, K. Yu, Z. Bo and J. Chen, *Adv. Mater.*, 2010, **22**, 3521–3526.
535 Y. Chen, B. Jiang, Y. Xiang, Y. Chai and R. Yuan, *Chem. Commun.*, 2011, **47**, 12798–12800.
536 Y. Du, S. Guo, S. Dong and E. Wang, *Biomaterials*, 2011, **32**, 8584–8592.
537 H. Chang, X. Wu, C. Wu, Y. Chen, H. Jiang and X. Wang, *Analyst*, 2011, **136**, 2735–2740.
538 F. Cui and X. Zhang, *J. Electroanal. Chem.*, 2012, **669**, 35–41.
539 S. Palanisamy, S.-M. Chen and R. Sarawathi, *Sens. Actuators, B*, 2012, **166–167**, 372–377.
540 T. Kavitha, A. I. Gopalan, K. P. Lee and S. Y. Park, *Carbon*, 2012, **50**, 2994–3000.
541 S. Gadipelli and Z. X. Guo, *Prog. Mater. Sci.*, 2015, **69**, 1–60.
542 L. Zhang, Y. Tian, Y. Guo, H. Gao, H. Li and S. Yan, *RSC Adv.*, 2015, **5**, 44096–44106.
543 T. S. Sreeprasad, S. M. Maliyekkal, K. P. Lisha and T. Pradeep, *J. Hazard. Mater.*, 2011, **186**, 921–931.
544 N. Li, Z. Geng, M. Cao, L. Ren, X. Zhao, B. Liu, Y. Tian and C. Hu, *Carbon*, 2013, **54**, 124–132.
545 X. H. Guan, B. T. Zheng, M. Lu, X. Guan, G. S. Wang and L. Guo, *ChemPlusChem*, 2012, **77**, 50–60.
546 W. Zhang, X. Shi, Y. Zhang, W. Gu, B. Li and Y. Xian, *J. Mater. Chem. A*, 2013, **1**, 1745–1753.
547 J. Zhang, Z. Xiong and X. S. Zhao, *J. Mater. Chem.*, 2011, **21**, 634–640.
548 V. Chandra, J. Park, Y. Chun, J. W. Lee, I. C. Hwang and K. S. Kim, *ACS Nano*, 2010, **4**, 3979–3986.
549 Z. Geng, Y. Lin, X. Yu, Q. Shen, L. Ma, Z. Li, N. Pan and X. Wang, *J. Mater. Chem.*, 2012, **22**, 3527–3535.
550 J. Zhu, S. Wei, H. Gu, S. B. Rapole, Q. Wang, Z. Luo, N. Haldolaarachchige, D. P. Young and Z. Guo, *Environ. Sci. Technol.*, 2012, **46**, 977–985.
551 G. Xie, P. Xi, H. Liu, F. Chen, L. Huang, Y. Shi, F. Hou, Z. Zeng, C. Shao and J. Wang, *J. Mater. Chem.*, 2012, **22**, 1033–1039.
552 C. Santhosh, P. Kollu, S. Doshi, M. Sharma, D. Bahadur, M. T. Vanchinathan, P. Saravanan, B.-S. Kim and A. N. Grace, *RSC Adv.*, 2014, **4**, 28300–28308.
553 W. Lu, Y. Wu, J. Chen and Y. Yang, *CrystEngComm*, 2014, **16**, 609–615.
554 Q. Min, X. Zhang, H. Zhang, F. Zhou and J.-J. Zhu, *Chem. Commun.*, 2011, **47**, 11709–11711.
555 M. Seredych, O. Mabayoje and T. J. Bandosz, *Langmuir*, 2012, **28**, 1337–1346.
556 K. Turcheniuk, R. Boukherroub and S. Szunerits, *J. Mater. Chem. B*, 2015, **3**, 4301–4324.
557 K. Z. Kamali, A. Pandikumar, G. Sivaraman, H. N. Lim, S. P. Wren, T. Sund and N. M. Huang, *RSC Adv.*, 2015, **5**, 17809–17816.
558 J. Cui, C. Hu, Y. Yang, Y. Wu, L. Yang, Y. Wang, Y. Liu and Z. Jiang, *J. Mater. Chem.*, 2012, **22**, 8121–8126.
559 N. Salam, A. Sinha, A. S. Roy, P. Mondal, N. R. Jana and S. M. Islam, *RSC Adv.*, 2014, **4**, 10001–10012.
560 J. Li and C. Liu, *Eur. J. Inorg. Chem.*, 2010, 1244–1248.
561 A. H. Al-Marri, M. Khan, M. Khan, S. F. Adil, A. Al-Warthan, H. Z. Alkhathlan, W. Tremel, J. P. Labis, M. R. H. Siddiqui and M. N. Tahir, *Int. J. Mol. Sci.*, 2015, **16**, 1131–1142.
562 J. A. Dougan and K. Faulds, *Analyst*, 2012, **137**, 545–554.
563 S. Dutta, C. Ray, S. Sarkar, M. Pradhan, Y. Negishi and T. Pal, *ACS Appl. Mater. Interfaces*, 2013, **5**, 8724–8732.
564 J. R. Lombardi and R. L. Birke, *Acc. Chem. Res.*, 2009, **42**, 734–742.
565 J. Lee, S. Shim, B. Kim and H. S. Shin, *Chem.–Eur. J.*, 2011, **17**, 2381–2387.
566 J. Zabel, R. R. Nair, A. Ott, T. Georgiou, A. K. Geim, K. S. Novoselov and C. Casiraghi, *Nano Lett.*, 2012, **12**, 617–621.
567 X. Ling, L. M. Xie, Y. Fang, H. Xu, H. L. Zhang, J. Kong, M. S. Dresselhaus, J. Zhang and Z. Liu, *Nano Lett.*, 2010, **10**, 553–561.
568 Y. He and H. Cu, *J. Mater. Chem.*, 2012, **22**, 9086–9091.
569 S. Murphy, L. Huang and P. V. Kamat, *J. Phys. Chem. C*, 2013, **117**, 4740–4747.
570 G. Lu, H. Li, C. Liusman, Z. Yin, S. Wu and H. Zhang, *Chem. Sci.*, 2011, **2**, 1817–1821.
571 S. Sun and P. Wu, *Phys. Chem. Chem. Phys.*, 2011, **13**, 21116–21120.
572 Z. Luo, L. A. Somers, Y. Dan, T. Ly, N. J. Kybert, E. J. Mele and A. T. C. Johnson, *Nano Lett.*, 2010, **10**, 777–781.
573 H. Zhou, C. Qiu, F. Yu, H. Yang, M. Chen, L. Hu and L. Sun, *J. Phys. Chem. C*, 2011, **115**, 11348–11354.
574 Z. Zhang, F. Xu, W. Yang, M. Guo, X. Wang, B. Zhang and J. Tang, *Chem. Commun.*, 2011, **47**, 6440–6442.
575 W. Ren, Y. Fang and E. Wang, *ACS Nano*, 2011, **5**, 6425–6433.
576 M. Manikandan, H. N. Abdelhamid, A. Talib and H.-F. Wu, *Biosens. Bioelectron.*, 2014, **55**, 180–186.
577 H. Zhang, D. Hines and D. L. Akins, *Dalton Trans.*, 2014, **43**, 2670–2675.
578 K. Jasuja and V. Berry, *ACS Nano*, 2009, **3**, 2358–2366.
579 F. Schedin, E. Lidorikis, A. Lombardo, V. G. Kravets, A. K. Geim, A. N. Grigorenko, K. S. Novoselov and A. C. Ferrari, *ACS Nano*, 2010, **4**, 5617–5626.
580 J. Lee, K. S. Novoselov and H. S. Shin, *ACS Nano*, 2011, **5**, 608–612.

581 Y. Chen, C. Tan, H. Zhang and L. Wang, *Chem. Soc. Rev.*, 2015, **44**, 2681–2701.
582 A. E. Jakus, E. B. Secor, A. L. Rutz, S. W. Jordan, M. C. Hersam and R. N. Shah, *ACS Nano*, 2015, **9**, 4636–4648.
583 S. Ahadian, M. Estili, V. J. Surya, J. R. Azcón, X. Liang, H. Shiku, M. Ramalingam, T. Matsue, Y. Sakka, H. Bae, K. Nakajima, Y. Kawazoecm and A. Khademhosseini, *Nanoscale*, 2015, **7**, 6436–6443.
584 J.-M. Shen, G. Huang, X. Zhou, J. Zou, Y. Yang, Y.-F. Chen and S.-K. Mena, *RSC Adv.*, 2014, **4**, 50464–50477.
585 L. Ren, S. Huang, W. Fan and T. Liu, *Appl. Surf. Sci.*, 2011, **258**, 1132–1138.
586 X. Fan, G. Jiao, W. Zhao, P. Jin and X. Li, *Nanoscale*, 2013, **5**, 1143–1152.
587 W. Chen, P. Yi, Y. Zhang, L. Zhang, Z. Deng and Z. Zhang, *ACS Appl. Mater. Interfaces*, 2011, **3**, 4085–4091.
588 X. T. Zheng and C. M. Li, *Mol. Pharmaceutics*, 2012, **9**, 615–621.
589 V. Urbanova, M. Magro, A. Gedanken, D. Baratella, F. Vianello and R. Zboril, *Chem. Mater.*, 2014, **26**, 6653–6673.
590 Y. Ye, T. kong, X. Yu, Y. Yu, K. Zhang and X. Wang, *Talanta*, 2012, **89**, 417–421.
591 H.-J. Song, X.-H. Jia, N. Li, X.-F. Yang and H. Tang, *J. Mater. Chem.*, 2012, **22**, 895–902.
592 M. Khan, S. T. Khan, M. Khan, S. F. Adil, J. Musarrat, A. A. Alkhedhairy, A. Al-Warthan, M. R. H. Siddiqui and H. Z. Alkhathlan, *Int. J. Nanomed.*, 2014, **9**, 3551–3565.
593 E. Alarcon, K. Udekwu, M. Skog, N. L. Pacioni, K. G. Stamplecoskie, M. González-Béjar, N. Polisetti, A. Wickham, A. Richter-Dahlfors, M. Griffith and J. C. Scaiano, *Biomaterials*, 2012, **33**, 4947–4956.
594 O. Akhavan and E. Ghaderi, *ACS Nano*, 2010, **4**, 5731–5736.
595 Y. Zhou, J. Yang, T. He, H. Shi, X. Cheng and Y. Lu, *Small*, 2013, **9**, 3445–3454.
596 J. Tang, Q. Chen, L. Xu, S. Zhang, L. Feng, L. Cheng, H. Xu, Z. Liu and R. Peng, *ACS Appl. Mater. Interfaces*, 2013, **5**, 3867–3874.
597 L. Liu, J. Liu, Y. Wang, X. Yan and D. D. Sun, *New J. Chem.*, 2011, **35**, 1418–1423.
598 J. Ma, J. Zhang, Z. Xiong, Y. Yong and X. S. Zhao, *J. Mater. Chem.*, 2011, **21**, 3350–3352.
599 Y. Gu, M. Xing and J. Zhang, *Appl. Surf. Sci.*, 2014, **319**, 8–15.
600 V. Stengl, D. Popelkova and P. Vlacil, *J. Phys. Chem. C*, 2011, **115**, 25209–25218.
601 H. J. Zhang, P. P. Xu, G. D. Du, Z. W. Chen, K. Oh, D. Y. Pan and Z. Jiao, *Nano Res.*, 2011, **4**, 274–283.
602 J. Guo, S. Zhu, Z. Chen, Y. Li, Z. Yu, Q. Liu, J. Li, C. Feng and D. Zhang, *Ultrason. Sonochem.*, 2011, **18**, 1082–1090.
603 L. Gu, J. Wang, H. Cheng, Y. Zhao, L. Liu and X. Han, *ACS Appl. Mater. Interfaces*, 2013, **5**, 3085–3093.
604 X. Liu, L. Pan, T. Lv, G. Zhu, T. Lu, Z. Sun and C. Sun, *RSC Adv.*, 2011, **1**, 1245–1249.
605 B. Qiu, M. Xing and J. Zhang, *J. Am. Chem. Soc.*, 2014, **136**, 5852–5855.
606 V. H. Nguyen and J. J. Shim, *Mater. Sci. Eng., B*, 2014, **180**, 38–45.
607 L. Zhao, H. Li, S. Gao, M. Li, S. Xu, C. Li, W. Guo, C. Qu and B. Yang, *Electrochim. Acta*, 2015, **168**, 191–198.
608 C. Zhang, A. Boudiba, M.-G. Oliver, R. Snyders and M. Debliquy, *Thin Solid Films*, 2012, **520**, 3679–3683.
609 Z. S. Wu, W. Ren, D.-W. Wang, F. Li, B. Liu and H.-M. Cheng, *ACS Nano*, 2010, **4**, 5835–5842.
610 J. Zhang, J. Jiang and X. S. Zhao, *J. Phys. Chem. C*, 2011, **115**, 6448–6454.
611 Y. Jin, H. Chen, M. Chen, N. Liu and Q. Li, *ACS Appl. Mater. Interfaces*, 2013, **5**, 3408–3416.
612 X. Zhang, X. Sun, Y. Chen, D. Zhang and Y. Ma, *Mater. Lett.*, 2012, **68**, 336–339.
613 H. Wang, L.-F. Cui, Y. Yang, H. S. Casalongue, J. T. Robinson, Y. Liang, Y. Cui and H. Dai, *J. Am. Chem. Soc.*, 2010, **132**, 13978–13980.
614 X. Dong, L. Li, C. Zhao, H.-K. Liu and Z. Guo, *J. Mater. Chem. A*, 2014, **2**, 9844–9850.
615 S. Baek, S. H. Yu, S. K. Park, A. Pucci, C. Marichy and D. C. Lee, *RSC Adv.*, 2011, **1**, 1687–1690.
616 Y. C. Dong, R. G. Ma, M. J. Hu, H. Cheng, C. K. Tsang, Q. D. Yang, Y. Y. Li and J. A. Zapien, *J. Solid State Chem.*, 2013, **201**, 330–337.
617 X. Yang, X. Zhang, Y. Ma, Y. Wang and Y. Chen, *J. Mater. Chem.*, 2009, **19**, 2710–2714.
618 X. Fan, G. Jiao, L. Gao, P. Jin and X. Li, *J. Mater. Chem. B*, 2013, **1**, 2658–2664.
619 W. Xiao, Z. Wang, H. Guo, X. Li, J. Wang, S. Huang and L. Gan, *Appl. Surf. Sci.*, 2013, **266**, 148–154.
620 Z. Wang, C. Ma, H. Wang, Z. Liu and Z. Hao, *J. Alloys Compd.*, 2013, **552**, 486–491.
621 J. Yan, T. Wei, J. Feng, Z. Fan, L. Zhang and F. Wei, *Carbon*, 2012, **50**, 2356–2358.
622 N. Li, M. Zheng, X. Chang, G. Ji, H. Lu, L. Xue, L. Pan and J. Cao, *J. Solid State Chem.*, 2011, **184**, 953–958.
623 S. Min, C. Zhao, G. Chen and X. Qian, *Electrochim. Acta*, 2014, **115**, 155–164.
624 Y. Zhang, X. Xiao, Y. Sun, Y. Shi, H. Dai, P. Ni, J. Hu, Z. Li, Y. Song and L. Wang, *Electroanalysis*, 2013, **25**, 956–966.
625 K. H. Chang, Y. F. Lee, C. C. Hu, C. I. Chang, C. L. Liu and Y. L. Yang, *Chem. Commun.*, 2010, **46**, 7957–7959.
626 W. He, H. Jiang, Y. Zhou, S. Yang, X. Xue, Z. Zou, X. Zhang, D. L. Akins and H. Yang, *Carbon*, 2012, **50**, 265–274.
627 W. Qin and X. Li, *J. Phys. Chem. C*, 2010, **114**, 19009–19015.
628 Z. Gao, J. Liu, F. Xu, D. Wu, Z. Wu and K. Jiang, *Solid State Sci.*, 2012, **14**, 276–280.
629 B. Li, H. Cao, G. Yin, Y. Lu and J. Yin, *J. Mater. Chem.*, 2011, **21**, 10645–10648.
630 A. K. Rai, L. T. Anh, J. Gim, V. Mathew, J. Kang, B. J. Paul, N. K. Singh, J. Song and J. Kim, *J. Power Sources*, 2013, **244**, 435–441.
631 J. Zhu, G. Zeng, F. Nie, X. Xu, S. Chen, Q. Hana and X. Wang, *Nanoscale*, 2010, **2**, 988–994.
632 W.-P. Xu, L.-C. Zhang, J.-P. Li, Y. Lu, H.-H. Li, Y.-N. Ma, W.-D. Wang and S.-H. Yu, *J. Mater. Chem.*, 2011, **21**, 4593–4597.

633 Y. Wang, S. Zhang, H. Chen, H. Li, P. Zhang and Z. Zhang, *Electrochem. Commun.*, 2012, **17**, 63–66.
634 L. Zheng, G. Zhang, M. Zhang, S. Guo and Z.-H. Liu, *J. Power Sources*, 2012, **201**, 376–381.
635 C. Liu, D. Yang, Y. Jiao, Y. Tian, Y. Wang and Z. Jiang, *ACS Appl. Mater. Interfaces*, 2013, **5**, 3824–3832.
636 Z. Chen, N. Zhang and Y.-J. Xu, *CrystEngComm*, 2013, **15**, 3022–3030.
637 X. Sun, C. Zhou, M. Xie, H. Sun, T. Hu, F. Lu, S. M. Scott, S. M. George and J. Lian, *J. Mater. Chem. A*, 2014, **2**, 7319–7326.
638 F.-X. Xiao, J. Miao and B. Liu, *J. Am. Chem. Soc.*, 2014, **136**, 1559–1569.
639 X. Zhao, S. Zhou, L.-P. Jiang, W. Hou, Q. Shen and J.-J. Zhu, *Chem.–Eur. J.*, 2012, **18**, 4974–4981.